**UNIVERSIDADE ESTADUAL DE CAMPINAS**

FACULDADE DE ENGENHARIA MECÂNICA E INSTITUTO DE GEOCIÊNCIAS

**JUAN FRANCISCO VILLACRESES MORALES**

# Structural Elements Characterization Using Tridimensional Seismic Data Analysis in Brazilian Pre-Salt Reservoirs, Santos Basin.

# Caracterização de Elementos Estruturais Usando Análise de Dados Sísmicos Tridimensionais em Reservatórios do Pré-Sal do Brasil, Bacia de Santos.

CAMPINAS

2021

**JUAN FRANCISCO VILLACRESES MORALES**

# Structural Elements Characterization Using Tridimensional Seismic Data Analysis in Brazilian Pre-Salt Reservoirs, Santos Basin.

# Caracterização de Elementos Estruturais Usando Análise de Dados Sísmicos Tridimensionais em Reservatórios do Pré-Sal do Brasil, Bacia de Santos.

Dissertation presented to the School of Mechanical Engineering and Institute of Geosciences of the University of Campinas in partial fulfillment of the requirements for the degree of Master in Science and Petroleum Engineering in the area of reservoirs and management.

Dissertação apresentada à Faculdade de Engenharia Mecânica e Instituto de Geociências da Universidade Estadual de Campinas como parte dos requisitos exigidos para a obtenção do título de Mestre em Ciências e Engenharia de Petróleo, na Área de reservatórios e gestão.

Orientador: Prof. Dr. Alexandre Campane Vidal

ESTE TRABALHO CORRESPONDE À VERSÃO FNAL DA DISSERTAÇÃO DEFENDIDA PELO ALUNO JUAN FRANCISCO VILLACRESES MORALES E ORIENTADA PELO PROF. DR. ALEXANDRE CAMPANE VIDAL.

**CAMPINAS**
**2021**

FICHA CATALOGRÁFICA ELABORADA PELA

BIBLIOTECA DA ÁREA DE ENGENHARIA - BAE – UNICAMP

Ficha catalográfica
Universidade Estadual de Campinas
Biblioteca da Área de Engenharia e Arquitetura
Rose Meire da Silva - CRB 8/5974

| | |
|---|---|
| | Villacreses Morales, Juan Francisco, 1996- |
| V711s | Structural elements characterization using tridimensional seismic data analysis in Brazilian pre-salt reservoir, Santos Basin / Juan Francisco Villacreses Morales. – Campinas, SP : [s.n.], 2021. |
| | Orientador: Alexandre Campane Vidal. |
| | Dissertação (mestrado) – Universidade Estadual de Campinas, Faculdade de Engenharia Mecânica. |
| | Em regime multiunidades com: Instituto de Geociências. |
| | 1. Falhas (Geologia). 2. Fraturas (Geologia). 3. Pré-sal. 4. Prospecção sísmica. 5. Ondas sismicas. I. Vidal, Alexandre Campane, 1969-. II. Universidade Estadual de Campinas. Faculdade de Engenharia Mecânica. III. Título. |

<u>Informações para Biblioteca Digital</u>

**Título em outro idioma:** Caracterização de elementos estruturais usando análise de dados sísmicos tridimensionais em reservatorios do pré-sal do Brasil, Bacia de Santos
**Palavras-chave em inglês:**
Faults
Fracture
Pre-salt
Seismic prospection
Seismic waves
**Área de concentração:** Reservatórios e Gestão
**Titulação:** Mestre em Ciências e Engenharia de Petróleo
**Banca examinadora:**
Alexandre Campane Vidal [Orientador]
Bruno César Zanardo Honório
Ulisses Miguel da Costa Correia
**Data de defesa:** 26-08-2021
**Programa de Pós-Graduação:** Ciências e Engenharia de Petróleo

**Identificação e informações acadêmicas do(a) aluno(a)**
- ORCID do autor: https://orcid.org/0000-0002-5493-7072
- Currículo Lattes do autor: http://lattes.cnpq.br/7205640186615739

**UNIVERSIDADE ESTADUAL DE CAMPINAS**

**FACULDADE DE ENGENHARIA MECÂNICA
E INSTITUTO DE GEOCIÊNCIAS**

**DISSERTAÇÃO DE MESTRADO ACADÊMICO**

# Structural Elements Characterization Using Tridimensional Seismic Data Analysis in Brazilian Pre-Salt Reservoirs, Santos Basin

# Caracterização de Elementos Estruturais Usando Análise de Dados Sísmicos Tridimensionais em Reservatórios do Pré-Sal do Brasil, Bacia de Santos

Autor: Juan Francisco Villacreses
Orientador: Alexandre Campane Vidal

A Banca Examinadora composta pelos membros abaixo aprovou esta Dissertação:

**Prof. Dr. Alexandre Campane Vidal, Presidente**
**DGRE/IGE/UNICAMP**

**Dr. Bruno César Zanardo Honório**
**Centro de Pesquisa e Tecnologia da Equinor, EQUINOR**

**Dr. Ulisses Miguel da Costa Correia**
**CGG GeoConsulting, Reservoir Americas**

A Ata de Defesa com as respectivas assinaturas dos membros encontra-se no SIGA/Sistema de Fluxo de Dissertação/Tese e na Secretaria do Programa da Unidade.

Campinas, 26 de agosto de 2021

## Dedicatória

*A Dios trinidad por el amor, la sabiduría y la fortaleza.*

*A mi amada familia Rubiela, Carolina y Juan José.*

*A Francisco, siempre estarás presente*

*Los amo con todo mi corazón*

*A Deus, a trindade, pelo amor, sabedoria e força.*

*À minha valiosa família Rubiela, Carolina e Juan José.*

*Para Francisco, você estará sempre presente*

*Amo vocês com todo o meu coração*

## Agradecimentos

Agradeço a Deus por tudo na minha vida. À minha família por todo o amor e apoio na distância. Um especial agradecimento à Sayeny de Ávila Gonçalves, que sempre esteve presente nos momentos que eu mais precisava desde o início deste trabalho. Obrigado pela sua companhia e amor.

Devo agradecer pela oportunidade e confiança que me foi dada pelo meu orientador Professor Doutor Alexandre Campane Vidal, que me proporcionou junto do Laboratório de Modelagem Geológica de Reservatórios condições para participar e desenvolver o projeto de pesquisa.

Agradeço a empresa Equinor pela oportunidade de trabalhar em associação com o seu projeto e a Fundação de Amparo à Pesquisa do Estado de São Paulo (FAPESP) pela bolsa de Mestrado que me foi concedida. O presente trabalho foi realizado sob o processo no 2020/02039-5.

Agradeço ao pessoal do laboratório MGR, tive momentos muito especiais com todos e aprendi algo valioso para a minha vida com cada um deles, apesar do pouco tempo que compartilhamos.

Devo agradecer ao Doutor Bruno César Zanardo Honório e Doutor Ulisses Miguel da Costa Correia devido à valiosa orientação e conhecimento transmitido na qualificação, seus comentários foram muito importantes para meu crescimento profissional e acadêmico e a melhoria deste trabalho.

# Resumo

## Dissertação de Mestrado

A compreensão da tectônica que impacta a subsuperfície é crítica para o sucesso de caracterização de reservatórios de petróleo. Elementos estruturais, como falhas e fraturas, podem definir a distribuição de sedimentos durante a deposição na evolução da bacia e atuar como barreiras ou condutos para o fluxo de fluido, influenciando o armazenamento de hidrocarbonetos. Os dados sísmicos permitem detectar esses elementos estruturais. geralmente visualizados como descontinuidades nos refletores sísmicos. A interpretação estrutural de reservatórios carbonáticos é particularmente desafiadora devido à alta heterogeneidade, caracterizada pela baixa continuidade espacial e por estruturas de pequena escala, como fraturas sub-sísmicas e características relacionadas a certificação. O objetivo principal deste estudo foi investigar os elementos estruturais das rochas carbonáticas do pré-sal através da interpretação de falhas e fraturas. Para isso, foi usado sísmica tridimensional e análise de dados de poços na Bacia de Santos. Com base nesses dados, foi possível obter informações sobre a morfologia das falhas e a interação entre as estruturas regionais. Nesse sentido, a interpretação foi feita utilizando técnicas de processamento sísmico e atributos sísmicos que aprimorou o processo interpretativo. Com base em um fluxo de trabalho sistemático, ruído coerente e randômico do volume sísmico foram removidos. A caracterização das descontinuidades baseada na análise atributos sísmicos permitiram entender a deformação estrutural e a relação entre as estruturas regionais. A orientação das descontinuidades foi fundamental para detectar regiões potencialmente fraturadas. Uma vez selecionados os diversos atributos sísmicos, a análise multiatributos, baseada em uma rede neural artificial não supervisionada, foi possível detectar e caracterizaras áreas com alta probabilidade de ocorrência de falha. Na fase de validação, as características estruturais de perfis de imagem de poço calibraram o azimute das descontinuidades sísmicas e o campo de tensões tectônica local, confirmando as tendências interpretadas a partir dos atributos sísmicos.

**Palavras Chave:** Falhas, Redes de Fratura, Atributos Sísmicos, Interpretação Sísmica, Bacia de Santos.

# Abstract

### Master's degree

Understanding the tectonic activity that impacts the subsurface is critical for the successful characterization of petroleum reservoirs. Structural elements, such as faults and fractures, may constrain the sediment distribution during deposition into the basin evolution and perform as barriers or conduits for fluid flow, influencing hydrocarbon storage. These structural elements are commonly detected using seismic data are often imaged as discontinuities on the seismic reflectors. In particular, carbonate reservoirs are structurally challenging due to the high heterogeneity, which often presents low spatial continuity and sub-seismic fractures and karst-related features. The main objective of this study is to increase the scientific knowledge of faults and fractures interpretation in the pre-salt reservoirs based on three-dimensional seismic and well data analysis in Santos Basin. This study provides insights into the fault morphology and the interaction among structures. In that sense, the identification of structural elements was carried out using seismic processing techniques and seismic attributes, which improved the interpretive process. A systematic data conditioning workflow removed coherent and random noise from the seismic volume. The characterization of the structural elements based on seismic attributes allowed understanding the structural deformation and the relation with regional structures. The discontinuities orientation was the key to predicting potential fractured regions. Once we selected the seismic attributes, the multi-attribute analysis approach, based on the unsupervised artificial neural network, characterized the areas with a high probability for fracturing. In the validation stage, structural features from the borehole image calibrated the azimuth of the seismic discontinuities and the local tectonic stress field, which confirmed the main structural trends interpreted from the seismic attributes.



**Keywords:** Faults, Fracture networks, Seismic Attributes, Seismic Interpretation, Santos Basin.

# Index of figures

**ARTIGO 1: Impact of seismic data conditioning on the structural elements detection for the pre-salt reservoir, Santos Basin, Brazil.**

Figure 1. (a) Regional distribution of the main geological features in Santos Basin and study area location (modified from Cardoso and Hamza, 2014). (b) Base map indicating the area covered by 3D seismic and drilled wells. .......... 23

Figure 2. Workflow of seismic data processing and attribute analysis. The workflow adopted for the present study consists of three phases: data conditioning, well-to-seismic tie, and attribute analysis. .......... 24

Figure 3. Trace segments show how the steering cube method uses inline and crossline locations (modified from Brouwer and Huck, 2011). .......... 25

Figure 4. Curvature definition. a) Positive, negative, and zero curvature are related to antiforms, synforms, and flat surfaces, respectively. b) Fault might exist in the zone where the most positive and the most negative are parallel bands (modified from Roberts, 2001). .......... 28

Figure 5. Seismic zones and amplitude spectrum behavior separation, a) Seismic volume displaying the characteristics of seismic reflector in the shallow (yellow box), intermediate (blue box), and deep interval (red box). Amplitude spectrum according to b) shallow (50 Hz), c) intermediate (25 Hz), and d) deep (17 Hz) intervals showing the dominant frequency. .......... 30

Figure 6. Amplitude maps at Barra Velha Formation time slice. a) Original data shows strong parallel stripes in inline direction with a size of 300m (yellow ovals), b) First iteration, noise is partially attenuated. Remnant noise is still observed with a size of 120m approximately (yellow ovals) and c) the second iteration attenuated the coherent noise; despite, random noise remains on the seismic data. d) Comparison amplitude spectra from original, first iteration and second iteration extracted at deep interval .......... 31

Figure 7. Time slice at Barra Velha Formation sampled through a) FFT steering cube and b) BG steering cube. Comparison of noise impacts on the calculation of dip values at the crossline through c) FFT steering cube and d) BG steering cube. The yellow arrows show zones with extreme negative dip values in a predominantly NE-SW direction and orange ovals indicate the locations of dip information associated with noise. .......... 32

Figure 8. Crossline is shown after applying a) Destriping Filter, b) Dip-Steered Median filter results, and c) residual noise from Dip-Steered Median Filter. White boxes indicate the location where noise overlapped the seismic reflectors before data conditioning. d) Yellow boxes show the Spectral Whitening effect in zones where the energy from the reflectors was increased. .......... 33

Figure 9. Comparison amplitude spectra from crossline X180 between a) Destriping Filter, b) Dip-Steered Median Filter, and c) Spectral Whitening. .......... 33

Figure 10. Time slices at Barra Velha Formation sampled through a) Steering Cube and b) second-generation Steering Cube, and Crossline through c) Steering Cube and d) second-

generation Steering Cube. Yellow arrows indicate zones with extreme negative dip values in a predominantly NE-SW orientation. Orange ovals show the locations of contrasting dip values associated with noise. The second-generation steering cube generated more continuous dip and azimuth volume. ........................................................................................................34

Figure 11. Seismic-Well tie for well A. a) Sonic and Density logs used to calculate b) Acoustic Impedance (AI) and Reflectivity logs. c) Original and d) conditioned seismic data are compared with the synthetic seismic traces produced by convolution between reflectivity log and extracted wavelet from the original seismic data. d) Well A tying the reflectors of filtered seismic data. Formations tops for Barra Velha, Itapema, and Camboriu Formations are represented by pink, green and red color, respectively. ..............................................................................35

Figure 12. Crossline displaying (a) Dip-Steered Diffusion Filter and (b) Edge Preserving Smoother filter. White boxes indicate zones where discontinuities were enhanced. ...............36

Figure 13. Dip-steered Similarity attribute displayed at time slice of Barra Velha Formation utilizing a) raw data, b) dip-steered median filter, and c) edge-enhancing filters. Yellow arrows indicate zones where the discontinuities were highlighted. The Crosslineshows Dip-steered Similarity d) before and e) after data conditioned. Conditioned data shows the direct relationship of discontinuities enhanced by the Similarity attribute. Blue dashed line indicates the respective position regarding crossline and time slice. ...................................................37

Figure 14. Curvature attributes were displayed at the top of the Barra Velha formation. The most negative curvature (a, c) and the most-positive curvature (b, d) indicate the flexural characteristics of the seismic reflectors. Curvature attributes calculated from the raw data (a, b) showed distorted lineaments (yellow arrows) and accentuated acquisition footprint artifacts in the inline direction. Curvature attributes computed from second-generation Steering Cube (c, d) displayed continuous structures without the influence of the acquisition footprint (yellow arrows). ........................................................................................................................38

Figure 15. The most positive curvature (blue color) and the most negative curvature (red color) from the second-generation Steering Cube show the relationship between the curvatures and the main discontinuities detected (yellow arrows). The Dip-steered Similarity attribute (white color) from the conditioned seismic data highlights the principal structural elements at the top of the Barra Velha formation. .........................................................................................39

Figure 16. The horizon at the top of the Barra Velha Formation shows the most negative curvature (blue colors), most-positive curvature (red colors), and dip-steered similarity (white color), highlighting the flexures characteristics caused by faulting (black arrows). ................39

**ARTIGO 2: Seismic attributes and unsupervised artificial neural network for fault and fracture interpretation: an example from Brazilian pre-salt reservoir, Santos Basin.**

Figure 1. (a) Location map of the study area in the Santos basin, Brazil (modified from Gamboa et al., 2019). (b) Base map of the survey indicating the area covered by 3D seismic lines and drilled wells. ........................................................................................................................ 48

Figure 2. Workflow adopted. It consists of seismic interpretation, attribute computation, artificial neural network, and validation. .................................................................... 48

Figure 3. Diagram showing the dip components on a reflector. Pink and green arrows are dips along the inline and crossline direction, respectively. The red arrow is the polar dip, and the orange arrow is the dip azimuth (Modified from Chopra and Marfurt, 2007b). ...................... 50

Figure 4. Diagram illustrating the REF computation in four directions (inline, crossline, and two diagonals oriented in 45 and 315°). The most significant values are extracted surrounding the evaluation point (Modified from Brouwer and Huck, 2011). ............................................ 51

Figure 5. Illustration of seismic traces pairs position used as input in the computation of similarity attribute regarding a central seismic trace (red square). Four different directions can be used, two diagonal(yellow and green squares) and two perpendiculars (purple and blue squares)(Modified from Brouwer and Huck, 2011). ............................................................. 52

Figure 6. Curvature diagram showing the characteristics of the curvature analysis (extracted from Roberts, 2001). .......................................................................................................... 53

Figure 7. Main structural elements interpretation using borehole image log. Some examples from an interpreted a) Fault, b) Fracture, c) Breakouts, and d) DIF (Drilling Induced Fractures). The white arrow indicates faults and fractures, the green area the occurrence of breakouts, and the black arrows the presence of drilling-induced fractures. The scale bar in all examples corresponds to 1 meter in vertical position. ................................................................. 56

Figure 8. a) Regional faults and lineaments illustrated over the study area with the main trend in NW-SE direction. Seismic crossline-section b) and c) highlights the regional fault with the apparent high dip affecting the time maps of d) Barra Velha, e) Itapema, and f) Camboriu Formation. ........................................................................................................................ 58

Figure 9. Time slice showing (a) polar-dip, (b) inline-dip, and (c) crossline-dip based on Steering Cube data. The black lines and arrows show dip values related to major structures. Red and blue arrows indicate the sudden dip changes in inline direction and crossline direction, respectively. .................................................................................................................. 59

Figure 10. Time slices showing a) Dip-Steered Similarity and b) REF. Red arrows follow structures with a preferential NE-SW trend. Pink circles indicate areas where discontinuities are improved. ................................................................................................................ 60

Figure 11. Time slices showing a) directional REF in W-E orientation and b) N-S orientation. Green and purple arrows point out discontinuities by the directional REF............................. 61

Figure 12. Curvature maps on the Barra Velha horizon shows (a) the most positive curvature, (b) the most negative curvature, and (c) the blend of the most positive curvature and the most negative curvature. The pink arrows point out the principal structures, and the yellow arrows show variation in the principal direction. The yellow, green, and pink polygons indicate the separation of structural patterns. ........ 62

Figure 13. The diagram shows the relationship between different structural elements directions interpreted by seismic attributes and compared to the regional structures of Santos Basin. .... 63

Figure 14. a) TFL cube showing the faults likelihood values close to the interpreted major faults and opacity between conditioned seismic and TFL at crossline (b) and (c). Black lines represent zones of the interpreted faults manually. ........ 64

Figure 15. Automatic fault planes extraction shows the orientation of five groups of possible discontinuities in the study area. a) N20°W, b) N10°E and c) N55°W, d) E-W and e) N45°W. Cool colors referred to the upper part of the reservoir, and warm colors referred to the lower part of the reservoir. ........ 65

Figure 16. Interactions among different trends in shallow and deep zones. a) NE-trending, b) E-W trend and the shallow N20°W trend, and c) deep trends N45°W and N20°W. Cool colors refer to times from shallow structures, and warm colors refer to deep structures. ........ 66

Figure 17. The fracture density attribute shows the most positive curvature scenario with a searching window of a) 125 m and b) 375 m, and the TFL scenario using a) low threshold and b) high threshold. The yellow arrows show some regions of maximum fracture activity. ...... 67

Figure 18. The fracture proximity attribute emphasized the relationship between the center of discontinuities and the adjacent structures. The yellow arrows show the regions where the interaction among possible structures was compared. The most positive curvature scenario uses a searching window of a) 125 m and b) 375 m and the TFL scenario uses c) low and d) high threshold. ........ 68

Figure 19. The result of the curvature scenario highlighted the possible fracture network from a) upper, b) middle, and c) lower part of the Barra Velha Formation. Yellow arrows show the cluster of possible fractures following the NE-SW trend. ........ 70

Figure 20. The results of the TFL scenario highlight the possible fractured areas from a) upper, b) middle, and c) lower part of the Barra Velha Formation. Yellow arrows exhibit the clusters of fractures following the NNE-SSW trend. ........ 70

Figure 21. Interpretation of main structural trends using strike data from the interpreted fractures and faults in the borehole image logs. The black arrow indicates the predominant direction of faults and fractures. ........ 71

Figure 22. Well location with borehole image logs. Fractures trends in the Barra Velha Formation were plotted in rose diagrams for individual wells. The red rose diagram shows seismic discontinuities interpreted from the TFL attribute, and the pink rose diagram the fracture direction for wells. The red boxes indicate local structures with changes in the main trends. ........ 72

Figure 23. Interpretation of tectonic stress field using the strike data from Breakout and DIF interpreted in the borehole image logs for the a) Well A, b) Well C, c) Well E, and d) Well F. Blue and red points indicate the dip azimuth from DIF and breakouts, respectively. Blue and red arrows show the directions of maximum and minimum horizontal stress, respectively.... 73

# Table of contents

**INTRODUCTION** ..... **16**

**REFERENCES** ..... **18**

**ARTICLE 1: Impact of seismic data conditioning on the structural elements detection for pre-salt reservoir, Santos Basin, Brazil.** ..... **20**

**ABSTRACT** ..... **20**

**INTRODUCTION** ..... **21**

**GEOLOGICAL SETTINGS** ..... **22**

**DATA AND METHODS** ..... **23**

Data Conditioning ..... 24

Dip-azimuth computation ..... 25

Structural Enhancement ..... 26

Well-to-Seismic tie ..... 27

Seismic attributes analysis ..... 27

**RESULTS AND DISCUSSION** ..... **29**

Noise attenuation ..... 29

Impact on seismic attributes ..... 36

**CONCLUSIONS** ..... **39**

**REFERENCES** ..... **41**

**ARTICLE 2: Seismic attributes and unsupervised artificial neural network for fault and fracture interpretation: an example from Brazilian pre-salt reservoir, Santos Basin** ..... **43**

**ABSTRACT** ..... **43**

**INTRODUCTION** ..... **44**

**GEOLOGICAL SETTING** ..... **46**

**DATA AND METHOD** ..... **47**

Interpretation of seismic fault framework ..... 49

Seismic attributes selection and analysis ... 49

Dip Attributes ... 49

Dip-steered Similarity and Ridge-enhancement Filter ... 50

Curvatures Attributes ... 52

Thinned Fault likelihood ... 53

Fracture Density and Fracture Proximity ... 54

Unsupervised Artificial Neural Network ... 55

Well Image Log Validation ... 56

**RESULTS AND DISCUSSION ... 57**

Structural Framework Interpretation ... 57

Structural characterization through seismic attributes ... 59

Detailed structural characterization ... 63

Multi-attribute Analysis through Unsupervised Artificial Neural Networks ... 69

Seismic Attribute Map and Well Validation ... 71

**CONCLUSION ... 74**

**REFERENCES ... 75**

**APEPENDIX 1A.FINAL CONSIDERATIONS ... 80**

**APPENDIX 2A. WELL-TO-SEISMIC TIE ... 81**

**APPENDIX 2B. REPRESENTATIVE FREQUENCY SPECTRA AND VERTICAL RESOLUTION ... 82**

**APPENDIX 3A. COMPARISON SEISMIC AND WELL STRUCTURAL ELEMENTS ... 84**

## INTRODUCTION

Carbonate reservoirs have always been of interest in the oil and gas industry due to the enormous potential in hydrocarbon reserves, the world's largest oil and gas reserves (Nelson, 2001). The inherent heterogeneity and complex geological properties on these reservoirs are usually produced by external agents, such as tectonic activity. Notably, structural elements such as faults and fractures may crucially impact reservoir architecture, improve the storage capacity and fluid flow, or cause leakage and instabilities in borehole walls.

Fracturing occurs naturally associated with brittle deformation over the earth's entire crust. Different mechanisms can be the driving force behind the generation of these structural elements, such as tectonics, salt-tectonics, water escape, or differential compaction (Alves et al., 2020). According to Gabrielsen and Braathen (2014), an approximation to the architecture of fracture networks and faults is often composed of a fault core and an associated damage zone. Mainly, steep structures may display symmetrical zonation of fracture patterns as joint swarms or fracture corridors around the central area. The orientations are essential due to the likelihood to affect the permeability (Richard et al., 2014). However, fault zones do not always correspond to interconnected spaces; sealing across the discontinuities is crucial for analyzing fault risk or modified hydrocarbon traps.

These geological processes have led researchers to challenge issues regarding the characterization of fractures in reservoirs. It may include mapping fault architecture and understanding the connectivity of fracture networks. Mostly, in carbonate reservoirs, it is necessary to properly understand the nature, intensity, and geometric distribution of fractures for optimum hydrocarbon production (Aguilera, 1995). Thus, the seismic expression of such structures is relevant for the investigation, as suggested by the seismic attributes mapping of lineaments in the subsurface (Chopra and Marfurt, 2007b).

Seismic attributes are a different representation of seismic data based on mathematical tools and analysis of seismic traces (Barnes, 2000). They can facilitate structural and stratigraphic interpretation and identify faults and fracture zones that cannot be easily detected on amplitude data. In most cases, dependent on the quality of the data, it is necessary to create workflows that include a pre-conditioning for noise attenuation and structural enhancement using filters or a combination of more than one seismic attribute to detect geological features successfully.

On the other hand, the pre-salt reservoirs in Santos Basin, composed mainly of microbial carbonates, have been affected by the basin settings that conditioned their facies distribution (Moreira et al., 2007). These reservoirs often presented structural elements such as fractures and karst features, which are essential in the development plan of oilfields (Boyd et al., 2015). The distribution of these heterogeneities is mainly related to the tectonic activity and the depositional conditions (Gomes et al., 2008).

Through 3D seismic data, this work proposes identifying faults and fracture networks in a pre-salt field from Santos Basin, southeast Brazil. To this end, a first article is presented, which implements a systematic workflow of seismic data pre-conditioning to remove noises and highlight the discontinuities. In complement, a second article is presented focusing on the characterization of seismic discontinuities using several seismic attributes. An artificial neural network analyzes multiple seismic attributes, looking for areas with a high probability of faults and fractures. In the end, the structural elements extracted from the seismic data are cross-correlated with borehole image data for validation.

**REFERENCES**


Aguilera, R., 1995. Naturally Fractured Reservoirs-. Pennwell Books.

Alves, T., Fetter, M., Busby, C., Gontijo, R., Cunha, T.A., Mattos, N.H., 2020. A tectono-stratigraphic review of continental breakup on intraplate continental margins and its impact on resultant hydrocarbon systems. Marine and Petroleum Geology 117, 104341. https://doi.org/10.1016/j.marpetgeo.2020.104341

Barnes, A.E., 2000. Weighted average seismic attributes. Geophysics 65, 275–285. https://doi.org/10.1190/1.1444718

Boyd, A., Souza, A., Carneiro, G., Machado, V., Trevizan, W., Santos, B., Netto, P., Bagueira, R., Polinski, R., Bertolini, A., 2015. Presalt Carbonate Evaluation for Santos Basin, Offshore Brazil. Petrophysics 56, 577–591.

Chopra, S., Marfurt, K.J., 2007. Seismic Attributes for Prospect Identification and Reservoir Characterization, Seismic Attributes for Prospect Identification and Reservoir Characterization. https://doi.org/10.1190/1.9781560801900

Gabrielsen, R.H., Braathen, A., 2014. Models of fracture lineaments - Joint swarms, fracture corridors and faults in crystalline rocks, and their genetic relations. Tectonophysics 628, 26–44. https://doi.org/10.1016/j.tecto.2014.04.022

Gomes, P.O., Kilsdonk, B., Minken, J., Grow, T., Barragan, R., 2008. The outer high of the Santos Basin, Southern São Paulo Plateau, Brazil: pre-salt exploration outbreak, paleogeographic setting, and evolution of the syn-rift structures. AAPG International Conference and Exhibition, Cape Town, South Africa 10193, 26–29.

Jaglan, H., Qayyum, F., Huck, H., 2015. Unconventional seismic attributes for fracture characterization. First Break 33, 101–109.

Moreira, J.L.P., Madeira, C.V., Gil, J.A., 2007. Bacia de Santos. Boletim de Geociencias da Petrobras, , Rio de Janeiro, v. 15, n. 2, p. 531-549, maio/nov. 2007 531–549.

Nelson, R., 2001. Geologic Analysis of Naturally Fractured Reservoirs, Geologic Analysis of Naturally Fractured Reservoirs. Gulf Professional Pub. https://doi.org/10.1016/b978-0-88415-317-7.x5000-3

Richard, P., Bazalgette, L., Kidambi, V.K., Laiq, K., Odreman, A., Al Qadeeri, B., Narhari, R., Pattnaik, C., Al Ateeqi, K., 2014. Structural evolution model for the North Kuwait Carbonate fields and its implication for fracture characterisation and modelling. Society of Petroleum Engineers - International Petroleum Technology Conference 2014, IPTC

2014: Unlocking Energy Through Innovation, Technology and Capability 5, 3365–3378. https://doi.org/10.2523/iptc-17620-ms

**ARTICLE 1: Impact of seismic data conditioning on the structural elements detection for the pre-salt reservoir, Santos basin, Brazil.**

**ABSTRACT**

The three-dimensional seismic data provides valuable insights into the geological structures and fluid flow in reservoirs, which are required in great detail when dealing with naturally fractured reservoirs, especially for sensitive projects like carbon sequestration and field enhancement & development. The characterization of structural elements, such as faults and fractures in pre-salt reservoirs using conventional approaches, is challenging due to a complex and heterogeneous overlying evaporitic unit that imposes noises in the seismic amplitude responses. Therefore, seismic data conditioning targeted at improving the seismic image is necessary for quality subsurface investigations. This work provides a systematic workflow of filters to enhance and detect discontinuities in seismic sections, especially through the removal of migration artifacts and salt multiple, thereby maintaining the true geological characteristics of the data. We emphasize the delineation of fault and fracture zones by computing seismic attributes in a post-stack time migrated 3D seismic on Santos Basin deep-waters. Initially, the seismic signal was analyzed, and a sequence of structural-oriented filters and spectral balancing were applied to generate vertically refined images with improved seismic amplitudes. In order to assess the quality of the conditioned data, we implemented the Similarity and Curvature attributes to identify the distribution of discontinuities and compare the before-and-after denoising approach. The data conditioning and analysis of seismic attributes improved our understanding of the distribution and possible compartmentalization of the reservoirs, highlighting discontinuities predominantly NE-trending. The systematic workflow significantly improved the seismic data quality, allowing us to identify better structural elements and insights into potential fractured zones.

**Keywords:** Data Conditioning, Fault Enhancement, Seismic Attributes, Pre-salt Santos Basin.

## INTRODUCTION

The tectonic activity during the evolution stages of the Santos Basin influenced the deposition systems and facies distribution of the pre-salt carbonate reservoirs (Moreira et al., 2007). Structural elements, such as faults or fractures, can have considerable effects on the permeability and quality of reservoirs, directly impacting the productivity of the wells. Thus, identifying zones with those geological features using seismic data is essential in characterizing these reservoirs located in ultra-deep waters. However, an overlying thick layer of stratified salt challenges seismic imaging and processing, imposing considerable uncertainties in the seismic interpretation of pre-salt reservoirs. The salt layer produces shadow zones, loss of high frequencies, and high noise levels in conventional seismic profiles, which affect the computation of seismic attributes and the structural interpretation (Meneguim et al., 2016).

In order to enhance the signal-to-noise ratio and seismic interpretability, particularly the geometries of structural elements, numerous data conditioning techniques have been implemented in the last decades. Tingdahl (1999) introduced the Dip-steering technique using the well-known median filter to enhance the continuity of seismic events and preserve the edges of seismic reflectors. Later, Tingdahl and de Groot (2003) presented an edge-preserving filtering workflow improving the identification of faults with seismic attributes. Similarly, Chopra and Marfurt (2008) showed how structure-oriented filters sharpen interesting subsurface features and decrease the noise levels.

In the same way, Brouwer and Huck (2011) proposed a method based on four main stages to optimize the identification of discontinuities. This method suggests removing discontinuities related to coherent noise, filtering local dips to improve dip volumes, balancing the frequency spectrum, and sharpening the termination of reflector close to potential faults, which increases the quality of the results. Recently, several developments have occurred in interpretation techniques driven by filters and seismic attributes. Jaglan et al. (2015) showed a sequential approach of seismic data conditioning that plays a fundamental role in removing undesired coherent and random noises and characterizing faults and fractures from seismic attributes. Therefore, most authors have effectively illustrated the application of data conditioning through step-by-step processes to attenuate noise, improve the continuity of reflectors, and highlight subsurface structural elements, such as faults or fractures.

This study aims to optimize the denoising process on a seismic volume from Santos Basin, Brazil, based on a sequential approach of data conditioning to identify discontinuity zones. The impacts on the seismic image quality are shown and evaluated at each stage. In addition, the enhancement effects on the geometry and location of discontinuities are provided by seismic attributes, comparing the initial dataset and the outputs from the workflow.

## GEOLOGICAL SETTINGS

The Santos Basin, located on the southeastern Brazilian margin (Figure 1), was formed by separating South American and African plates during the Latest Jurassic to Early Cretaceous (Cainelli and Mohriak, 1999). The current basin was greatly influenced by two main tectonic phases that characterize the evolution from active rifting mechanism on earlier stages to a post-rift thermal subsidence and basin relief movements on latter stages (Alves et al., 2017). The main structures are characterized by faulted and rotated blocks associated with the rifting, NE-trending, and locally segmented by transfer zones (Gomes et al., 2008). Consequently, the tectonostratigraphy framework includes three primary sequences: the syn-rift, post-rift, and drift sequence, separated by regional unconformities (Moreira et al., 2007). In the syn-rift phase, the half-graben structures are constituted by the basement of the Camboriu Formation. Then, a thick succession of no-marine sediments of the Piçarras and Itapema formations were deposited on these depocenters. On the top, a regional unconformity marked the end of this sequence. Overlapping, the carbonates of the Barra Velha formation were deposited, involving the beginning of the post-rift phase. These carbonates consist mainly of microbial carbonates, laminites, spherulites, and magnesium-rich claystone (Moreira et al., 2007; Wright and Barnett, 2015).

On the other hand, a layer of 2 km-thick of stratified evaporites from the Ariri Formation was precipitated overlying the Barra Velha formation. They constitute the principal pre-salt reservoir and the seal in deep-water areas of the Santos Basin. Later, the beginning of the drift sequence was established by raising the sea level and thermal subsidence, forming a passive margin (Moreira et al., 2007).

**DATA AND METHODS**

The data used in this study is a 3D post-stack time migrated data with zero-phase that covers approximately 260 km2 located in Santos Basin (Figure 1). The seismic volume record 1,375 samples at a vertical interval of 4 ms. The bin size of the seismic data is 12.5 m in the inline direction and 12.5 m in the crossline direction, which provides the horizontal seismic resolution. The data are presented using SEG American polarity convention, where a peak with positive amplitude is an increment in acoustic impedance (blue on seismic sections). We also used wireline data from four boreholes: formation tops, checkshots, density, and sonic logs. It is important to emphasize that the measured depth of the well logs is focused on the pre-salt interval. Therefore, the well logs from the salt layer to the sea bottom are restricted.

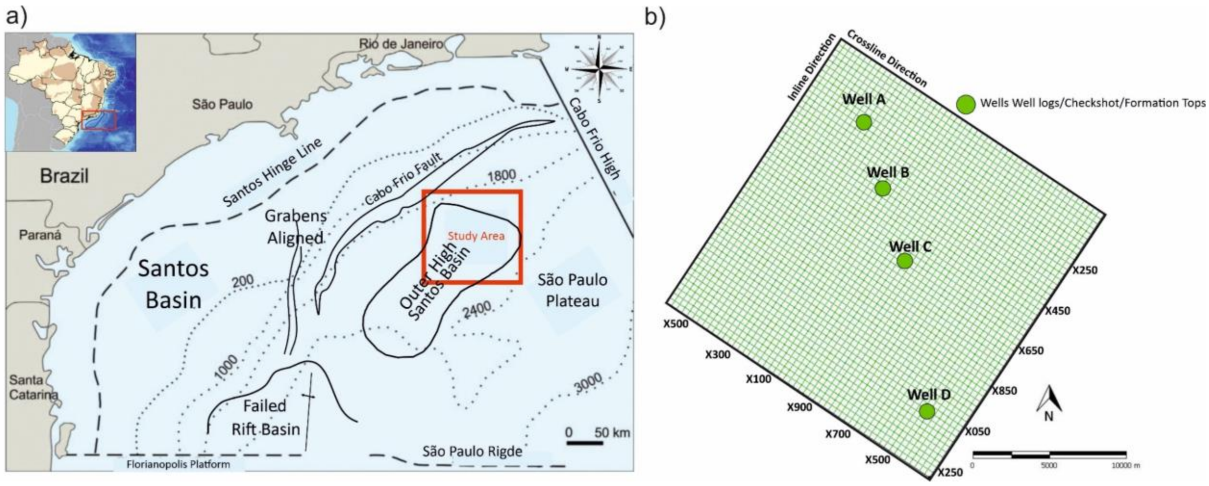


**Figure 1.** (a) Regional distribution of the main geological features in Santos Basin and study area location (modified from Cardoso and Hamza, 2014). (b) Base map indicating the area covered by 3D seismic and drilled wells.

The workflow is divided into two phases: First, a systematic approach of attenuating noises and enhancing the seismic features based on seismic data conditioning. It also includes the input data analysis, filtering evaluation, and comparison of outputs and residuals. Second, applying seismic attributes and analyzing the impact on the characterization of seismic discontinuities. The methodology of this study is summarized in Figure 2.

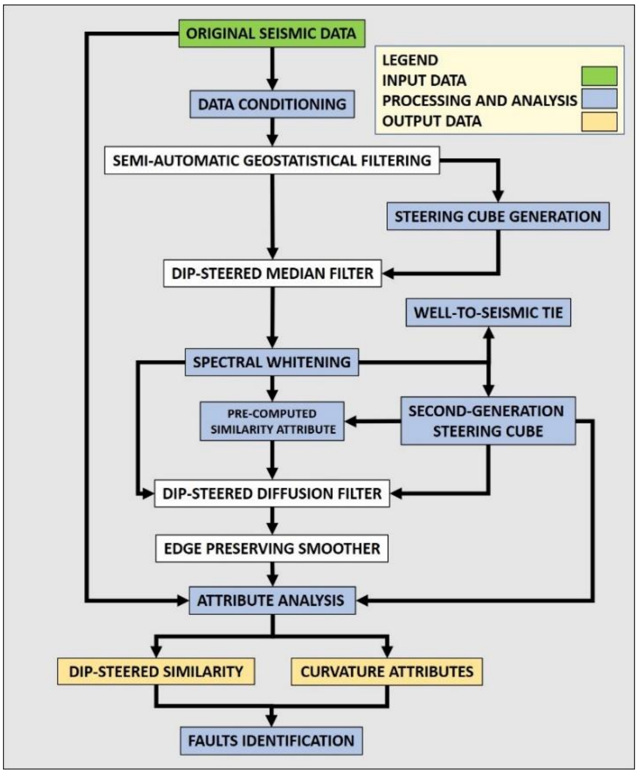


**Figure 2.** Workflow of seismic data processing and attribute analysis. The workflow adopted for the present study consists of three phases: data conditioning, well-to-seismic tie, and attribute analysis.

### Data Conditioning

Initially, we evaluated the 3D time-migrated seismic data through amplitude maps and amplitude spectra on correlated intervals with the tectonostratigraphic framework described by Moreira et al. (2007). We assessed the undesired seismic anomalies that the processing stage might maintain, such as acquisition footprints or multiples.

A semi-automated geostatistical filter (Destriping Filter) was applied based on the first noise analysis. The filter employs a local underlying variogram model composed of the signal and noise. Most of the variogram parameters are optimized during an iterative process; however, other parameters, such as the noise orientation, the signal-to-noise variability, and noise distribution, are defined from the data analysis. Once the parameters are specified, the factorial kriging filters out the noise using the local noise and signal characteristics (Magneron et al., 2009). We then used this denoised data for dip-azimuth computation and structural enhancement as described as follows.

### Dip-azimuth computation

The Steering Cube was used to compute the dip-azimuth volume. The process consists of a surface intercepting the equal seismic phase in a searching radius trace-to-trace (phase-locked) (Figure 3). It extracts the dip in inline direction and cross-line direction at each sample position (Tingdahl and de Groot, 2003). Three algorithms are used to extract the Steering Cube: Principal component analysis (PCA), Phase-gradient (BG), and Fast Fourier Transform (FFT). The PCA estimates the dips using eigenvalue decomposition to extract the direction in three components of maximum seismic amplitude changes. The BG is based on the instantaneous seismic phase's vertical and horizontal amplitude gradient analysis. The FFT depends on the highest energy value on the 3D Fourier transformed domain to compute the dips (dGB-Beheer, 2021).

In some cases, the BG and PCA algorithms may be sensitive to noise and lose details from the reflectors, creating outliers due to the data quality and making smoother dip and azimuth values relatively. For that reason, in most cases, Steering Cube is filtered depending on the scale of structures to be enhanced and data quality. In this study, the FFT algorithm was used following the approach proposed by Huck (2007). First, we created a raw steering cube with 7/7/7 step out (inline/crossline/number of samples), and later median filtering was applied with size 0/0/2 (inline/crossline/number of samples). The Steering Cube was utilized further as an input for the structural enhancement of seismic data.

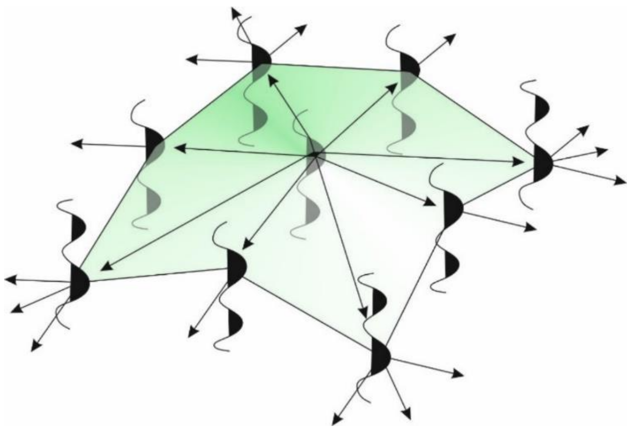

**Figure 3.** Trace segments show how the steering cube method uses inline and crossline locations (modified from Brouwer and Huck, 2011).

**Structural Enhancement**

The structure-oriented filters (SOF) carried out the noise attenuation and seismic enhancements, which removed the artifacts by aligning the seismic reflector using the dip-steering principle and separating the dip-azimuth from seismic reflectors and overlying noise (Chopra and Marfurt, 2008). These filters evaluate three simple components: the orientation of seismic reflectors, the geometry of reflection terminations, and the relative preservation of these terminations while smoothing seismic reflectors data (Fehmers and Höcker, 2003). Following these assumptions, Dip Steered Median Filter (DSMF) was applied to the seismic cube with a 3×3 filtering step out using the pre-computed Steering Cube. The median operator collects samples within the chosen seismic trace window and replaces the central position with the defined statistical operator. It is characterized by improving the continuity of the reflectors and preserving the edge of seismic reflectors (Jaglan et al., 2015). Once we computed the noise-reduced seismic data, we flattened out the amplitude spectrum content through the Spectral Whitening (SW). This method determinates a decay rate of the frequencies from the input data, and then an inverse decay function is applied, flattening the amplitude spectrum (Chopra, 2011). The SW used a specific bandwidth of frequencies as parameters, which was adjusted to optimize the result. High-frequency noise might be included when the range of frequencies differs overmuch from the original amplitude spectrum. Therefore, a narrow frequency range regarding the dominant frequency was applied using a trapezoid-pass filter (Yilmaz, 2001). Later, a second-generation Steering Cube was computed, following the method mentioned in the dip-azimuth computation stage (Huck, 2007).

Despite refining the continuity of reflectors, we also need to enhance the reflector edges to analyze the direction of dips. For that, Dip Steered Diffusion Filter (DSDF) adjusted the diffused terminations of the seismic reflectors with a pre-computed Similarity attribute, which identifies the dissimilar seismic traces to improve the edge of the reflectors (Jaglan et al., 2015). Consequently, the structural enhancement was completed through the Edge-Preserving Smoother filter (EPS), which generated razor-sharp edges on the termination of the reflectors (Luo et al., 2002). It performs a statistical analysis based on the variance of the amplitudes and then replaces the area with the lowest variance by the average amplitude. The operator size is an important parameter that defines the zone around the sample point (Tingdahl and De Groot, 2003). We considered three-size parameters: a small filter size that captures small-scale discontinuities, a restricted search radius to avoid the over-smoothing effect, and a low fault smoothing likelihood due to the low number of well-defined linear structures on the seismic data. The EPS volume and the second-generation Steering Cube were used as inputs for extracting discontinuity attributes.

**Well-to-Seismic tie**

After the filtering process, we tied the available wells to adjust the relationship between time and depth. The overall well-to-seismic tie uses the density and sonic logs to calculate the acoustic impedance log. The time and depth information from checkshot data might be used to calibrate the velocity relation of the sonic log. The contrasts on the impedance log describe the reflective coefficient or the fraction of reflected energy when the acoustic wave finds an interface. Then, an extracted wavelet from the seismic is convoluted with the reflectivity log to generate the synthetic traces. The seismic traces at well locations are compared with the synthetic seismic to find the depth-time relationship.

Initially, a zero-phase wavelet of 120ms was extracted from the seismic data at each well location in a variable interval between the salt base and the maximum seismic recording length (5.5 s) and used as input. The process mainly enabled the correlation of Barra Velha, Itapema, and Camboriu formation tops with the seismic events and mapped the subsurfaces. In addition, the correlation coefficients before-and-after data conditioning were compared to understand the impact of the filtering process; we used Well A to exemplify the differences between the synthetic and real seismic traces. The well-to-seismic tie for the other three wells is presented in Appendix 1A.

**Seismic attributes analysis**

Discontinuity seismic attributes are a proven effective tool for structural elements identification using conventional seismic data. We discussed the enhancement over the discontinuities applying Similarity and Curvature attributes before and after the data conditioning on pre-salt reflectors. The Steering Cube assists these geometric attributes to delineate and predict the distributions of discontinuities. According to Rijks and Jauffred (1991), the dip and dip azimuth may illuminate subtle faults with a thrown significantly less than the size of a seismic wavelength. Thus, the dip-steered attributes yield superior results over the non-steered attributes, showing more subtle geometries than artifacts.

The Similarity attribute quantifies the similarities between two or more traces as a percentage. High values indicate that seismic traces are identical in waveform and amplitude. Meanwhile, low similarity values represent seismic reflections with inconsistent phase and amplitude, revealing a break in the continuity of the seismic reflector that might result from seismic-scale faults. The second-generation Steering Cube was used as an input to improve the Similarity attribute. The output is called Dip-Steered Similarity (Tingdahl and De Groot, 2003). The Dip-Steered Similarity was extracted using a time window of 50ms, which matches the vertical extent of the features with the dominant period and improves the detection capability.

The Curvature Attributes are used to characterize subtle discontinuities, based on the fact that areas with brittle deformation, mainly folding, can produce faults and fractures (Roberts, 2001). They measure the subsurface bending at a particular point using the intersection of infinite planes and focusing on seismic shape deformation instead of analyzing the multi-trace amplitude variations (Chopra and Marfurt, 2007). When the curvature attributes follow the dip and azimuth information trace by trace, it may simulate mapping of local subsurfaces, assigning local curvature values and producing a volumetric attribute (De Rooij and Tingdahl, 2002). According to Roberts (2001), the positive values of curvature are associated with antiforms or upthrow of faults, negative values correspond to synforms or downthrown of faults, and zero curvature is referred a flat surface or inflection zones (Figure 4a). Thus, the most positive and the most negative curvature can highlight isolated features, making the results less ambiguous than those generated by other types of curvature attributes (Figure 4b).

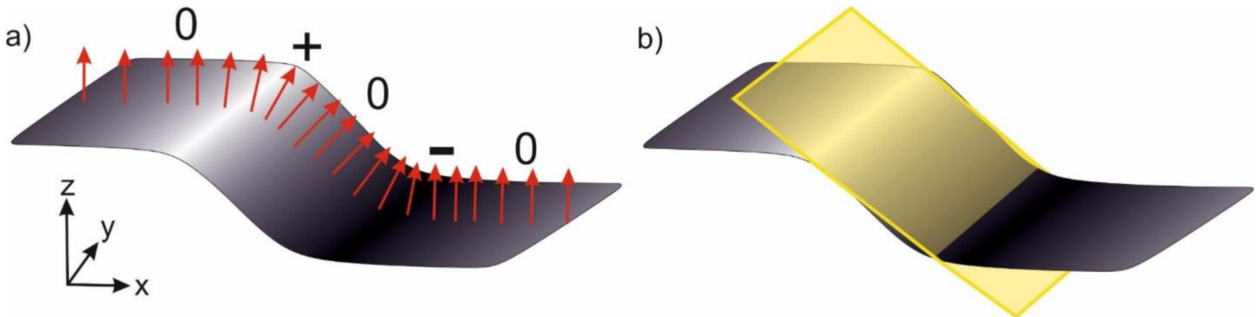


**Figure 4.** Curvature definition. a) Positive, negative, and zero curvature are related to antiforms, synforms, and flat surfaces, respectively. b) Fault might exist in the zone where the most positive and the most negative are parallel bands (modified from Roberts, 2001).

# RESULTS AND DISCUSSION

## Noise attenuation

Initially, the extracted amplitude spectra at remarkable reflector intervals showed the seismic signal distribution on the data (Figure 5a). Representative data samples were analyzed since the dominant frequency shows high variation, generating uncertainty of a specific value in the seismic data (Appendix 1B). The dominant frequency differed from 30-40 Hz for the shallow interval (2800-3500 ms) (Figure 5b) to 20-25 Hz in the intermediate interval (3500-4200 ms) (Figure 5c) and 20-17 Hz in the deeper interval (4200-5500ms) (Figure 5d). The limit between the sub-horizontal reflectors and the antiform structures (~3500ms) was related to strong impedance contrasts on the top of the salt structures. Here, undesired seismic artifacts were homogeneously distributed on the dataset and might be confused with geological features on the pre-salt reflectors (Figure 5a). According to Krueger et al. (2019), the most dominant internal artifacts are characterized by long periods associated with the top of the salt in the Santos Basin. Thus, the noise might mainly mix up with the signal between 30 Hz and 60 Hz. Similarly, the vertical resolution ranged from approximately 20 m for the shallow intervals to 55 m for the deeper intervals, showing in-depth amplitude energy attenuation (Appendix 1B). We noticed that the resolution of the seismic data over the study area was considerably less than ideal for the interpretation of small-scale discontinuities, but large-scale structures may be improved.

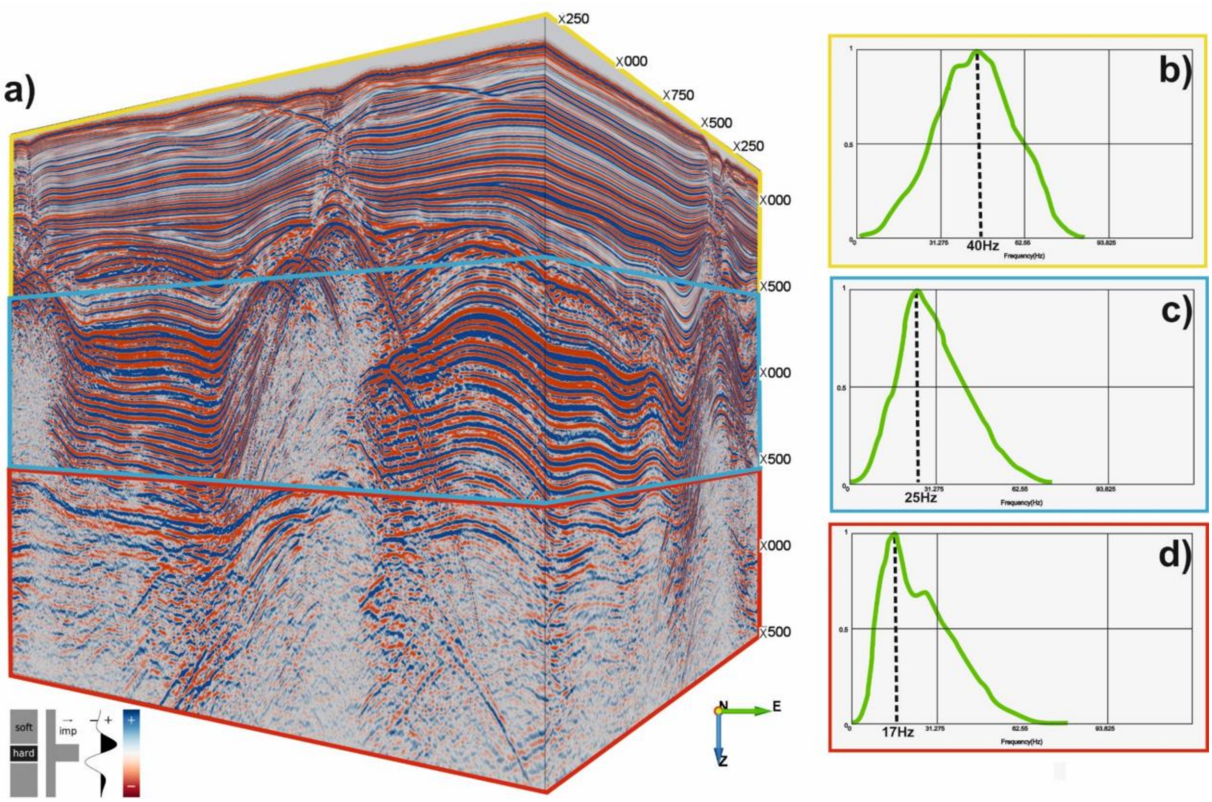


**Figure 5.** Seismic zones and amplitude spectrum behavior separation, a) Seismic volume displaying the characteristics of seismic reflector in the shallow (yellow box), intermediate (blue box), and deep interval (red box). Amplitude spectrum according to b) shallow (50 Hz), c) intermediate (25 Hz), and d) deep (17 Hz) intervals showing the dominant frequency.

Overall, the seismic data are highly susceptible to noise, generating uncertainty and making mapping a problematic task. On the amplitude maps, two periodic linear stripes were recognized as acquisition footprints with a width of 150 m (Figure 6a) and 60 m (Figure 6b) in the inline direction. The width of these acquisition footprints was measured regarding the half period of the coherent noise, where the period was the average distance between two stripes at several positions on the seismic data (Figure 6).

This periodic noise blurred and altered the shape of seismic reflectors, making the artifacts easily confused for geological features (Figure 6a). Marfurt and Alves (2015) emphasized that this seismic noise generates pitfalls that may accumulate errors in the subsequent extraction of seismic attributes. Hence, at the beginning of the data conditioning stage, this preliminary inspection facilitated the noise comprehension for the filtering approach. Then, the Destriping Filter attenuated the periodic signatures of those artifacts, improving the shape of the seismic reflectors (Figure 6b-c). The filter was optimized employing two iterations because of the two periods identified in the inspection stage. Although the frequency spectra comparison showed attenuation of amplitude energy between 25 Hz and 50 Hz and preservation of frequencies below 20 Hz, random noise remained in the seismic image (Figure 6c).

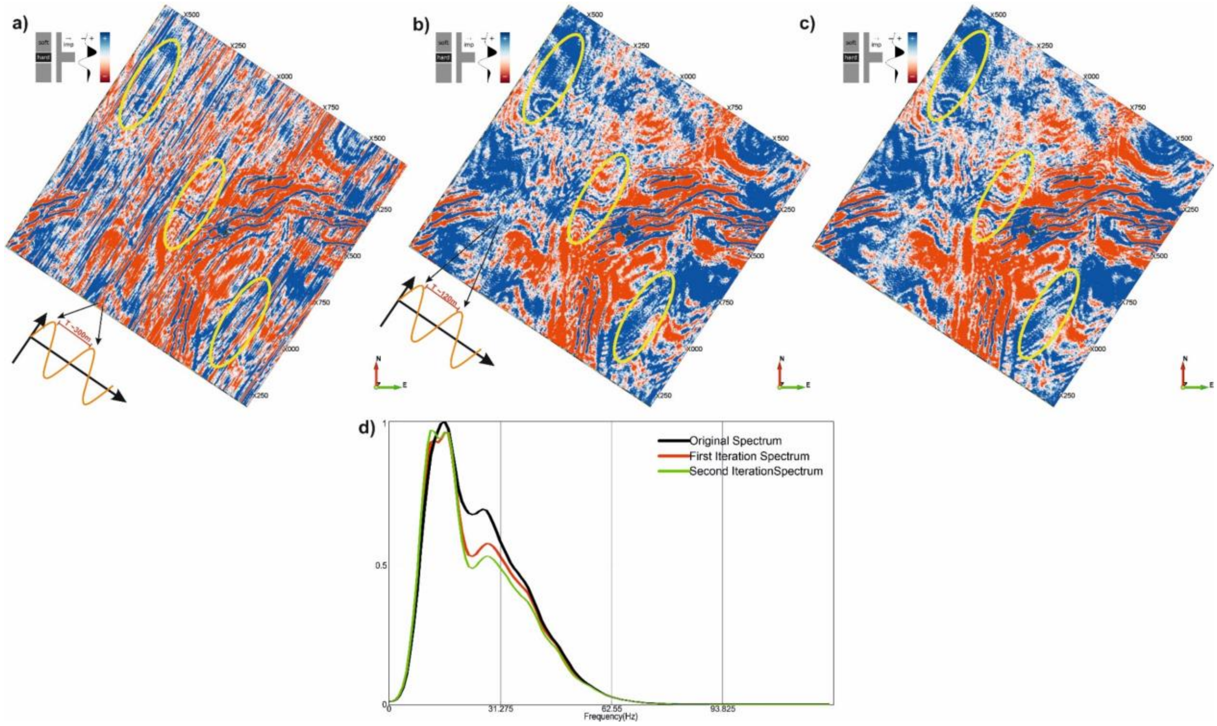


**Figure 6.** Amplitude maps at Barra Velha Formation time slice. a) Original data shows strong parallel stripes in inline direction with a size of 300m (yellow ovals), b) First iteration, noise is partially attenuated. Remnant noise is still observed with a size of 120m approximately (yellow ovals) and c) the second iteration attenuated the coherent noise; despite, random noise remains on the seismic data. d) Comparison amplitude spectra from original, first iteration and second iteration extracted at deep interval.

The Steering Cube established dip and azimuth information for SOF computation and seismic attributes. The quality of the Steering Cube has a meaningful impact on filters and seismic attributes results. According to Huck (2007), the most favorable and similar results are attributed to BG and FFT algorithms, which follow an individual filtering configuration. Both approaches were applied and compared on the dataset; black and white shades represent the distribution of opposite dipping values in Figure 7. As a result, the BG algorithm exhibited conflicting dips and distortion on larger structures due to remnant noise (Figure 7b-d). In contrast, the FFT algorithm showed a low noise influence, more homogeneous dip values in zones characterized by high noise levels, and high contrasting dip regions that might describe better structural trends (Figure 7a-c). Thus, the FFT algorithm with minimum vertical filtering yielded good quality results despite the high noise levels from the dataset.

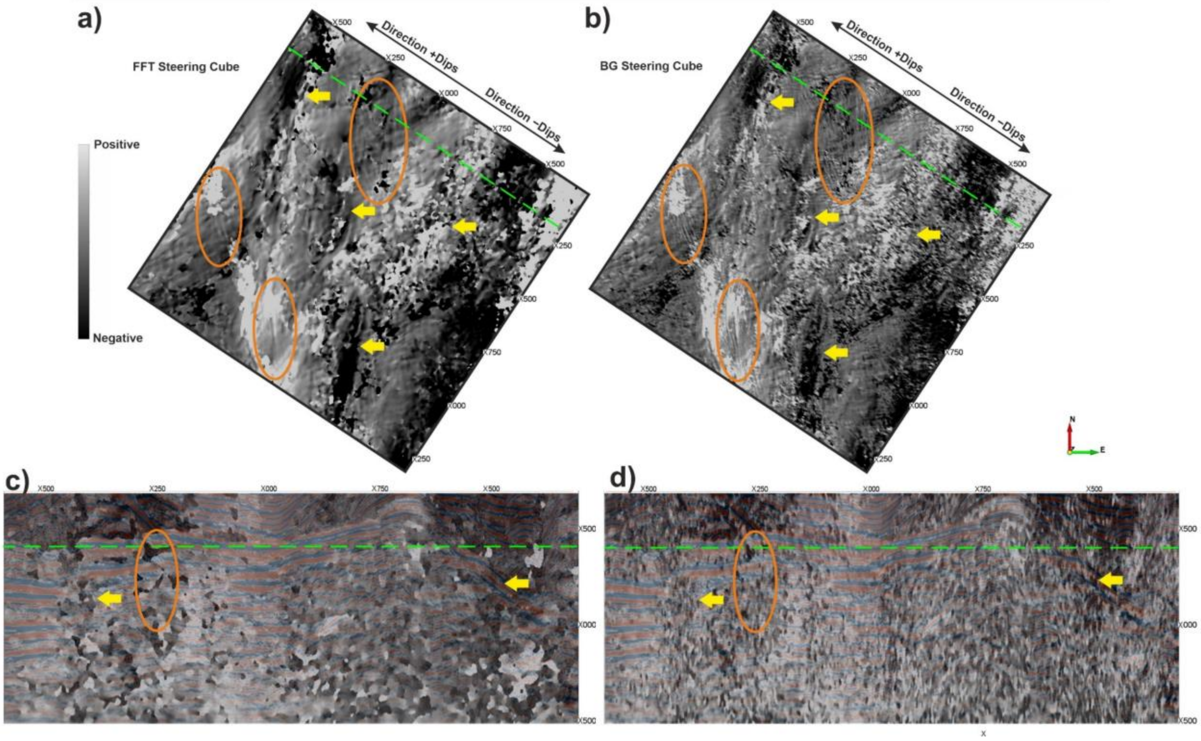


**Figure 7.** Time slice at Barra Velha Formation sampled through a) FFT steering cube and b) BG steering cube. Comparison of noise impacts on the calculation of dip values at the crossline through c) FFT steering cube and d) BG steering cube. The yellow arrows show zones with extreme negative dip values in a predominantly NE-SW direction and orange ovals indicate the locations of dip information associated with noise.

The structural-oriented filter, DSMF, significantly reduced the random noise and increased the continuity of the seismic reflectors. This filter produced a noticeable background and highlighted amplitudes on the seismic image compared to the original input (Figure 8a-b). The residual signal visually revealed the most undesired high-dip noise artifacts associated with the overlying evaporitic unit (Figure 8c). Even though the DSMF is well-known edge preservation, Jaglan et al. (2015) stated that fault zones are preserved larger than the DSFM size. Thus, fault zones with horizontal lengths smaller than around 75m were smoothed from the dataset and some seismic signal losses might be involved, even with the significant attenuated noise. On the other hand, comparing the amplitude spectra from Destriping Filtered and DSMF, we found a significant reduction of the high-frequency amplitudes, particularly between 20Hz and 60Hz, where the noise had been previously characterized (Figure 8a-b).

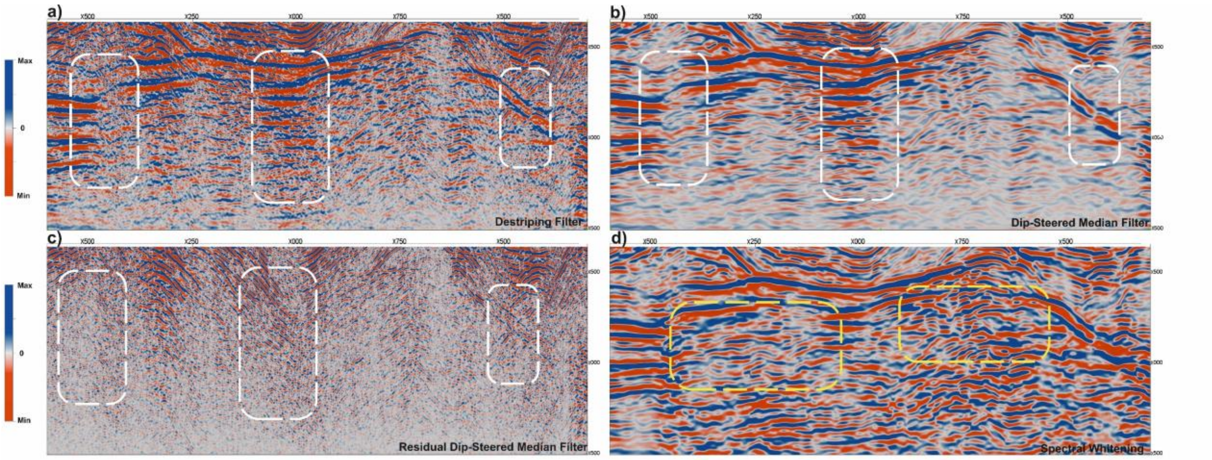


**Figure 8.** Crossline is shown after applying a) Destriping Filter, b) Dip-Steered Median filter results, and c) residual noise from Dip-Steered Median Filter. White boxes indicate the location where noise overlapped the seismic reflectors before data conditioning. d) yellow boxes show the Spectral Whitening effect in zones where the energy from the reflectors was increased.

On the other hand, the spectral enhancement by SW improved the visualization of reflectors, balancing the energy of seismic image and flattening frequencies close to the dominant frequency between 20Hz and 30Hz (Figure 9). In most cases, the spectral enhancement produces a broader frequency bandwidth enhancing the subtle geological characteristics. However, according to Chopra (2011), the high-frequency noise usually increases applying the SW. We found that by increasing frequencies greater than 30Hz, the seismic data might generate uncertainty due to the low seismic data quality, obscuring the seismic image or causing false geological trends. In addition, a narrow and high energy amplitude spectrum was more reliable to distinguish general geological trends (Figure 9d).

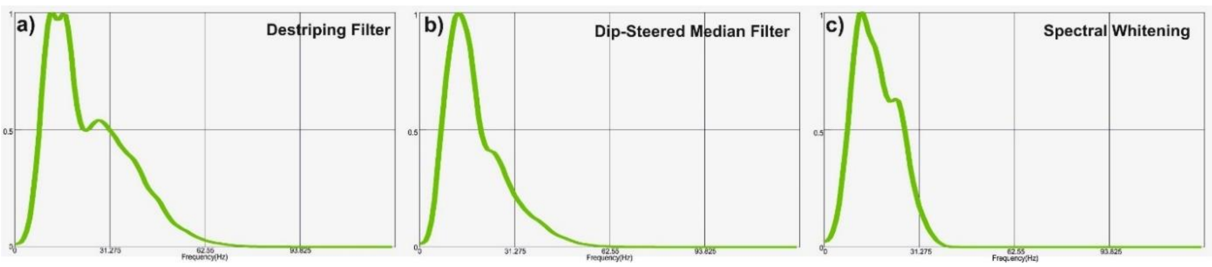


**Figure 9.** Comparison amplitude spectra from crossline X180 between a) Destriping Filter, b) Dip-Steered Median Filter, and c) Spectral Whitening.

The second-generation Steering Cube was computed as an optimized approach that decreased noise levels on dip-azimuth volume, taking advantage of the DSFM (Figure 10). Contrasting the first- Steering Cube and the second-generation Steering Cube, the sharp and sudden disturbances of dip values were associated with the noise on the Steering Cube before the filtering process (Figure 10b). According to Brouwer and Huck (2011), the Steering Cube might be optimized, focusing on removing this local dips to favor larger dips since local values calculated near faults may create artifacts and obscure the fault traces. Thus, the second-generation Steering Cube showed more visible and continuous distribution of dip values, revealing well-defined trends of contrasting dips in the NW-SE direction (Figure 10a). This simple approach was essential to improve the fault-enhancement filters and the seismic attribute extraction from the dataset.

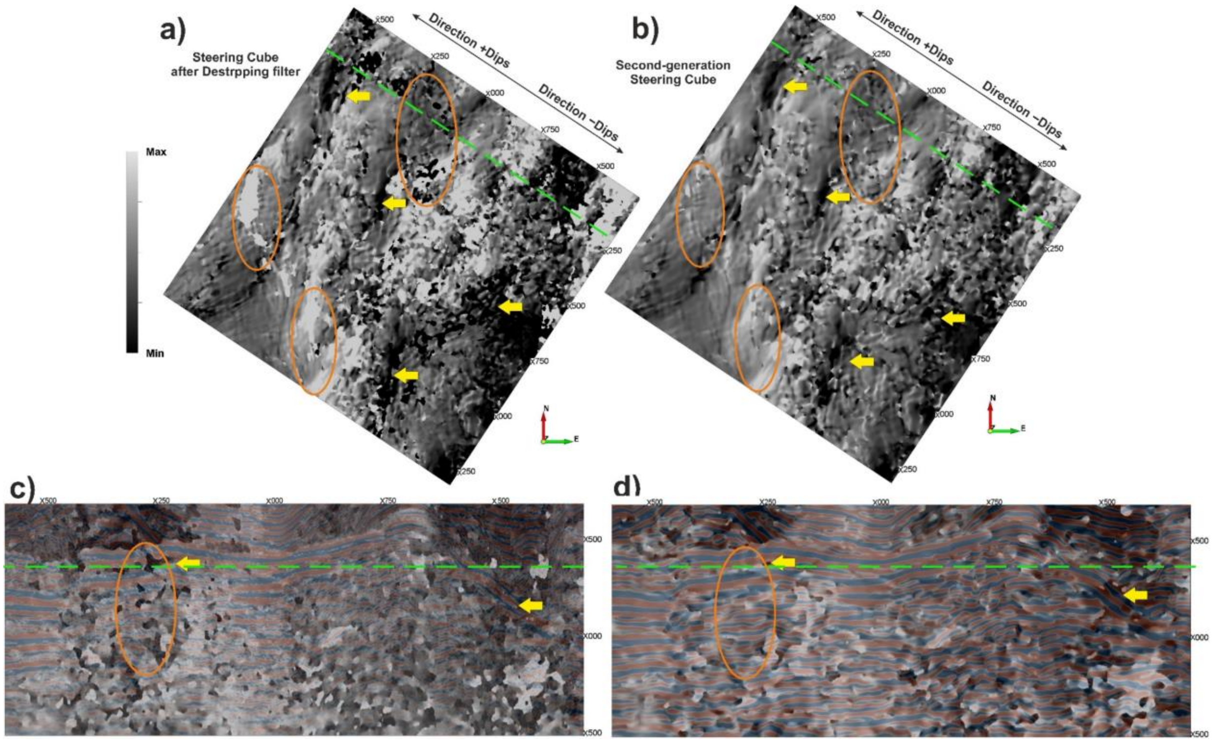


**Figure 10.** Time slices at Barra Velha Formation sampled through a) Steering Cube and b) second-generation Steering Cube, and Crossline through c) Steering Cube and d) second-generation Steering Cube. Yellow arrows indicate zones with extreme negative dip values in a predominantly NE-SW orientation. Orange ovals show the locations of contrasting dip values associated with noise. The second-generation steering cube generated more continuous dip and azimuth volume.

In addition to the visual assessment of the reflector continuity, the impact of the data conditioning on the seismic data was further investigated using a before-and-after comparison of seismic and synthetic data during the well-to-seismic tie shown in Figure 11. The original seismic data had a correlation coefficient of 75% from Barra Velha to Camboriu formation on the Well A. On the other hand, the correlation coefficient indicated a match of 77% for the conditioned seismic data, even over a much narrow frequency range. Moreover, the waveform of the conditioned seismic data evidenced a reduction on subtle seismic features and smoother peaks and troughs than the original one because of the less high-frequency range.

Despite the high correlation coefficient between seismic and well, three key aspects about the uncertainty in the process were contemplated. First, the uncertainty produced by the restricted continuity of the well logs focuses only on the pre-salt interval that might generate a probable overestimating correlation coefficient. Second, the uncertainty is related to the noise produced by the salt layer. This aspect might be considered during the filtering process; however, the filters are far from perfect in removing noise; thus, the noise may continue in subsequent stages after the data conditioning. Finally, the uncertainty from the interval of the wavelet extraction may impact the reflectivity log and provide ambiguous synthetic traces. We used these insights to evaluate the response from the seismic-well tying of the heterogeneous reservoirs of the pre-salt, when the lateral continuity has high variations, for instance, for the Itapema Formation from wells A to D.

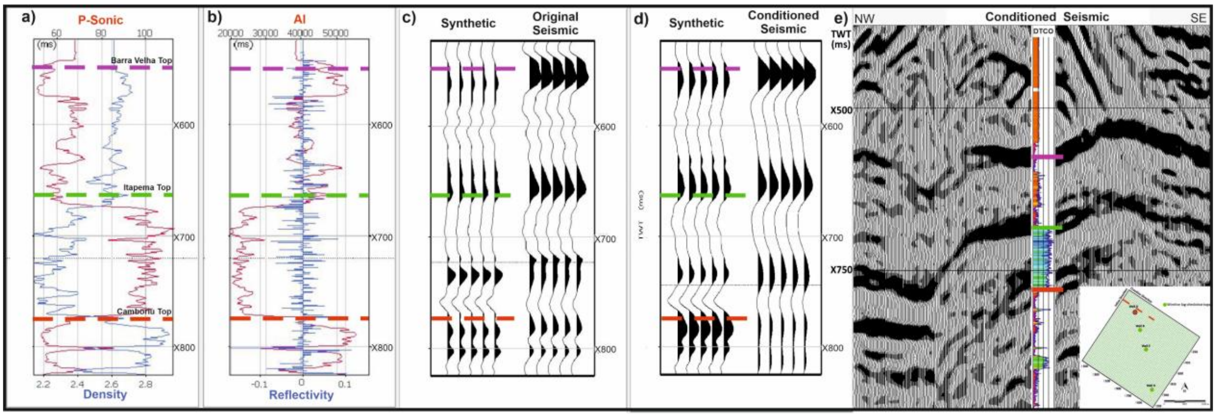


**Figure 11.** Seismic-Well tie for well A. a) Sonic and Density logs used to calculate b) Acoustic Impedance (AI) and Reflectivity logs. c) Original and d) conditioned seismic data are compared with the synthetic seismic traces produced by convolution between reflectivity log and extracted wavelet from the original seismic data. d) Well A tying the reflectors of filtered seismic data. Formations tops for Barra Velha, Itapema, and Camboriu Formations are represented by pink, green and red color, respectively.

The correlation coefficient between the conditioned seismic data and the wells B, C, and D remained at the same level along the study area regarding well A (Appendix 1A). The interfaces of contrasting acoustic impedance for Barra Velha and Itapema Formations were more reliable at wells A, B, and C than wells E and F. For well D, only the reflector of the Barra Velha formation was correlated due to the absence of the well marker for Itapema Formation. The interface of the Camboriu Formation was ambiguous due to the energy loss, even with the most remarkable continuity achieved by the conditioned seismic data.

Once the seismic events were released from noise, the DSDF and EPS increased the detailed structural interpretation based on the edge-enhancing. Since the seismic data presented a reduced definition of structural elements, firstly, the DSDF promoted the breaking effect on the termination of the reflectors (Figure 12a). Then, the EPS emphasized the sharpness on the edges (Figure 12b). Both played an essential role in finding zones with high discontinuity distribution. The discontinuities became more explicit and continuous than in previous stages, where they were undetectable.

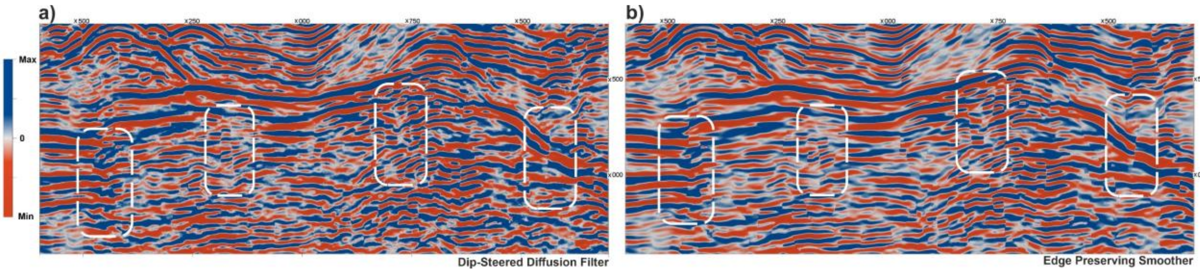


**Figure 12.** Crossline displaying (a) Dip-Steered Diffusion Filter and (b) Edge Preserving Smoother filter. White boxes indicate zones where discontinuities were enhanced.

## Impact on seismic attributes

The Dip-Steered Similarity and Curvature attributes were used to compare original seismic data and conditioned seismic data supporting the detection of offsets on seismic reflectors (Figure 13). On the original data, the attributes emphasized the periodic noise showing the footprint artifacts, which obscured the interpretability of the seismic data and showed inadequate definition and high distortion of seismic features. The substantial contamination of the acquisition footprint was highlighted by ellipses on the time slice (Figure 13a).

Once the Destriping Filter and the DSMF were applied, the Dip-steered Similarity discretized in more homogeneous zones with high and low similarity. It illustrated more continuous features associated with discontinuities; the arrows pointed to linear black shades in Figure 13b. In addition, the results obtained using fault enhancement methods showed a sharper definition of these possible structural elements (Figure 13c). We also used the crossline direction as a control to assess insights obtained from the seismic attributes, as shown in Figure 13d-e. In the vertical direction, the Dip-steered Similarity detected various discontinuous segments of structural elements, which assisted us in getting insights into the limits of the spatial distribution of the discontinuities. Two structural zones were exposed; the eastern zone was dominated by intense faulting, and the western zone where the reflectors were more continuous with low discontinuities (Figure 13e). The improvement of the conditioned data over conventional seismic data was explicit regarding structural elements illumination.

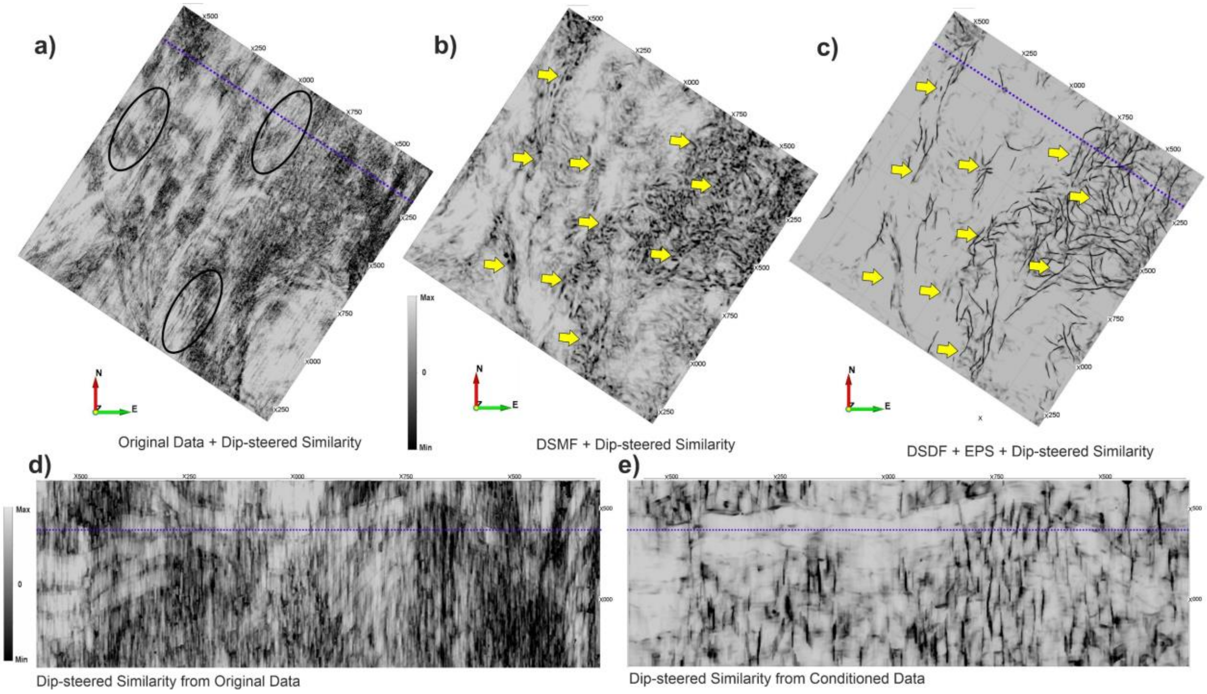


**Figure 13.** Dip-steered Similarity attribute displayed at time slice of Barra Velha Formation utilizing a) raw data, b) dip-steered median filter, and c) edge-enhancing filters. Yellow arrows indicate zones where the discontinuities were highlighted. The Crosslineshows Dip-steered Similarity d) before and e) after data conditioned. Conditioned data shows the direct relationship of discontinuities enhanced by the Similarity attribute. Blue dashed line indicates the respective position regarding crossline and time slice.

Additionally, maps at the top of the Barra Velha formation displayed the most negative and positive curvature values in red and blue. The Curvature attributes showed the impact of footprint artifacts regarding the Steering Cube; this noise distorted the shape of seismic reflectors (Figure 14a-b). After data conditioning, the curvature values showed better distribution and continuity, highlighting seismic elements on the top of the Barra Velha Formation. These features might be related to folding structures and discontinuities with a NE-SW trend **(**Figure 14c-d). The high intensity of seismic elements illuminated by the more positive curvature produced low interpretability of geological features compared to the most negative curvature, which showed trends with more definition associated with the extensive structures in the evolution of the Santos Basin. (Figure 14)**.**

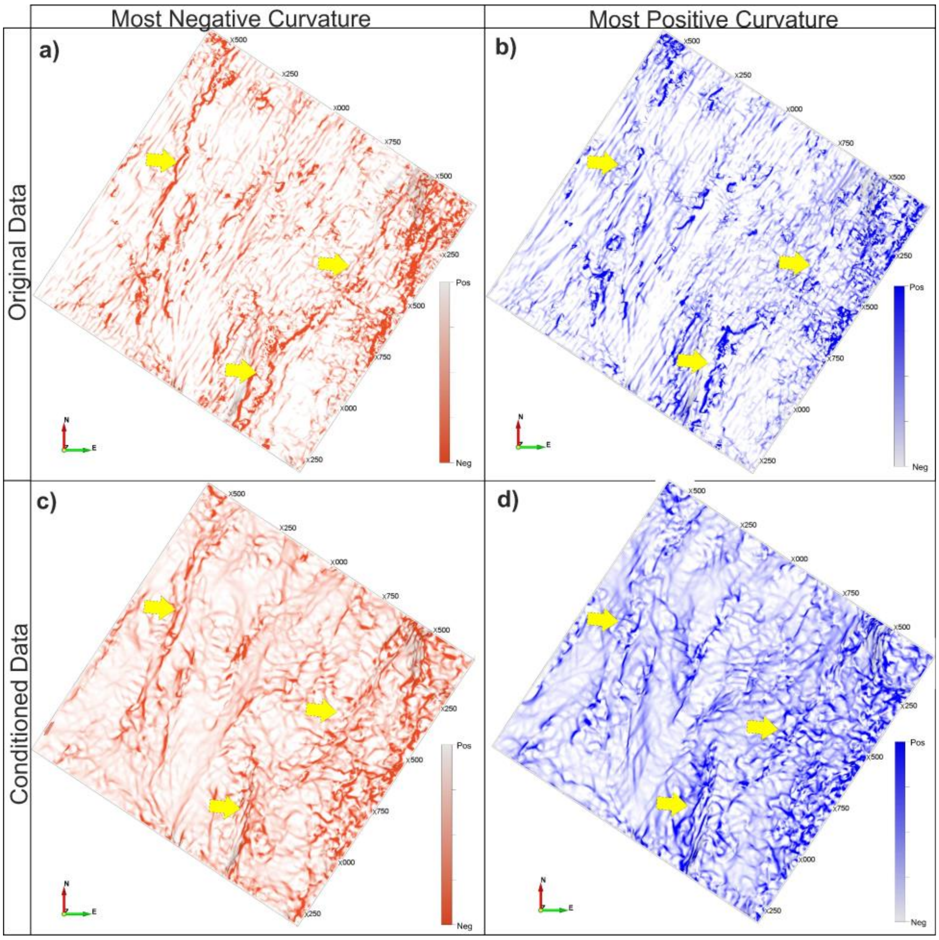


**Figure 14.** Curvature attributes were displayed at the top of the Barra Velha formation. The most negative curvature (a, c) and the most-positive curvature (b, d) indicate the flexural characteristics of the seismic reflectors. Curvature attributes calculated from the raw data (a, b) showed distorted lineaments (yellow arrows) and accentuated acquisition footprint artifacts in the inline direction. Curvature attributes computed from second-generation Steering Cube (c, d) displayed continuous structures without the influence of the acquisition footprint (yellow arrows).

The improved Dip-steered Similarity and Curvature attributes were compared to analyze a co-rendering perception at the top of the Barra Velha Formation. We identified structural elements concentrated primarily in the eastern and central zones of the study area. The highlighted major and minor lineaments from the conditioned data might give insights into associated faults zones and adjacent fracture systems. These lineaments are related to a deformation system with a predominant trend in the NE-SW direction, which is consistent with the regional evolution trend of Santos Basin (Figure 15) (Gomes et al., 2008). In some cases, the attributes showed a precise relationship with the fault geometry, as shown by the interpretation of faults (Figure 16). The normal faults were represented by negative curvature in the footwall and positive curvature in the hanging wall. The positive and negative curvatures allowed us to infer the relation between the throw and the direction of the fault dip.

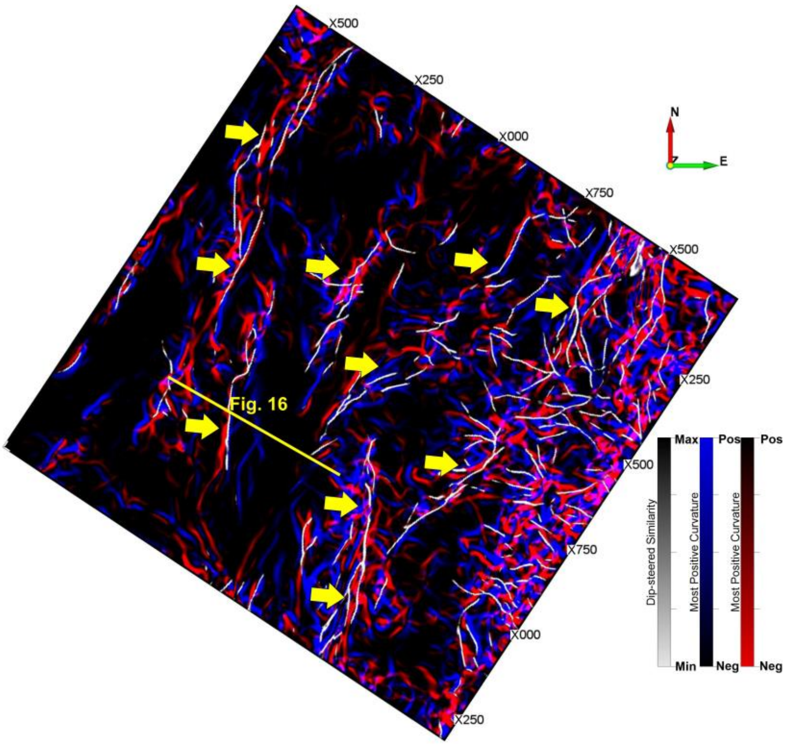


**Figure 15.** The most positive curvature (blue color) and the most negative curvature (red color) from the second-generation Steering Cube show the relationship between the curvatures and the main discontinuities detected (yellow arrows). The Dip-steered Similarity attribute (white color) from the conditioned seismic data highlights the principal structural elements at the top of the Barra Velha formation.

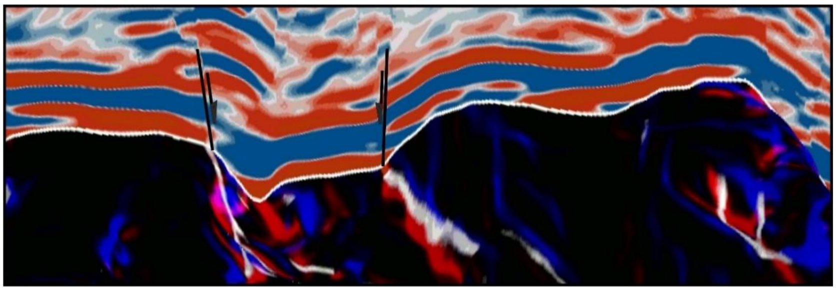

**Figure 16.** The horizon at the top of the Barra Velha Formation shows the most negative curvature (blue colors), most-positive curvature (red colors), and dip-steered similarity (white color), highlighting the flexures characteristics caused by faulting (black arrows).

## CONCLUSIONS

The optimization of the seismic data conditioning process was a valuable tool for denoising and enhancing conventional seismic data, directly impacting the detection of discontinuities through geometric seismic attributes for the studied area. The initial analysis stage was necessary to manage the filtering process, attenuating the coherent and random noise produced by the salt layer that directly impacts the enhancement and the subsequent identification of discontinuities. The edge-enhancing filters proved to be an effective option for highlighting discontinuities after a complete denoising process. In addition, the step-by-step assessment during filtering generates more confidence about seismic elements highlighted by seismic attributes. However, applying these filters must be extremely careful since the over-optimized parameters might generate misleading structures, distorting the results. The Dip-Steered Similarity and Curvature attributes validated the effects of the seismic data conditioning process and helped to detect the presence, concentration, and trends of discontinuities on the seismic reflectors. It also provided us insights into potential fractured areas on the pre-salt reflectors. Systematic seismic data conditioning improves the seismic image and subsequent attribute analysis.

**Acknowledgments**

The authors would like to thank Fundação de Amparo à Pesquisa do Estado de São Paulo (FAPESP) and Equinor for the financial assistance, and Agência Nacional do Petróleo, Gás Natural e Biocombustíveis (ANP) for providing the seismic data in this research. We are also grateful to Opendtect (dGB) and Kingdom (IHS Markit) for donating the academic seismic processing packages.

**REFERENCES**


Al-Dossary, S., Marfurt, K.J., 2006. 3D volumetric multispectral estimates of reflector curvature and rotation. Geophysics 71. https://doi.org/10.1190/1.2242449

Alves, T.M., Fetter, M., Lima, C., Cartwright, J.A., Cosgrove, J., Gangá, A., Queiroz, C.L., Strugale, M., 2017. An incomplete correlation between pre-salt topography, top reservoir erosion, and salt deformation in deep-water Santos Basin (SE Brazil). Marine and Petroleum Geology 79, 300–320. https://doi.org/10.1016/j.marpetgeo.2016.10.015

Brouwer, F., Huck, A., 2011. An Integrated Workflow to Optimize Discontinuity Attributes for the Imaging of Faults, Attributes: New Views on Seismic Imaging–Their Use in Exploration and Production.

Cainelli, C., Mohriak, W.U., 1999. General evolution of the eastern Brazilian continental margin. The Leading Edge 18, 1–5. https://doi.org/10.1190/1.1438387

Chopra, S., 2011. Extracting meaningful information. CSEG Recorder 9–12.

Chopra, S., Marfurt, K., 2008. Gleaning meaningful information from seismic attributes. First Break 26, 43–53. https://doi.org/10.3997/1365-2397.2008012

Chopra, S., Marfurt, K., 2007. Curvature attribute applications to 3D surface seismic data. The Leading Edge 26, 404–414. https://doi.org/10.1190/1.2723201

de Rooij, M., Tingdahl, K., 2002. Meta-attributes-the key to multivolume, multiattribute interpretation. Leading Edge (Tulsa, OK) 21, 1050–1053. https://doi.org/10.1190/1.1518445

dGB-Beheer, B.V., 2021. OpendTect User Documentation - 6.6 [WWW Document]. URL https://doc.opendtect.org/6.6.0/doc/od_userdoc/Default.htm (accessed 6.15.21).

Farias, F., Szatmari, P., Bahniuk, A., França, A.B., 2019. Evaporitic carbonates in the pre-salt of Santos Basin – Genesis and tectonic implications. Marine and Petroleum Geology 105, 251–272. https://doi.org/10.1016/j.marpetgeo.2019.04.020

Fehmers, G.C., Höcker, C.F.W., 2003. Fast structural interpretation with structure-oriented filtering. Geophysics 68, 1286–1293. https://doi.org/10.1190/1.1598121

Gomes, P.O., Kilsdonk, B., Minken, J., Grow, T., Barragan, R., 2008. The outer high of the Santos Basin, Southern São Paulo Plateau, Brazil: pre-salt exploration outbreak, paleogeographic setting, and evolution of the syn-rift structures. AAPG International Conference and Exhibition, Cape Town, South Africa 10193, 26–29.

Huck, A., 2007. Steering Benchmark tests. [WWW Document]. URL https://doc.opendtect.org/5.0.0/doc/dgb_userdoc/content/ds/bnchmk_sc_create/bnchmk_sc_create.htm (accessed 6.15.21).

Jaglan, H., Qayyum, F., Huck, H., 2015. Unconventional seismic attributes for fracture characterization. First Break 33, 101–109.

Krueger, J., Donno, D., Pereira, R., Mondini, D., Souza, A., Espinoza, J., Khalil, A., 2019. Internal multiple attenuation for four pre-salt fields in the Santos Basin, Brazil. 2018 SEG International Exposition and Annual Meeting, SEG 2018 4523–4527. https://doi.org/10.1190/segam2018-2990024.1

Luo, Y., Marhoon, M., Al Dossary, S., Al-Faraj, M.N., 2002. 3D edge-preserving smoothing and applications. THE LEADING EDGE 71. https://doi.org/10.1190/1.2213050

Magneron, C., Bourges, M., Jeannee, N., 2009. M-Factorial Kriging For Seismic Data Noise Attenuation 1651–1654. https://doi.org/10.3997/2214-4609-pdb.195.1904_evt_6year_2009

Marfurt, K.J., Alves, T.M., 2015. Pitfalls and limitations in seismic attribute interpretation of tectonic features. Interpretation 3, SB5–SB15. https://doi.org/10.1190/INT-2014-0122.1

Meneguim, T.B.M.T.B., Proença, T.P.T., Pereira, C.E.L.P.C.E.L., De Almeida Junior, M.P.A.M.P., Da Silva, E.B.S.E.B., 2016. Effects of post stack Seismic data conditioning on impedance inversion for reservoir, Brazilian pre-salt, Santos Basin. 78th EAGE Conference and Exhibition 2016: Efficient Use of Technology - Unlocking Potential. https://doi.org/10.3997/2214-4609.201601340

Moreira, J.L.P., Madeira, C.V., Gil, J.A., 2007. Bacia de Santos. Boletim de Geociencias da Petrobras, , Rio de Janeiro, v. 15, n. 2, p. 531-549, maio/nov. 2007 531–549.

Rijks, E.J.H., Jauffred, J.C.E.M., 1991. Attribute extraction: An important application in any detailed 3-D interpretation study. GEOPHYSICS: THE LEADING EDGE OF EXPLORATION 774. https://doi.org/10.1190/1.1890330

Tingdahl, K.M., 2001. Improving seismic chimney detection using directional attributes. Developments in Petroleum Science 51, 157–173. https://doi.org/10.1016/S0376-7361(03)80013-4

Tingdahl, K.M., 1999. Improving seismic detectability using intrinsic directionality. Masters Thesis 41.

Tingdahl, K.M., de Groot, P.F.M., 2003. Post-stack-dip- and azimuth processing. Journal of Seismic Exploration 12, 113–126.

Tingdahl, K.M., de Rooij, M., 2005. Semi-automatic detection of faults in 3-D seismic data. Geophysical Prospecting, 533–542.

Wright, V.P., Barnett, A.J., 2015. An abiotic model for the development of textures in some South Atlantic early Cretaceous lacustrine carbonates. Geological Society Special Publication 418, 209–219. https://doi.org/10.1144/SP418.3

Yilmaz, Ö., 2001. SEISMIC DATA ANALYSIS Processing, Inversion, and Interpretation of Seismic Data. Society of Exploration Geophysicists.

**ARTICLE 2: Seismic attributes and unsupervised artificial neural network for fault and fracture interpretation: an example from Brazilian pre-salt reservoir, Santos Basin.**

**ABSTRACT**

The characterization of faults and fracture systems in the Brazilian pre-salt rocks is challenging and time-consuming because of the inherent heterogeneities produced by the tectonic activity during the rifting evolution. The interpretation of these structural elements usually is based on 3D seismic data, which provides valuable insights into the geological deformation and fluid flow inside reservoirs. In this work, we present an integrated approach through multi-attribute analysis and artificial neural networks to identify the spatial distribution and orientation of these geological structures. The workflow brought out the details of subsurface geologic structures and regions of maximum probability of fault. All seismic attributes suggested a predominant NE-SW trend developed in an oblique extension regimen dominated by basement blocks. Such a tectonic arrangement may affect the distribution of discontinuities, geometry, and orientation in the Barra Velha Formation, giving rise to five different clusters of faults, as shown by the Dip, Similarity, Ridge Enahancemnt Filter, Curvature, and Tinned Fault Likelihood attributes. The complex distributions of these structural elements were analyzed by two scenarios using the unsupervised artificial neural networks (ANN), enabling the identification of probable faulting areas close to the basement highs. The structural trends were validated by the borehole image data comparing the strike direction. This detailed structural understanding may support the field development of pre-salt reservoirs, providing significant insights into faults and fracture distribution.

**Keywords:** Seismic Attributes, Data Conditioning, Pre-salt, Discontinuity, Faults, and Fractures.

## INTRODUCTION

In the last decade, Santos Basin has become one of the most prospective oil exploration and production areas globally due to its prolific carbonate reservoirs (Correa et al., 2019). The potential volume of reserves, the considerable accumulation of high-quality oil, and high well-productivity have strategically established the pre-salt oil fields on the global energy demand (Abelha and Petersohn, 2018). The evolution of the Santos Basin was marked by tectonic and thermal subsidence during the Gondwana break-up (Moreira et al., 2007). The basement structures generated during the rifting process formed high regions, which influenced the depositional environments, facies distribution, and reservoir quality of the pre-salt rocks (Fetter et al., 2018). Naturally, structural elements, such as faults and fractures, may impact the reservoir petrophysical properties creating zones that increase the oil productivity or cause unpredictable behavior in the injected fluids, which is essential for development plans of the pre-salt fields (Boyd et al., 2015).

Defining the structural framework with a detailed identification of the geometry and location of the discontinuities may be fundamental to the pre-salt reservoir characterization. The detection of these subsurface features usually considers the seismic data as the primary approach. In this case, the seismic attributes allow the prediction of the geometry and distribution patterns, particularly for the subtle discontinuities that might be missed using conventional interpretation methods. Geometric attributes such as curvature, coherency, dip, and similarity assist the detection of discontinuities due to high sensitivity to changes in the characteristics of the seismic reflectors, such as shape, edges, angle, and continuity (Roberts, 2001; Tingdahl and de Groot, 2003; Chopra and Marfurt, 2007a). Another attribute set, such as ridge-enhancement filter (REF), fracture proximity, fracture density, and thinned fault likelihood (TFL), adopt unconventional characterization that might describe the fault distribution and probability, fracture density or the connectivity, emphasizing insights of faults zones, and fracture networks (e.g., Jaglan et al., 2015). In addition, applying edge-enhancement filters before the seismic attributes computation allows the automatic detection and extraction of predominant fault networks (Luo et al., 2002).

Several authors have successfully implemented different techniques and seismic attributes to identify and classify the seismic pattern of the Brazilian pre-salt rocks

(Ribeiro da Silva and Pereira, 2017; Jesus et al., 2019; Ysaccis et al., 2019). Considering these previous studies, the uncertainty associated with identifying subsurface features may decrease by controlling seismic attribute parameters, mainly in areas where seismic noise affects seismic data (Meneguim et al., 2016; Oliveira et al., 2019).

In order to identify the occurrence probability of structural elements, de Groot et al. (2001) and Meldahl et al. (2001) applied the seismic-object detection method based on multiple attributes using a supervised and an unsupervised artificial neural network (ANN) to produce probability classes, which transformed the input data into a new cube where faults and gas chimneys were highlighted. Other approaches have included directional attributes (Tingdahl, 2001) and meta-attributes (Aminzadeh and de Groot, 2005) to improve the seismic classification and create outputs with desired geologic features such as salt diapirs, gas chimney, fault, fracture, or sand thickness. Tingdahl and de Rooij (2005) presented a semiautomatic fault detection with the seismic-object classification method, where the fault probability cube obtained better results regarding fault contrast and continuity than the single attributes. Recently, multi-attribute analyses through ANN have gained even more acceptance due to the efficient recognition of geological discontinuities. The ANN might provide fault probability maps in which the probable locations of discontinuities are defined from the seismic data and estimations of connectivity of the fracture networks (e.g., Ashraf et al., 2020; Kumar and Sain, 2020).

Generally, the seismic data resolution reaches out to detect structures from tens to hundreds of meters. On the other hand, borehole images can describe the high resolution of dip and azimuth of discontinuities, ranging from a few centimeters to several meters and being laterally limited and sparsed. Therefore, combining multiple scales might reduce the uncertainty in mapping and identifying the discontinuities. For example, the azimuth of discontinuity attributes might be extracted at each well location and compared with the azimuth of interpreted fractures to find a structural correlation. Then, the results obtained from the seismic data might be validated by the borehole image data.

Therefore, this study aims to identify the most probable faults and fractures areas through multi-attribute analysis in a 3D seismic survey in the pre-salt reservoir from Santos Basin, Brazil. Different seismic attributes were used to guide the detection of the main structures of the pre-salt reservoir and understand their relationship with the deformation events in the basin.

Unsupervised ANN was utilized to capture the main subsurface features and discriminate areas with a high and low fault occurrence probability. Finally, we compared the seismic orientation of discontinuities regarding the borehole image log to validate the extraction of seismic fracture families and the major structural trends.

## GEOLOGICAL SETTING

The continental breakup of Gondwana, dating from the Latest Jurassic to Early Cretaceous, resulted in a diachronous rifting along the Brazilian margin. The Santos Basin is described by faulted and rotated blocks with NE-trending, subparallel to the coastline, and locally segmented by transfer zones (Gomes et al., 2008). From the Hauterivian to the beginning of the Aptian, the extrusion of basaltic lavas covered the semi-graben structures of the igneous-metamorphic basement, constituting the Camboriú Formation. Subsequently, the fluvial and lacustrine sediments of the Itapema formations constituted a thick sedimentary succession in these semi-graben depocenters (Moreira et al., 2007).

A regional unconformity marked the end of the rift phase. The tectonic control progressed to a regional thermal subsidence setting, which created extensive sag-phase lacustrine deposits and, later, a restricted environment with extensive deposition of evaporites (Moreira et al., 2007). From Aptian to Early Albian, this post-rift phase comprises Barra Velha and Ariri Formations. The Barra Velha Formation is the main pre-salt reservoir in the Santos Basin deep-water areas, composed of microbial carbonates, laminites, spherulites, and magnesium-rich claystone (Farias et al., 2019). After the main stage, a thick evaporite layer of the Ariri Formation was precipitated with halite, anhydrite, and other soluble salts, such as carnallite and sylvinite (Moreira et al., 2007). It constitutes the main seal overlying the pre-salt reservoirs. Davison et al. (2012) stated that evaporites in the Santos Basin were deposited very quickly, which played a role in increasing the rate of subsidence and basin relief, even before any overburden sediment was deposited. Alves et al. (2017) confirmed this later stage of pre-salt tectonism, evidenced by significant faults displacement at the base salt.

From the Albian to the present, the Drift sequence was established by marine conditions and thermal subsidence. First, the South Atlantic opening generated a shallow carbonate platform, which led to the Itanhaem formation. After the Albian, the deep-marine clastic sediments were deposited in response to the progradation and moderate salt movement. The distal turbidites, submarine fans, and mass-transport deposit sequence are related to the Itajai-Acu to Marambaia Formation (Moreira et al., 2007).

## DATA AND METHOD

The input data for this study include a 3D post-stack time migrated seismic with 1300 inlines/1300 crosslines and a bin spacing of 12.5 m/12.5 m, covering an area of approximately 260 km2 in the deep waters of the Santos Basin, Brazil (Figure 1a). A cropped seismic volume is used, which extends from 4.1 s to 5.5 s with a sampling interval of 4 ms. The seismic was previously conditioned following a systematic workflow that includes data analysis, coherent and random noises removal, and generation of edge-enhanced seismic volume in our previous research (See Article 1). In addition, the seismic data was characterized according to the Society of Exploration Geophysicists' (SEG) American polarity, in which increases in acoustic impedance are shown in blue and related to positive amplitude. In contrast, decreases in acoustic impedance boundary are shown as red reflections and correlated with negative amplitudes.

Four wells with the time-depth model and well markers for Barra Velha, Itapema, and Camboriu Formation are shown in Figure 1b (Well A, B, C, and D). Borehole images from four wells (Well A, C, E, and F) with investigation depths between 300 m and 350 m were used. These borehole images were acquired by acoustic imaging tools (CAST and UBI) and micro-resistive tools (OMRI and OBMI). The time-depth model is employed to evaluate the interpretation of the borehole images regarding the seismic data. The dataset was provided by ANP (Agência Nacional do Petróleo) and analyzed in Opendtect software (dGB Earth Science) and Interactive Petrophysics software (IP).

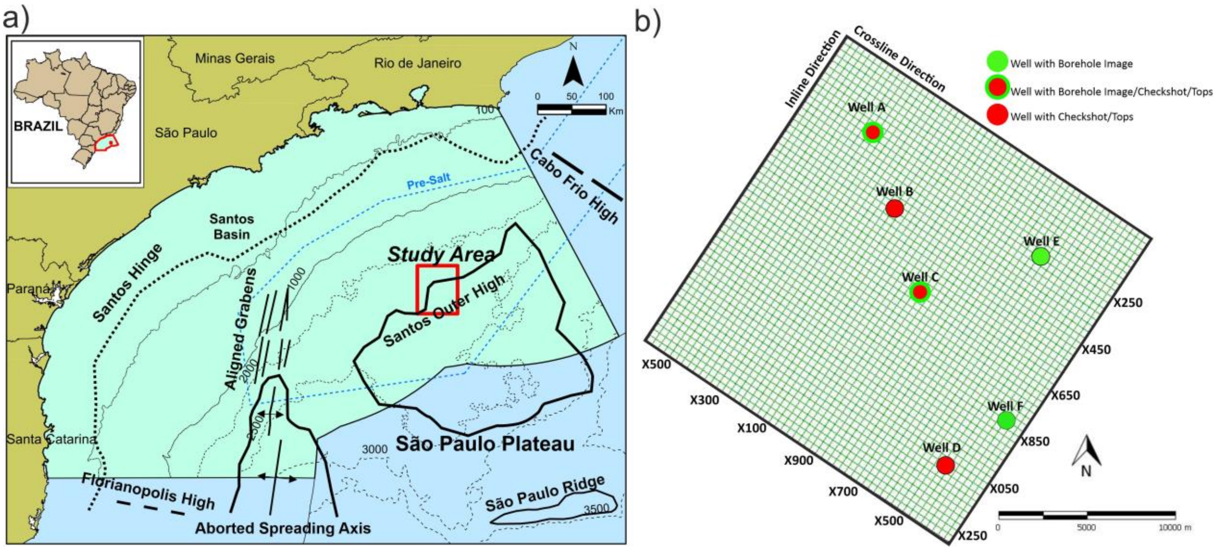


**Figure 1.** (a) Location map of the study area in the Santos basin, Brazil (modified from Gamboa et al., 2019). (b) Base map of the survey indicating the area covered by 3D seismic lines and drilled wells.

The research workflow was divided into two main sections. The first section dealt with the computation and optimization of seismic attributes to generate the most agreement framework for the fault and fracture characterization. The second section determined fault and fractures probability zones using unsupervised ANN and validated the scenarios by comparing the borehole image data. The methodology of this study is summarized in Figure 2.

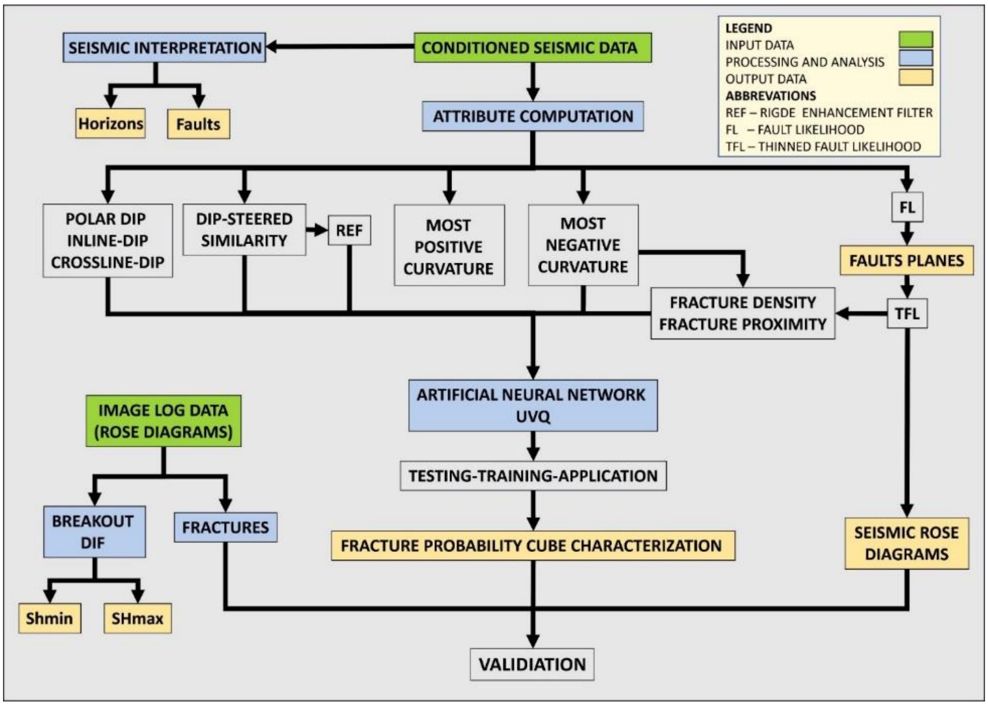


**Figure 2.** Workflow adopted. It consists of seismic interpretation, attribute computation, artificial neural network, and validation.

### Interpretation of seismic fault framework

The preliminary seismic interpretation was performed using the time-deep model and well markers from wells A, B, C, and D. We used crossline and inline sections to interpret the main horizons regarding Barra Velha, Itapema, and Camboriu Formation. In addition, the regional faults were interpreted based on the recognition of reflectors offset, changes in the dip, or contrasting seismic patterns.

### Seismic attributes selection and analysis

The dip steering was extracted from the preconditioned seismic data and used as input in the attribute's computation. Structural features detectable on seismic data were identified using seven edge-sensitive seismic attributes. Dip, Dip-steered Similarity, Curvature, REF, TFL, Fracture density, and Fracture proximity attributes were parameterized so that the detection of structural elements might be discretized by the direction. We mainly used time-window ratios around the dominant period of the seismic signal (48-50 ms) and step outs with increments of perpendicular trace pairs. The attributes were applied to the whole seismic cube to identify in time slice view the delineation of discontinuities.

### Dip Attributes

The dip attributes represent various dip components extracted from the seismic data (Chopra and Marfurt, 2007b) (Figure 3). The inline-dip and crossline-dip provide local dips in inline and crossline directions, respectively. Likewise, the polar dip describes the square root of the sum of the squares of inline-dip and crossline-dip. It measures the true dip from the horizontal plane in the positive ranges (Jaglan et al., 2015) (Figure 3). In our case, we calculated the polar dip and separated the inline and crossline components, comparing the results at time slices.

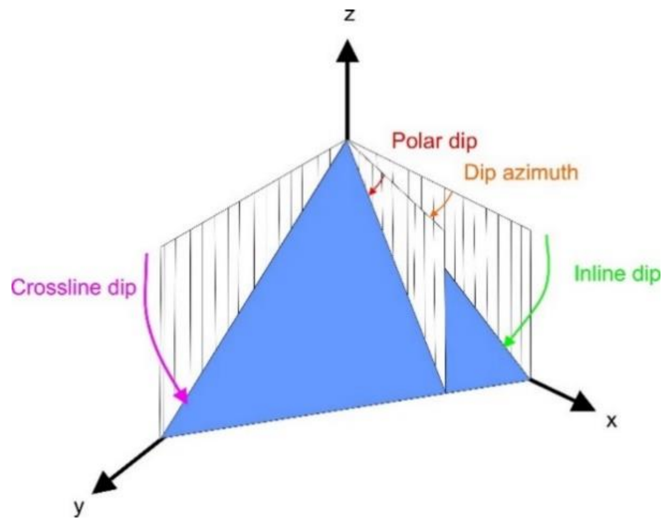


**Figure 3.** Diagram showing the dip components on a reflector. Pink and green arrows are dips along the inline and crossline direction, respectively. The red arrow is the polar dip, and the orange arrow is the dip azimuth (Modified from Chopra and Marfurt, 2007b).

### Dip-steered Similarity and Ridge-enhancement Filter

The dip-steered similarity estimates how similar are two segments of seismic traces using dip-steering as input. It is calculated along with a reflector by the Euclidean distance between the amplitude vectors of the traces $u(x, y, t)$. Considering two trace segments $(x_A, y_A)$ and $(x_B, y_B)$, centered at a time $t$, the similarity $(S)$ between these two trace segments can be expressed as (Tingdahl and de Groot, 2003; Tingdahl and de Rooij, 2005):

$$S = 1 - \frac{|a-b|}{|a| + |b|} \tag{1}$$

Where,

$$a = \begin{bmatrix} u(x_A, y_A, t_A + t_1) \\ u(x_A, y_A, t_A + t_1 + dt) \\ \dots \\ u(x_A, y_A, t_A + t_2 - dt) \\ u(x_A, y_A, t_A + t_2) \end{bmatrix}, \text{ and } b = \begin{bmatrix} u(x_B, y_B, t_B + t_1) \\ u(x_B, y_B, t_B + t_1 + dt) \\ \dots \\ u(x_B, y_B, t_B + t_2 - dt) \\ u(x_B, y_B, t_B + t_2) \end{bmatrix} \tag{2}$$

In Equation 2, $dt$ is the sampling interval, $t_1$ and $t_2$ are the starting and ending time of the selected time window, respectively; $t_A$ and $t_B$ are the dip-steered times of the trace segments at $(x_A, y_A)$ and $(x_B, y_B)$ respectively, and $u$ is the amplitude value in the seismic cube. Geologically, similar seismic traces indicate a continuous lithology, while phase changes in the seismic trace can indicate faults and fractures in the body of rocks.

On the other hand, the REF attribute sharpens lineaments comparing nine similarity values around a central point of evaluation on the time slice domain of the similarity attribute volume (Brouwer and Huck, 2011; Tingdahl and de Rooij, 2005). The values are extracted in four directions, two diagonal and two perpendiculars (Figure 4); thus, the value in each direction is defined by Equation 3:

$$REF = \frac{\sum values\ on\ either\ side\ of\ the\ central\ value}{2} - central\ value \tag{3}$$

REF attribute provides smaller values for the points with the absence of discontinuities, while large values are obtained at a perpendicular position to the discontinuity direction (Figure 4).

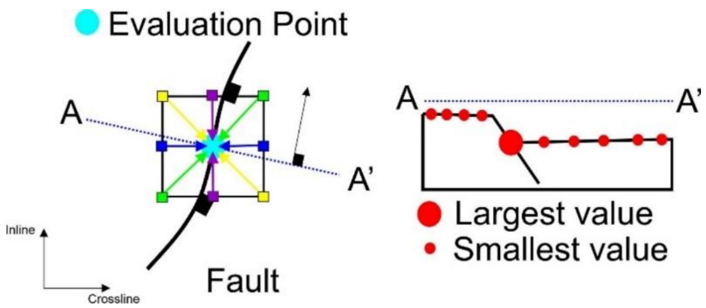


**Figure 4.** Diagram illustrating the REF computation in four directions (inline, crossline, and two diagonals oriented in 45 and 315°). The most significant values are extracted surrounding the evaluation point (Modified from Brouwer and Huck, 2011).

The directional component on these two attributes plays an essential role in separating the discontinuity attribute in different directions representing different fault sets (Brouwer and Huck, 2011). The seismic trace position settings might optimize the identification of discontinuities depending on the direction in which the seismic traces are compared. Four pairs of traces are used simultaneously; however, they can be decomposed in two diagonals and two perpendicular directions regarding the central seismic trace (Figure 5).

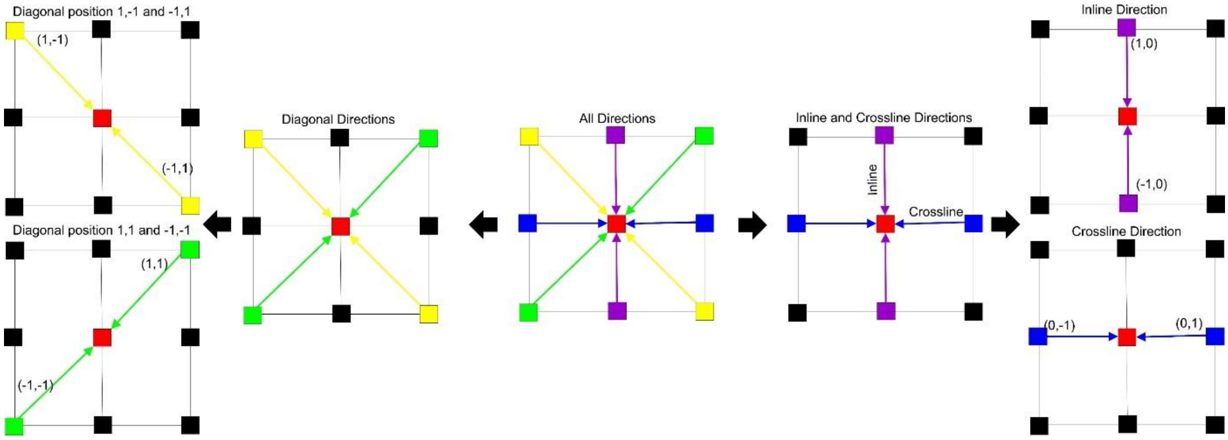


**Figure 5.** Illustration of seismic traces pairs position used as input in the computation of similarity attribute regarding a central seismic trace (red square). Four different directions can be used, two diagonal(yellow and green squares) and two perpendiculars (purple and blue squares)(Modified from Brouwer and Huck, 2011).

In this study, we computed the dip-steered similarity using a scenario with a time window of 48 ms, which describes the dominant period of the seismic data. Later, the REF was estimated using the dip-steered similarity as input. Here, we separated two diagonal trends according to a pair of seismic traces rotated 45 and 315° from the inline direction (Figure 5).

### Curvatures Attributes

The curvature measures the angle of a surface at a particular point. It describes subtle lateral and vertical variations in a dip often dominated by geological structures. Therefore, it is an effective tool to extract geometric features, for example, fault and fracture, derived from deformations of geological planes (Roberts, 2001). The seismic amplitude of the reflectors represents a quadratic surface where the curvature attribute is computed (Al-Dossary and Marfurt, 2006).

A wide variety of curvature attributes have been described by Roberts (2001). This study used the most positive and most negative volumetric curvature for interpreting subsurface structural features. The most positive curvature attribute defines normal vectors that diverge at various points on a surface, which might be associated with convex structures. Otherwise, the most negative curvature attribute returns converging vectors that might reveal depression forms, as presented in Figure 6. These attributes might magnify folds and the upthrown and downthrown parts of the faults.

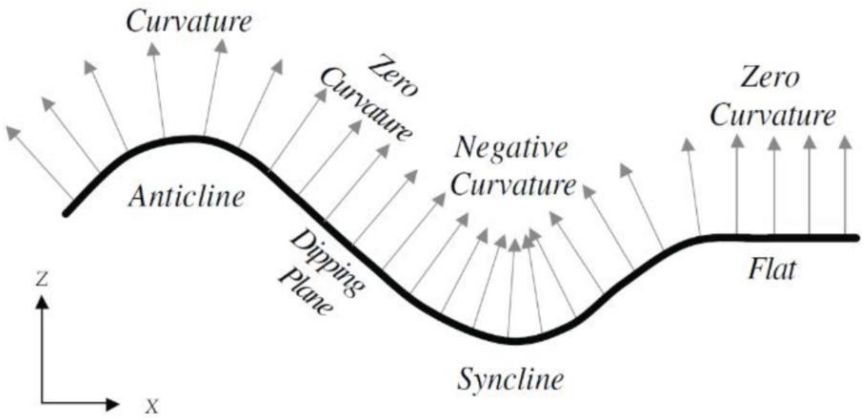


**Figure 6.** Curvature diagram showing the characteristics of the curvature analysis (extracted from Roberts, 2001).

### Thinned Fault likelihood

TFL is an unconventional fault attribute that generates sharp fault images and helps visualize discontinuities. The TFL attribute is a collapsed and thinner version of the fault likelihood (FL) attribute. They range between 0 and 1, where zero refers to the minimum likelihood of faults, and one refers to the maximum likelihood of faults (Jaglan et al., 2015). Hale (2013) developed the FL attribute generating images of fault likelihood related to the strikes and dip measures, allowing the extraction of fault planes through local maxima filtering of fault likelihood and the estimation of fault throw vectors. The FL attribute (f) is considered an amplified variant of the structural-oriented semblance and expressed according to Equation 4.

$$f = 1 - (semblace^{n}) \tag{4}$$

Where:

$$semblance = \frac{\langle\langle image\rangle_s^2\rangle_f}{\langle\langle image^2\rangle_s\rangle_f} \tag{5}$$

Here, $\langle\,.\rangle_s$ performs a structure–oriented averaging operation for the image sample values, which are expressed by the bin length and time samples in the seismic volumes. On the other hand, $\langle\,.\rangle_f$ denotes additional smoothing of the numerator and denominator, enabling the association of small and large semblance values in localized discontinuities and highlighting the reflections with wide offset. The computation of the FL attribute provides more accurate results when previous insights about the fault orientation and locations are parameterized. So that, strikes and dips ranges helps to correct the alignment of structures in their respective orientations, enhancing the imaging of structures in seismic data (Hale, 2013).

Herein, the FL attribute was parametrized employing sample values of four inlines, four crosslines, and one-hundred samples of time, enhancing the connectivity of more significant discontinuities. The strike direction was scanned from 0° to 360° that captures the maximum number of structural discontinuities from the seismic volume. Likewise, the dip angle was defined within a range from 45° to 85°. It was selected based on the stepped fault architecture described in the Outer High structure (Gomes et al., 2008). The smoothing operator for the strike and dip ranges was used on the minimum values, keeping the maximum values of fault likelihood on the discontinuities and reducing the creation of artifacts.

Subsequently, the FL attribute provided insights about the main orientation during the stage of fault plane extraction. They were filtered to remove the isolated features. Predominantly, noisy-small discontinuities were separated from the large-scale features according to the size of the skin (numbers of connected points on a fault plane). The TFL attribute volume is extracted from the images of faults planes and compared at different time slices with the most probable structural elements.

**Fracture Density and Fracture Proximity**

The fracture density attribute highlights the areas of high-density discontinuities through the relation between seismic traces classified as discontinuities and the total seismic traces in a search radius over time slices. Similarly, the fractures proximity attribute characterizes the interaction among discontinuity structures on fractured areas, assuming connectivity between them by the relative lateral distance (Jaglan et al., 2015). Here, the Fracture Density and Fracture proximity attributes provide insights about the areas of fractured rock bodies and possible fracture networks, respectively.

The TFL cube and the most negative curvature were utilized as input. The fracture proximity and density attributes use threshold values and searching radius to classify seismic traces as discontinuity or no-discontinuity. Since the TFL attribute defines a maximum fault likelihood threshold, we compared two cases of different thresholds to examine their impacts on the fracture density and proximity. On the other hand, the most negative curvature values might indicate areas with high potential of fractures associated with downthrown fault block; thus, two searching windows of 125 m and 375 m were assumed according to the bin size, observing their effect in recognition of the discontinuities. We compared and selected the most consistent scenario regarding the interaction among the structures.

**Unsupervised Artificial Neural Network**

The ANNs have been widely used to combine multiple attributes into a new volume and evaluate specific seismic patterns (Aminzadeh and de Groot, 2005). The unsupervised approaches enable the detection of possible structures in the data themselves, extracting the relevant properties or features from the seismic data. In particular, the unsupervised vector quantization (UVQ) algorithm, used in this study, can classify the data into a defined number of groups, similar to the K-means clustering algorithm (de Groot, 1998).

The UVQ takes samples at a random position from the calculated seismic attributes and converts them into vectors. These random vectors are classified according to the cluster center during the training phase. The center of the clusters is found by the ANN calculating the Euclidean distance to the vectors. The training ends when the classification curve reaches a stable average percentage match among the clusters. Then, the input attributes are compared to each cluster center. The UVQ computes the proximity between the input and the center of the winning cluster and assigns it to the closest cluster (Aminzadeh and de Groot, 2005). The outputs of the UQV application comprise the index number of the winning clusters, where the clusters are sorted to be adjacent to each other, and a degree of match (confidence measure between 1 and 0) between the cluster and the input attribute (de Groot, 1998).

Generally, the UVQ is used to classify seismic waveforms according to the data segmentation; however, it can also cluster tridimensional bodies. For that reason, the UVQ algorithm may also be used to restrict the area where the most common structural features occur using, for instance, TFL, fracture density, and fracture proximity attributes. It allows classifying zones with different probabilities of the fault and fractures intensity (Ashraf et al., 2020).

In the present study, we performed a multiattribute analysis using the UVQ algorithm through different scenarios of seismic attributes. They are based on the selection of a different set of computed attributes. We chose the polar dip, similarity, REF, and the fracture density and proximity calculated from the most negative curvature in the first scenario. In the second scenario, we used a combination of conventional and unconventional attributes, the crossline-dip, inline-dip, TFL, and the fracture density and proximity calculated from the TFL. Three classes were defined based on the insights of three zones: the central zone of the fault line, the immediately adjacent zone where the deformation is maintained, and the distal zone with possible affectation. The results of UVQ were analyzed considering several time slices, in which the distribution of the zones depends on the relative contribution of the input attributes.

### Well Image Log Validation

Finally, the insights obtained from seismic attributes were validated by borehole data through rose diagrams. The borehole images provided the dip and dip-direction of faults and fractures at well scale. Also, we interpreted other drilling features such as breakout and induced drilling fractures, which were used subsequently in the present-day stress analysis (Figure 7). All these structural elements were manually interpreted using graphic descriptions as examples, most of the elements identified in the interval between Barra Velha top and Itapema top. However, high uncertainty was considered due to the image quality and the low number of interpreted dip and azimuth data in the entire borehole image data.

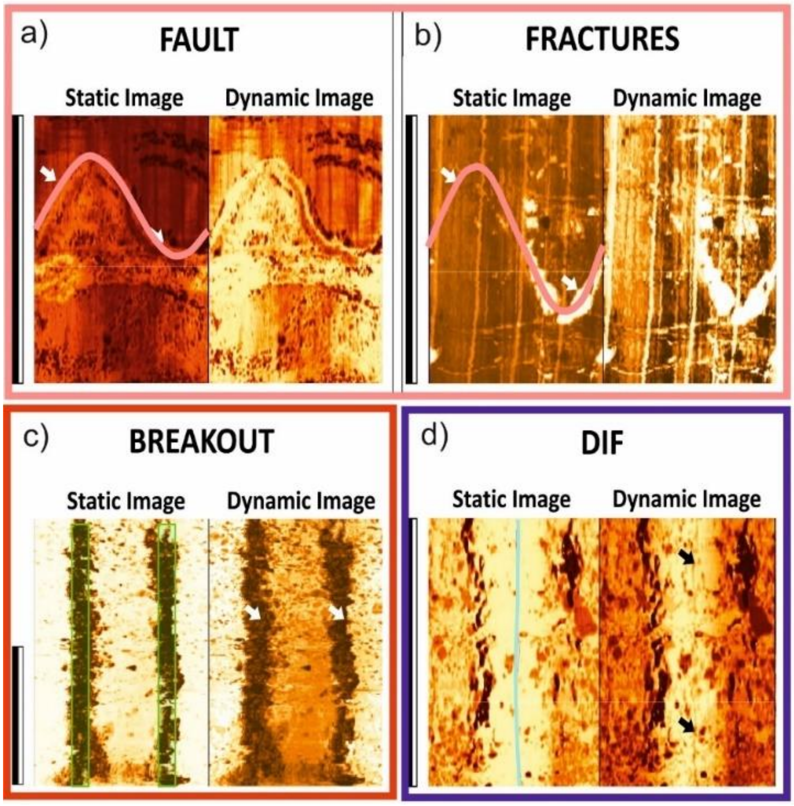


**Figure 7.** Main structural elements interpretation using borehole image log. Some examples from an interpreted a) Fault, b) Fracture, c) Breakouts, and d) DIF (Drilling Induced Fractures). The white arrow indicates faults and fractures, the green area the occurrence of breakouts, and the black arrows the presence of drilling-induced fractures. The scale bar in all examples corresponds to 1 meter in vertical position.

# RESULTS AND DISCUSSION

## Structural Framework Interpretation

The first stage of seismic interpretation revealed the major structural characteristics of the study area, focusing on the detection of regional structures (Figure 8a). Initially, the variation of seismic pattern provided insights into high-dip structures associated with the basement, where regional fault planes might be identified in the NE-SW trend. Then, the Camboriu Formation top was related to a non-continuous reflector with high uncertainty (Figure 8b-c).

The Itapema Formation was identified on a semi-continuous reflector, limited to the eastern by a probable structure associated with the basement (Figure 8b-c). Well D showed the absence of the Itapema Formation in the southeastern of the area. Some hypotheses about an erosional event or depositional hiatus might be suggested; however, the seismic data quality generated uncertainty about a reliable interpretation. On the other hand, the interpretation was also restricted in the northeastern zone due to no presence of well data and poor seismic quality, as shown in Figure 8e. The Camboriu and Itapema horizons showed possible offset or contrasting seismic patterns mainly related to the major structures on the underlying reflectors of the Barra Velha horizon. However, they were excluded from evaluating the seismic attributes due to the high uncertainty in the interpretation.

In contrast, we interpreted the Barra Velha Formation on a continuous reflector produced by the contrast impedance between the salt and carbonate layers. Some minor structures were detected in the NE-SW direction, suggesting a possible spatial influence from the major syn-rift structures, as presented in Figure 8d. However, the discontinuities within this interval challenged mapping due to the apparent smaller offsets of the faults.

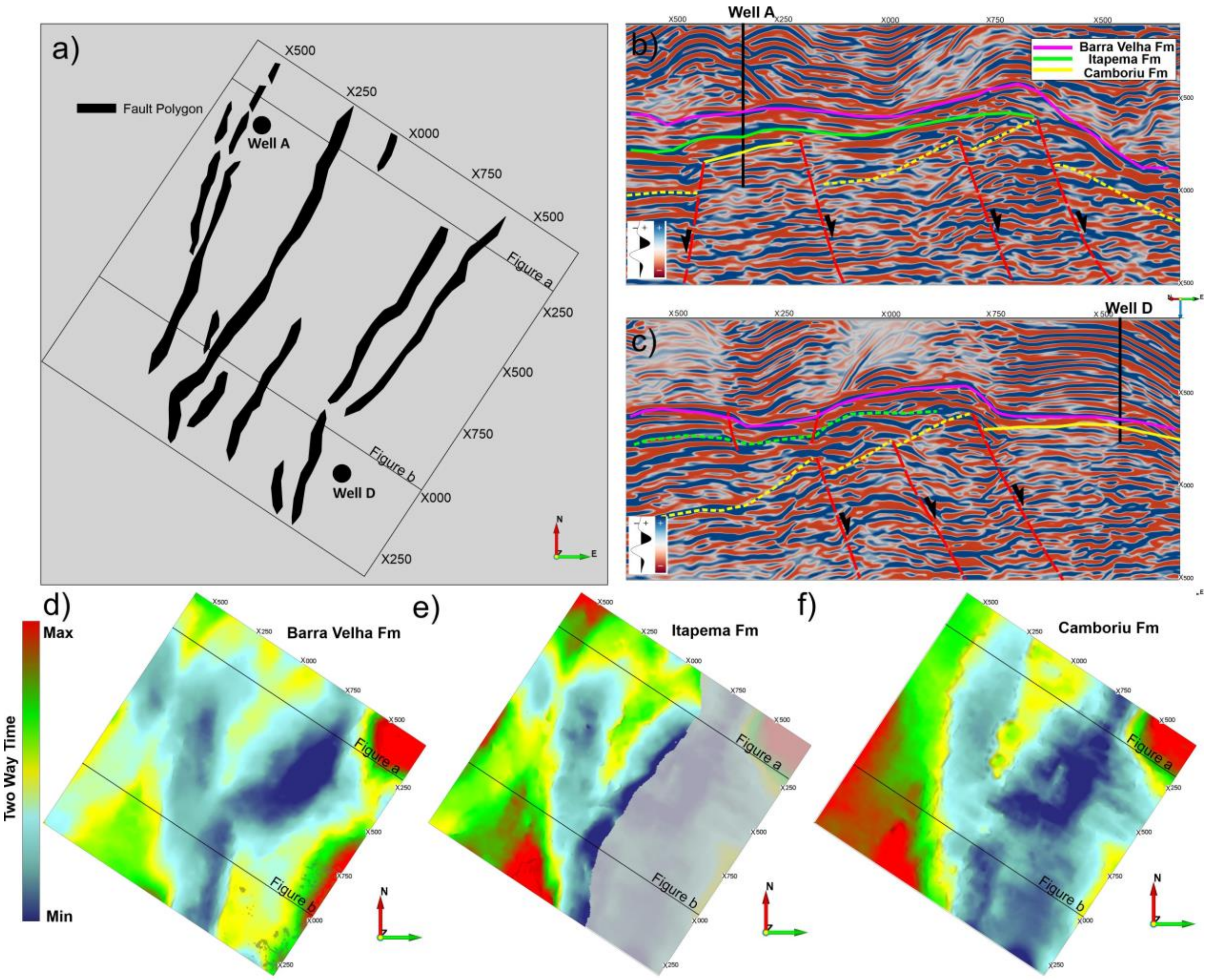


**Figure 8.** a) Regional faults and lineaments illustrated over the study area with the main trend in NW-SE direction. Seismic crossline-section b) and c) highlights the regional fault with the apparent high dip affecting the time maps of d) Barra Velha, e) Itapema, and f) Camboriu Formation.

The regional faults divided the area into two major structural domains, the eastern and western regions. We recognized a noticeable increase in layer thickness in the west region, which might mean lower fault influence than in the east region. In contrast, some reflectors may indicate the mechanical subsidence produced by the rifting phases in the east region identified through the divergent reflectors between Camboriu and Itapema formation (Moreira et al., 2007). In addition, these divergent geometries may define fault plane shapes, even though the lateral extension of the faults planes was better evaluated using time slices. This fault interpretation described a preliminary structural framework, which in conjunction with the analysis of further discontinuity attributes, may show the fault zones effects on the pre-salt rocks.

**Structural characterization through seismic attributes**

A time slice intersecting the Barra Velha Formation illustrated the structural characterization from the calculated seismic attributes in the study area. At first, the polar dip attribute highlighted the direction of main structural trends, characterized by higher dips values (Figure 9a). The first trend is identified in the central and northeastern zone with NE-SW orientation, while the second trend had an N-S direction in the south and northwest zone (Figure 9d). Inline-dip and crossline-dip components delineated sudden changes of dip values in detail. The inline-dip revealed major linear structures in the NE-SW direction, with some structures slightly rotated in an apparent NNE-SSW direction. Meanwhile, the crossline-dip showed minor lineament in the NW-SE direction (Figure 9b-c). The distribution of these discontinuities over the eastern zone may be considered fault zones.

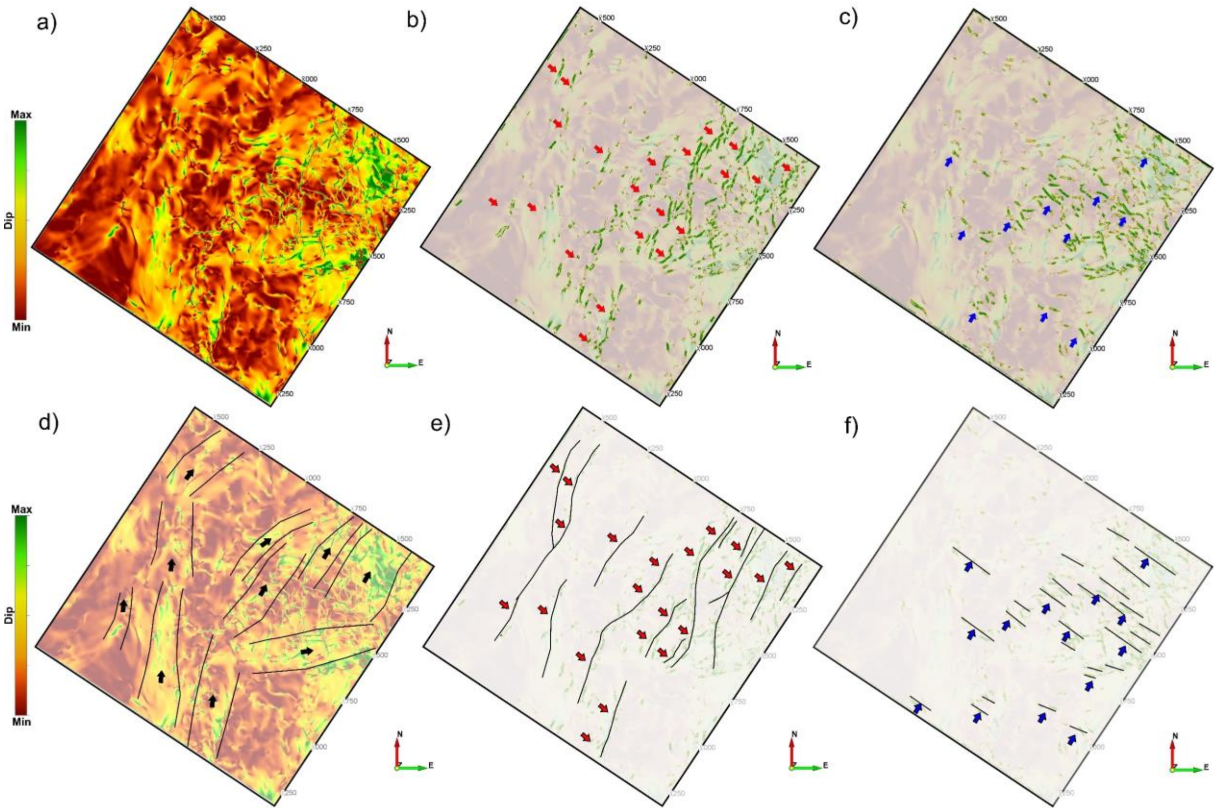


**Figure 9.** Time slice showing (a) polar-dip, (b) inline-dip, and (c) crossline-dip based on Steering Cube data. The black lines and arrows show dip values related to major structures. Red and blue arrows indicate the sudden dip changes in inline direction and crossline direction, respectively.

The dip-steered similarity attribute characterized discontinuities. Notably, low similarity values empathized areas with an intensive and random distribution of discontinuities in the eastern zone, following an apparent NE-SW trend. This concentrated pattern may be related to the surrounding areas of the stepped basement structures, where the brittle deformation influenced the adjacent regions, being prone to produce fragile zones with more intense discontinuities (Gabrielsen and Braathen, 2014). However, the Similarity attribute obscured the orientation of the minor discontinuities and connectivity among them in detail. On the other hand, the REF attribute generated a better background to visualize these minor discontinuities. The anomalous low similarity values disappeared due to the directional analysis accomplished by the REF attribute. Additionally, the distribution of discontinuities was better revealed in the study area, refining the morphology of the discontinuities even considering the minor lineaments (Figure 10).

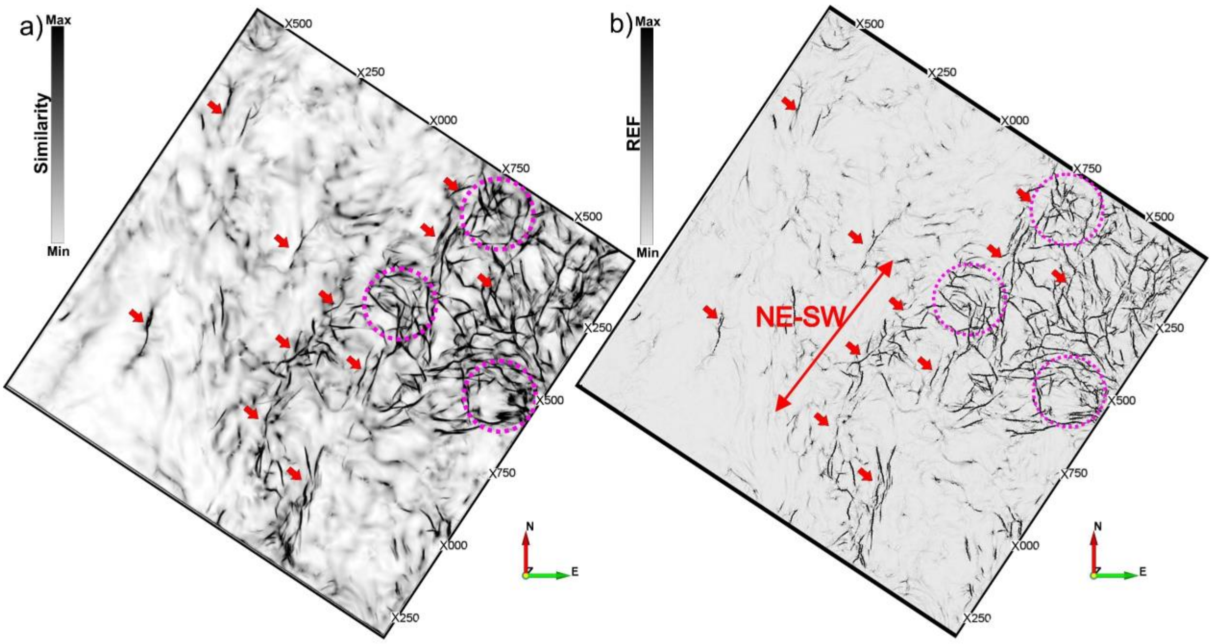


**Figure 10.** Time slices showing a) Dip-Steered Similarity and b) REF. Red arrows follow structures with a preferential NE-SW trend. Pink circles indicate areas where discontinuities are improved.

The directional components of the REF attribute also highlighted other different orientations from the inline and crossline direction, mainly in the chaotic pattern of discontinuities located in the eastern zone. These minor lineaments are characterized by E-W and NNW-SSE orientation, suggesting that the eastern zone is structurally more deformed than the western zone and showing a possible growth around the major structures within the study area (Figure 11). Although some minor lineaments seem to interact between them and the major structures, the cross-cutting relation that may establish a relative temporal position is unclear.

Meanwhile, the attribute showed some isolated features exposed a NE-SW orientation with poor continuity in the western zone (Figure 11).

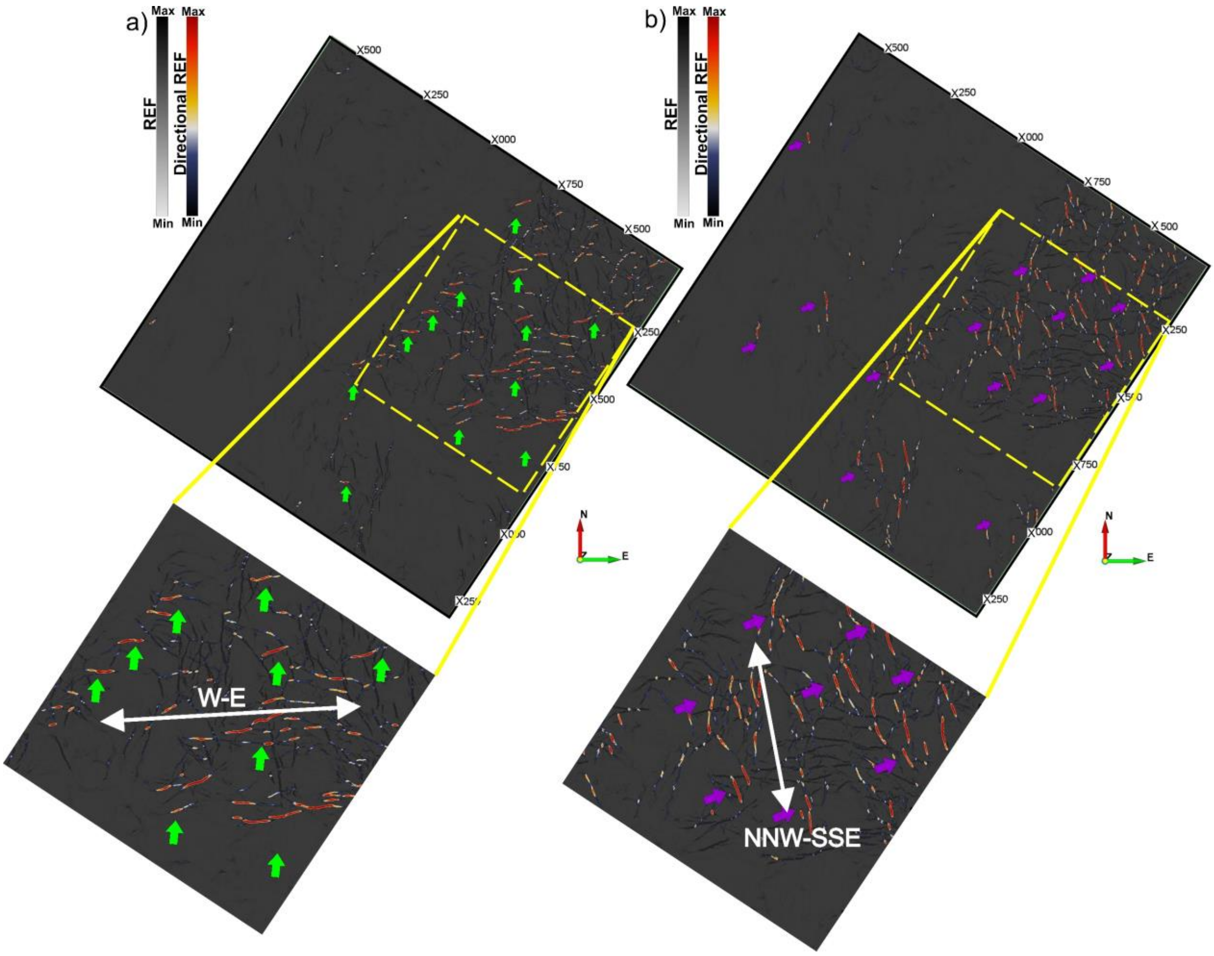


**Figure 11.** Time slices showing a) directional REF in W-E orientation and b) N-S orientation. Green and purple arrows point out discontinuities by the directional REF.

The curvature maps from the Barra Velha horizon revealed the principal trend of the structural elements along the NE-SW direction in the northeastern zone. In addition, the curvature maps showed NNE-SSW lineaments, sightly rotated from the principal structural trend, in the south and central-west part of the study area (Figure 12a-b). We noticed that the most negative curvature delineated more continuous structures than the most positive curvature. However, the random pattern of small lineaments on the eastern corner of the seismic survey resulted from uncertainty in the interpretation of the horizon.

The blended curvatures provided insights into the kinematic of interpreted structural elements (Figure 12c). We recognized three structural patterns according to the shape and the possible dip direction of the main structures. First, master faults in the east lead the zone to remain a continuous faulting pattern toward the east and suggest extensive fault shapes (Figure 12c). Second, curved faults in the west exhibited variations in the orientation regarding the main trend and showed narrow structures with apparent opposite dips and small structures within larger lineaments. Finally, narrowly opposed dips in the south and widely to the north characterized a transition zone between the master faults in the east and the short sinuous lineaments in the west (Figure 12c).

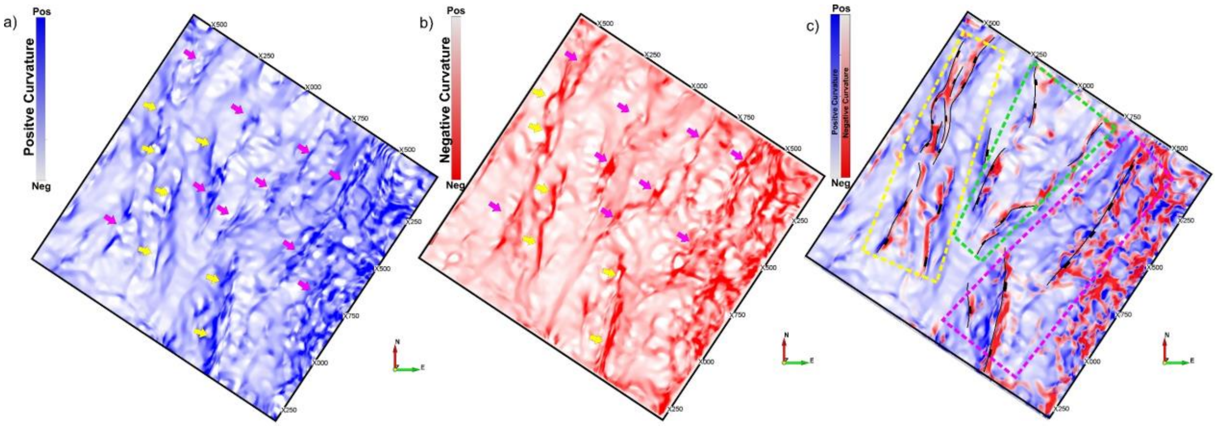


**Figure 12.** Curvature maps on the Barra Velha horizon shows (a) the most positive curvature, (b) the most negative curvature, and (c) the blend of the most positive curvature and the most negative curvature. The pink arrows point out the principal structures, and the yellow arrows show variation in the principal direction. The yellow, green, and pink polygons indicate the separation of structural patterns.

The dip, dip-steered similarity, and curvature attributes showed that the overall orientation of the structures followed a NE-SW trend, particularly in the eastern region. It coincided with the NE-trending fault system from the regional Outer High structure described by synthetic faults with vertical thrown (Gomes et al., 2008) (Figure 13).

Furthermore, as evidenced in the Dip and Curvature attributes, the structures with a NE-SW trend seemed to interact with some curved fault segments in the NNE-SSW direction. These NNE-SSW structures occurred in the northwestern, central, and southeastern zone. According to Ysaccis et al. (2019), similar lineaments with curved geometries were presented in some areas to the north. However, these structural elements in the north showed the more remarkable change of direction towards the N-S and NW-SE, attributed to the interaction with transfer zones from the oblique rift system (Cobbold et al., 2001) (Figure 13).

On the other hand, the minor discontinuities identified by REF attributes to the W-E directions were parallel to the transfer zone system that separates two basement high-structures adjacent to the southern part of the study area (Gomes et al., 2008) (Figure 13). The contrast between the pre-rift structures with ENE-WSW direction and the E-W obliques extension during the Mesozoic was associated with the orientation of these transfer zones (Meisling et al., 2001). Therefore, a plausible distal part of the immediate transfer system in the south might be evidenced by the orientation of these small discontinuities that seems hard-linked to the NE-SW lineaments (Figure 13).

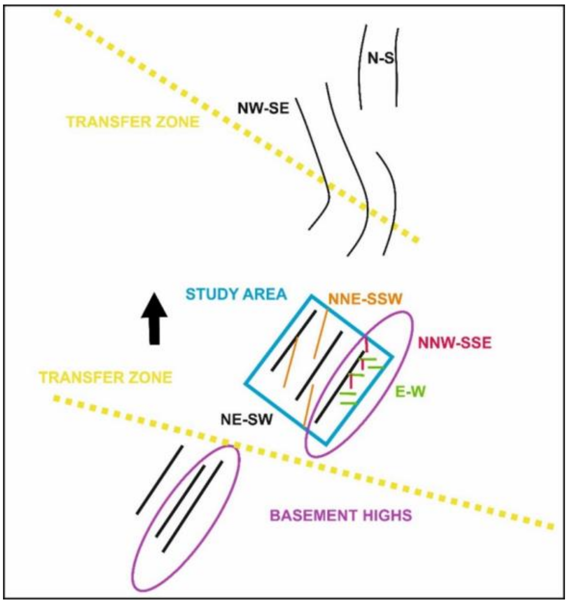


**Figure 13.** The diagram shows the relationship between different structural elements directions interpreted by seismic attributes and compared to the regional structures of Santos Basin.

### Detailed structural characterization

The FL attribute characterized the faults and recognized insights into the structural complexity from the seismic data in detail. The maximum fault likelihood values were found close to areas where faults in the NE-SW direction were previously interpreted manually. The maximum values were reached out in the eastern zone and some isolated regions in the western zone. The FL attribute provided the imaging of subsurface features by extracting fault planes when these maximum fault likelihood values were analyzed and scanned. The fault planes were categorized and described into five groups by the average orientation and the relative number of structures, as shown in Figure 15.

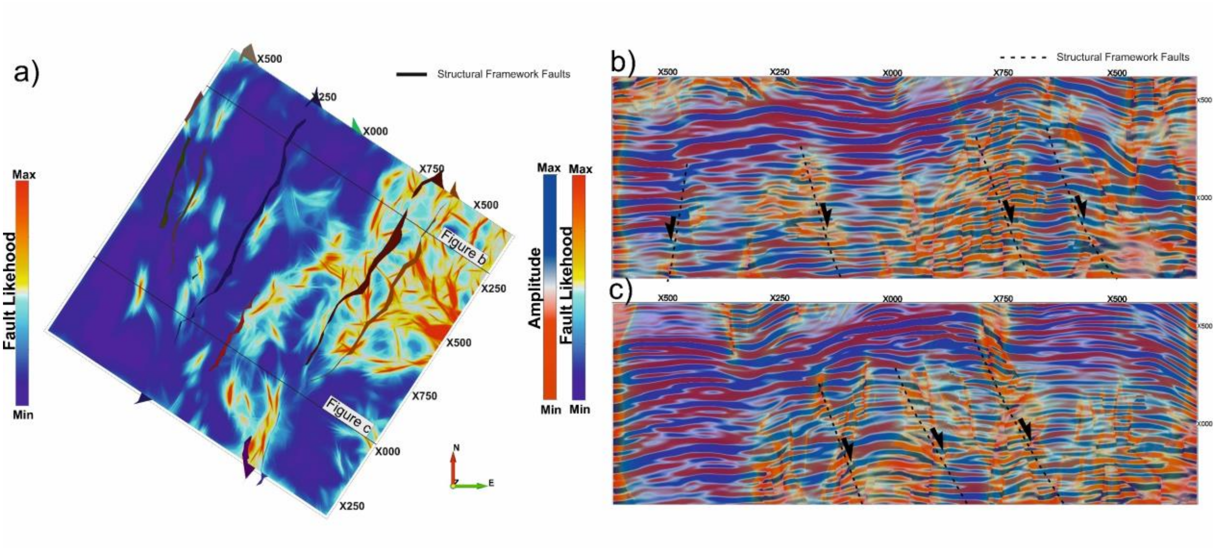


**Figure 14.** a) TFL cube showing the faults likelihood values close to the interpreted major faults and opacity between conditioned seismic and TFL at crossline (b) and (c). Black lines represent zones of the interpreted faults manually.

Initially, the opposite orientation distinguished two principal fault sets, NW- and NE-trending (Figure 15). The trend NW was separated into N20°W and N55°W. The first set showed shallow structures in the eastern region and deeper towards the west (Figure 15a). The distribution was accentuated in the east zone, where several discontinuities appeared. Otherwise, the N55°W set exhibited large structures in the east-central zone, mainly in the deeper zone (Figure 15c).

Also, two sets divided the NE-trending: N10°E (Figure 15b) and N45°E (Figure 15e). Two zones are identified regarding the distribution of structures, showing clusters to the northeast and northwest zone. The northeast trend had more prominent structural elements concentrated in the shallow zones than the northwest trends. In contrast to NE- and NW-trending, a minor set of discontinuities appeared in the E-W direction, only distributed over the eastern zone (Figure 15d).

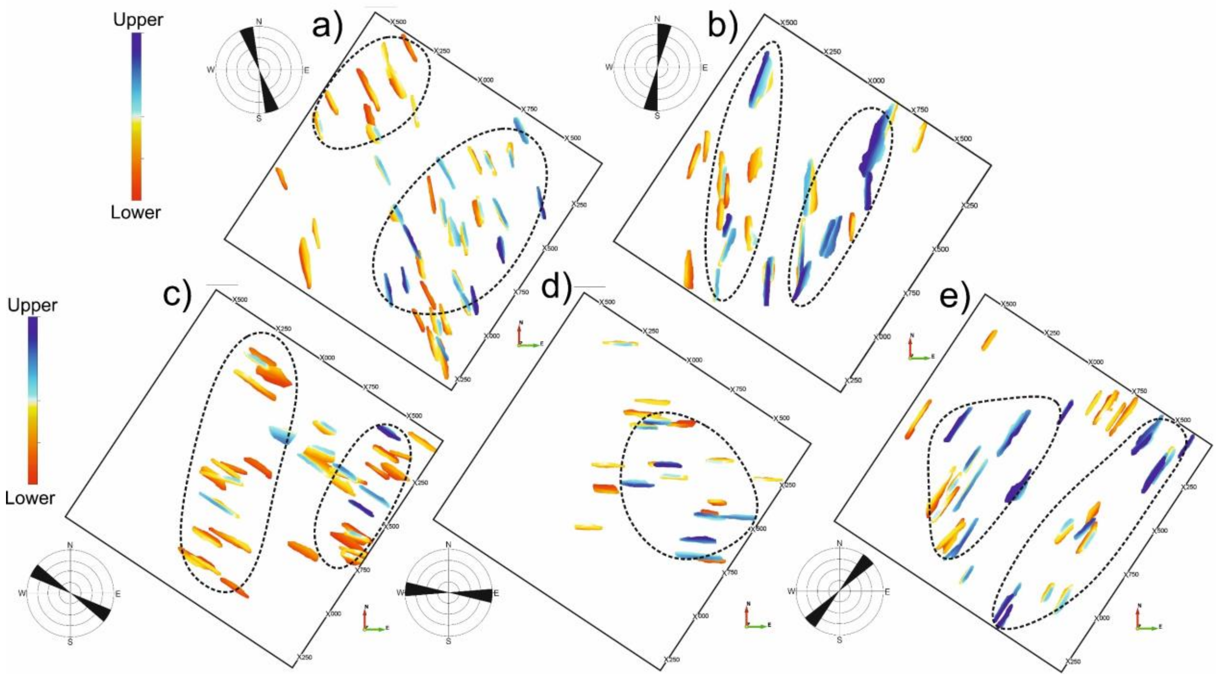


**Figure 15.** Automatic fault planes extraction shows the orientation of five groups of possible discontinuities in the study area. a) N20°W, b) N10°E and c) N55°W, d) E-W and e) N45°W. Cool colors referred to the upper part of the reservoir, and warm colors referred to the lower part of the reservoir.

Interactions among these different trends in shallow and deep zones may reveal insights into the structural connectivity or movement of the main basement blocks. For instance, the variations in the directions of the NE-trending might suggest that they may be formed by the same tectonic event through slight changes in the movements during the hyper-extensive stage in the rifting process, as indicated by Oliveira et al. (2019) (Figure 16a). Also, the E-W trend and the shallow N20°W trend may indicate minor structural elements in close interaction with the major basement highs in the eastern part (Figure 16b). For deeper structures, the N45°W trend dominated most of the area and was influenced by the N20°W trend in the southern and northern zones, resulting in clusters of faults connected by the tectonic control (Figure 16c).

These zones with different trends may have some conditions for the quality of the pre-salt reservoirs.

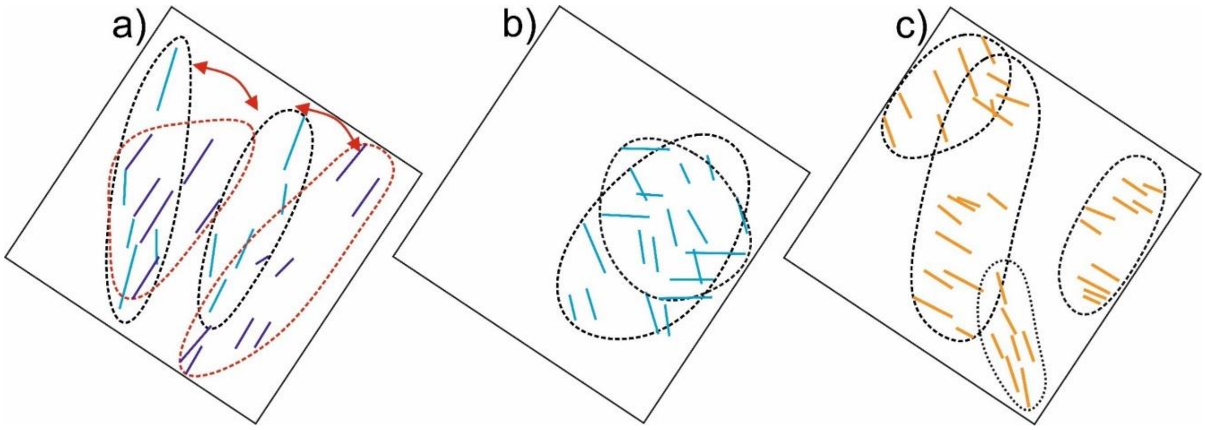


**Figure 16.** Interactions among different trends in shallow and deep zones. a) NE-trending, b) E-W trend and the shallow N20°W trend, and c) deep trends N45°W and N20°W. Cool colors refer to times from shallow structures, and warm colors refer to deep structures.

On the other hand, the fracture density attribute mapped the regions with a high quantity of discontinuities concerning possible structures highlighted by the TFL and curvature attributes. For the curvature attribute, we observed that searching windows smaller than 200 m created tiny zones that produced uncertainty on the distribution of fractures by comparing different searching windows. Besides, the distribution of possible fractures might be restricted, accumulating the highest fracture density values in isolated areas (Figure 17a). In contrast, a searching radius bigger than 200 m reveals a better distribution and connectivity of the zones, facilitating the differentiation of the number of discontinuities per area and showing the zonation of the intensity of fractures. Also, the maximum values, preferentially in the eastern part, may be emphasized by the same structural trend NE-SW identified in the regional characterization (Figure 17b).

Comparing the threshold values of the TFL, the fracture density attribute concentrated the maximum density of fractures in the most probable structures extracted from the TFL attribute. Using lower thresholds of TFL, the areas with a high density of fractures were characterized by a random distribution towards the eastern part without well-defined trends. Some of these areas might also be associated with the noise produced by low fault likelihood (Figure 17c)**.** In higher threshold values of TFL, the continuity of the trends was increased, and the intensity of fractures is better concentrated (Figure 17d). Generally, these zones might represent possible conductive regions; however, well data should be used to corroborate these regions' interpretation.

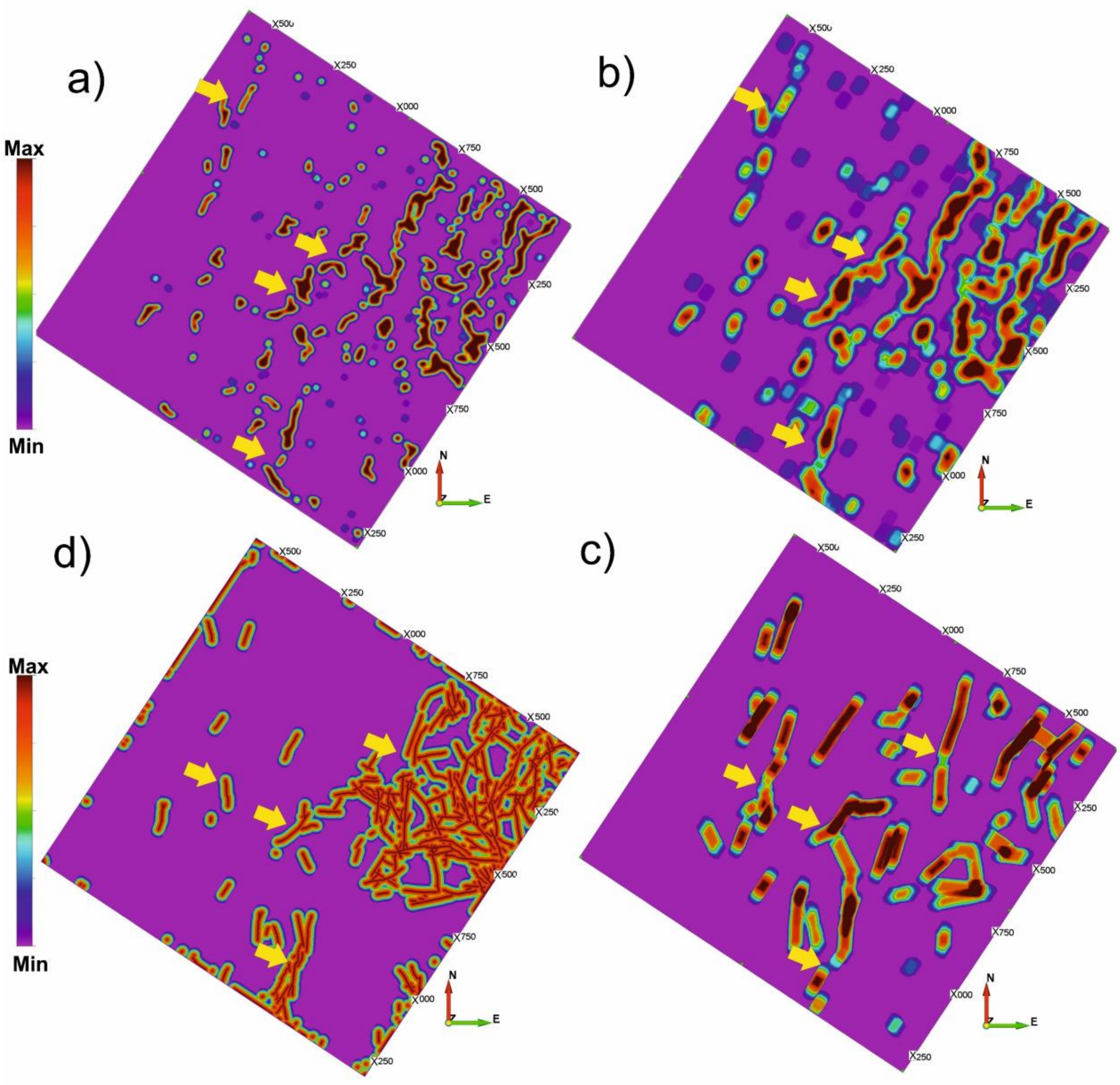


**Figure 17.** The fracture density attribute shows the most positive curvature scenario with a searching window of a) 125 m and b) 375 m, and the TFL scenario using a) low threshold and b) high threshold. The yellow arrows show some regions of maximum fracture activity.

On the other hand, the fracture proximity attribute emphasized the distances from the center of discontinuities and the interaction among other structures. These areas were partially isolated when low searching windows were applied, while high searching windows revealed a closer relationship among the discontinuities. In Figure 18b, the yellow-green colors indicate possible structures interacting between 185 m and 200 m.

The scenarios of the TFL attribute showed that different threshold values, which might strongly influence how the interaction among structures is presented. For instance, many structures were clustered in the northeastern sector using low threshold values, leading to high uncertainty due to the low values of fault likelihood. Otherwise, higher threshold values indicated an individual interaction of most structures, particularly impacting the discontinuities terminations, as shown in Figure 18.

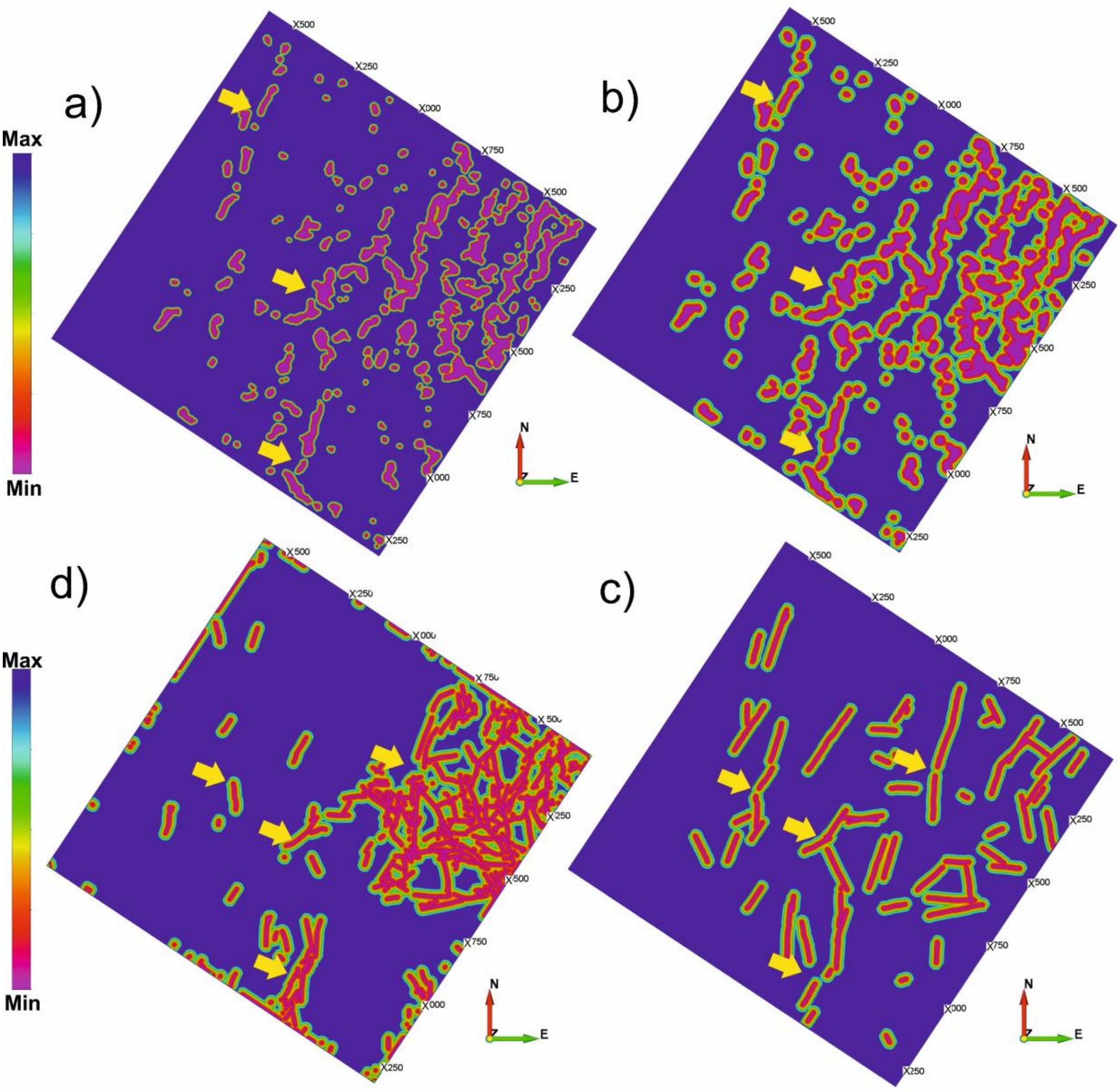


**Figure 18.** The fracture proximity attribute emphasized the relationship between the center of discontinuities and the adjacent structures. The yellow arrows show the regions where the interaction among possible structures was compared. The most positive curvature scenario uses a searching window of a) 125 m and b) 375 m and the TFL scenario uses c) low and d) high threshold.

### Multi-attribute Analysis through Unsupervised Artificial Neural Networks

The multi-attribute analysis was performed using the ANN to identify areas with the highest probability of faulting. Table 1 presents the relative contribution of each attribute in selecting the clusters and classification of the input data for each proposed scenario.

**Table 1**. Input node table illustrating the relative importance of every attribute used for each scenario of UVQ.

| Attribute | Relative Contribution Curvature Scenario | Relative contribution TFL Scenario |
|---|---|---|
| Polar dip | 17.2 | - |
| Inline-dip | - | 23.4 |
| Crossline-dip | - | 10.2 |
| Most negative curvature | 44.2 | - |
| Fracture Density | 65.5 | 52.3 |
| Fracture Proximity | 69.7 | 55.7 |
| Ridge Enhancement Filter | 95.5 | - |
| Dip-steered Similarity | 85.9 | - |
| Thinned Fault Likelihood | - | 98.5 |

The ANN scenarios were evaluated in three-time slices from the upper part to the lower part of the Barra Velha Formation. In the first scenario, the high faulting probability zones migrated from the east to the west side, showing the possible effect of basement structures on the intensity of faulting, as shown in Figure 18. This first scenario also showed a high distribution of structures, mainly influenced by the curvature and REF attributes, evidenced by the relative contribution of input attributes (Table 1). Although the high number of discontinuities may obscure the precise interpretation of zones with more continuous faults, the first scenario was helpful to recognize the connectivity between the structures. Then, we had insights into interpreted fracture networks associated with the major structures.

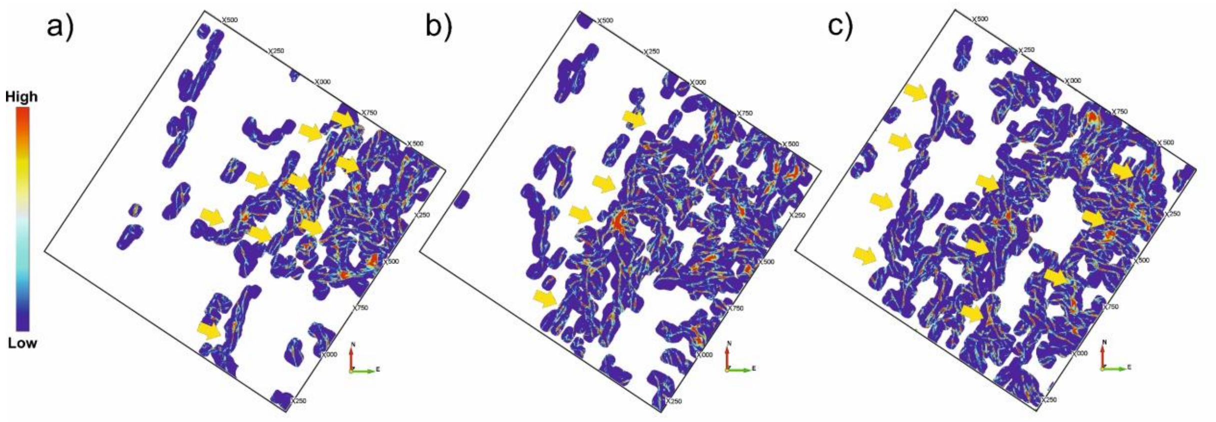


**Figure 19.** The result of the curvature scenario highlighted the possible fracture network from a) upper, b) middle, and c) lower part of the Barra Velha Formation. Yellow arrows show the cluster of possible fractures following the NE-SW trend.

The second scenario was related to larger-scale structures restricted by values of the fault likelihood distribution close to the main basement structures. The trends followed the NE-SW direction and were constant at different time slices. This scenario showed a better definition and concentration of areas with a high probability of discontinuities to identify more specific sectors with a possible high intensity of structures (Figure 20). These faulting zones also seem to have a more linear shape than in the first scenario, mainly produced by the relative weight contribution of attributes such as the TFL (Table 1).

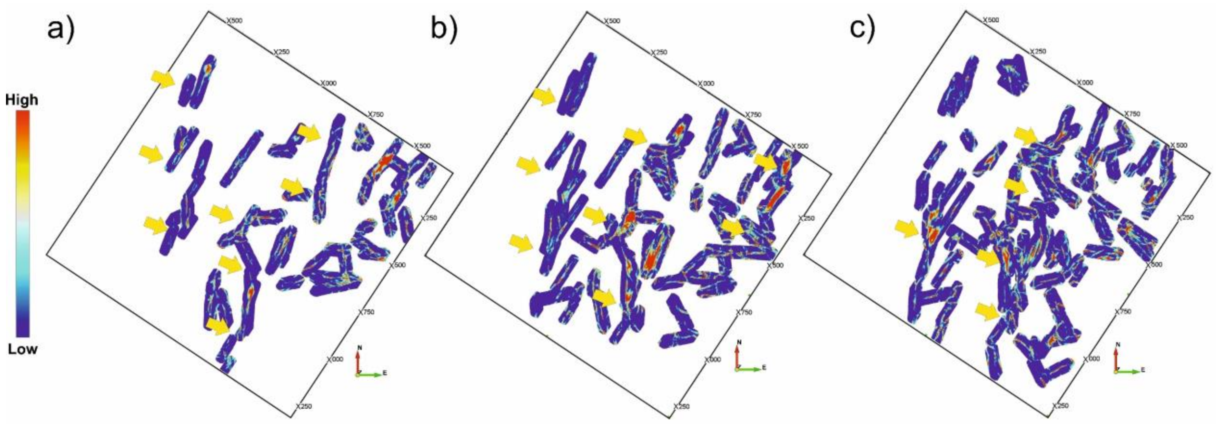


**Figure 20.** The results of the TFL scenario highlight the possible fractured areas from a) upper, b) middle, and c) lower part of the Barra Velha Formation. Yellow arrows exhibit the clusters of fractures following the NNE-SSW trend.

Comparing the zones with a high probability of faults and fractures, the ANN provided maps to recognize areas with detailed fracture probability. These scenarios were compared with the integrated prediction of structural elements performed by Zhang et al. (2020), which was carried out through the ant-colony algorithm and showed a distribution of fracture systems with a preferential NE-SW trend adjacent to uplifted areas. Also, these clusters of structural elements might be channels for hydrocarbon migration on the pre-salt rocks, but validating these structural trends with wells already drilled is essential (Refayee et al., 2016).

### Seismic Attribute Map and Well Validation

The strike direction of fracture and faults interpreted in the borehole images were plotted on the TFL attribute map to validate the discontinuities through the seismic-well integration. The borehole image interpretation for the wells A, C, E showed the principal structural in NE-SW direction. Meanwhile, well F exhibited a preferential direction in the NW-SE direction. Moreover, we recognized minor trends toward the west, where wells A and E showed an NW-trending, while wells C and F exhibited an SW-trending.

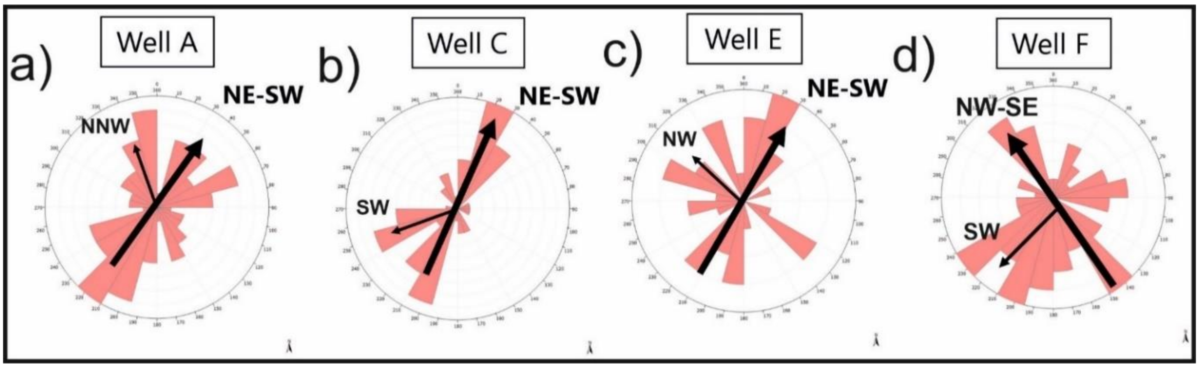


**Figure 21.** Interpretation of main structural trends using strike data from the interpreted fractures and faults in the borehole image logs. The black arrow indicates the predominant direction of faults and fractures.

Figure 21 shows the orientation of seismic discontinuities regarding the features observed in the borehole image logs. The strike direction from the TFL attribute was assessed as a volume around the wells. The wells A and B main trends exhibited a strike correlation with the TFL attribute of approximately 80%, while the wells E and F showed a correlation between 60% and 70%. In contrast, the minor trends exposed a considerable variability in fracture orientation, decreasing the seismic-well correlation to 50 % to 40% for all wells. All the correlations may be extended to the conventional attributes where we recognized similar insights about the orientation of discontinuities (Appendix 2A).

The NE-SW trending was the most predominant throughout the study area (Figure 22). This main trend in wells A, C, and E might be related to the position of basement blocks. Figure 22 shows that the NE-SW trend from the fracture set was correlated to the TFL attribute in the high areas. Meanwhile, in the lower areas (well F), the set of discontinuities presented the NW-SE direction. The NE-SW trend was oriented approximately 60° concerning the NW-SE trend.

According to Cobbold et al. (2001), the fault trends in the area were associated with the oblique rifting, where the transfer zones might compartmentalize the pre-salt reservoirs. Thus, the NW-SE and NE-SW structures might generate complex intra-rift structures. Meisling et al. (2001) described these structures with a possible strike-slip component that allowed the migration of hydrocarbons from lower to higher areas. In Figure 22, the red boxes showed variations in the NE-SW trend, which might evidence the orientation of the local stress field and the tectonic control of the large structures. Some insights into transtensive structures and relay ramps may be identified, which are related to the different rates of extensional movements that have been documented close to the study area (Alves et al., 2020; Cobbold et al., 2001; Meisling et al., 2001).

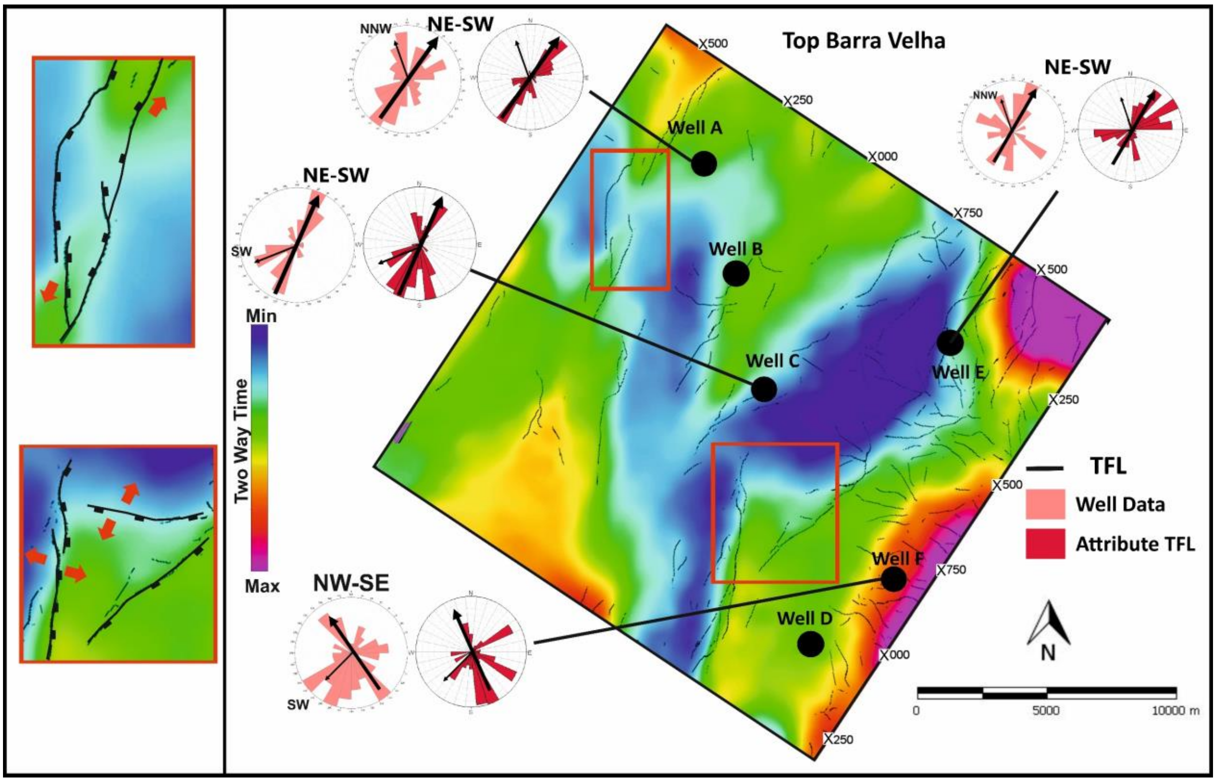


**Figure 22.** Well location with borehole image logs. Fractures trends in the Barra Velha Formation were plotted in rose diagrams for individual wells. The red rose diagram shows seismic discontinuities interpreted from the TFL attribute, and the pink rose diagram the fracture direction for wells. The red boxes indicate local structures with changes in the main trends.

On the other hand, the breakout and DIF direction from the wells provided the present-day tectonic stress field. For instance, the maximum horizontal stress direction (SHmax) might be related to the direction of breakouts; meanwhile, the minimum horizontal stress (Shmin) might be associated with the direction of DIF (Zoback et al., 2003). These features should be approximately 90° from each other; however, uncertainty associated with the quality of the image log and the interpretation might be considered. For wells A, C and F, the SHmax shows a dominant strike in the NE-SW direction, parallel to the DIF (Figure 23), and the Shmin is preferentially established in the NW-SE direction, parallel to the breakouts (Figure 23). Based on more detailed geomechanical assessments for nearby wells, Da Silva (2016) described the magnitude of the tectonic stress with a transitional behavior between normal fault (Sv > SHmax > Shmin) and transcurrent fault (SHmax > Sv > Shmin).

Therefore, fractures and fault sets may be impacted by the direction of the tectonic stress field, suggesting some insights into the quality of opening of these structural features. For example, structures in the SHmax direction might be more likely to be open than those in the Shmin direction, which may strongly influence the petrophysical properties such as permeability. Thus, the detailed structural characterization may help us understand the Brazilian pre-salt reservoirs more.

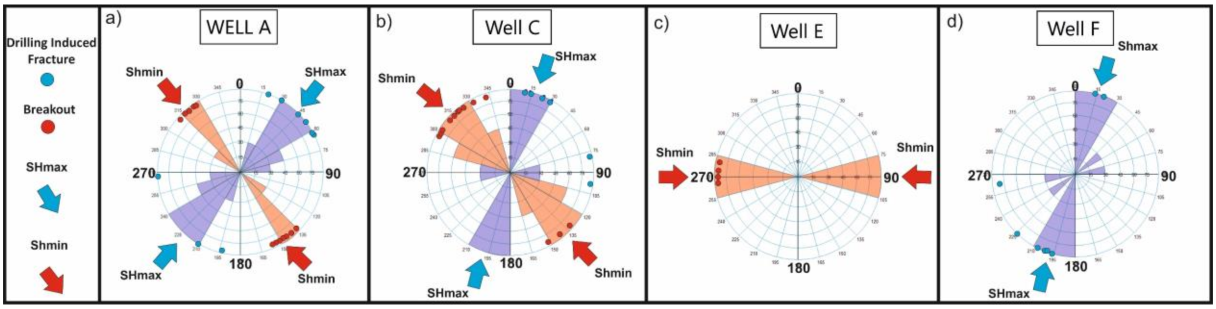


**Figure 23**. Interpretation of tectonic stress field using the strike data from Breakout and DIF interpreted in the borehole image logs for the a) Well A, b) Well C, c) Well E, and d) Well F. Blue and red points indicate the dip azimuth from DIF and breakouts, respectively. Blue and red arrows show the directions of maximum and minimum horizontal stress, respectively.

**CONCLUSION**

This study aimed to conduct an integrated analysis using seismic attributes and an unsupervised neural network to identify potential areas of occurrence for faults and fractures in the pre-salt reservoirs.

The dip attributes indicated orientations across the region with an overall trend in the NE-SW direction and small discontinuities in the NW-SE direction. The similarity and REF attributes minutely showed the clusters of subtle faults following the overall trend. The directional decomposition of the REF attribute showed detailed insights into faults, emphasizing the NNW-SSE and E-W trends in potential faulting areas. Regarding the attributes described along the horizon, the most positive and negative curvature provided insights into the normal faults that dominate the main structures, which allowed us to classify the area in three zones with different structural styles. These zones seemed to match with the tectonic control produced by the basement blocks. The most negative curvature emphasized the most continuous structures in the study area.

The FL presented a superior performance identifying discontinuities on pre-salt rocks. The strike and dip fault likelihood components allowed us to analyze different directions by automatically extracting faults planes. Five groups of discontinuities were classified, increasing the number of fault observations compared to the manual interpretation. The interaction of these different fault groups enabled the identification of three potential discontinuities areas.

Two cases of fracture density and fracture proximity attributes were used to characterize the distribution of faults and fractures based on the deformation along possible faults with the most negative curvature and maximum fault likelihood attribute. These scenarios generated insight into the distribution and connectivity among structures found mainly in the eastern zone.

The UVQ showed the distribution and location of the highest probability faulting areas based on the multi-attribute analysis, which comprised two scenarios. The scenario composed of conventional attributes limited most of these fractured zones to the NE-SW trend. These zones exhibited more significant clustering toward the region near the basement highs, showing possible fractures networks. In contrast, the scenario composed of conventional and unconventional attributes restricted the probability of faults to concentrated areas, following the NNE-SSW direction and showing a better definition of larger structures.

The borehole image data validated the interpreted trends from the seismic attributes. Rose diagrams at well location confirmed the NE-SW and NW-SE trend in the study area. Thus, the analysis of the rose diagrams allowed the recognition of potential structural zones in high areas. Also, the borehole breakouts and drilled-induced fractures evidenced the orientation for present-day Shmax and Shmin at each well location, which might be influenced the aperture of fractures on the Barra Velha Formation. We recommend that further detailed characterization of the Brazilian pre-salt reservoir might be carried out from higher resolution data for future studies.

## ACKNOWLEDGEMENTS

The study was financed by Fundação de Amparo à Pesquisa do Estado de São Paulo (FAPESP). National Petroleum Agency (ANP) is acknowledged for providing seismic and well data. The authors gratefully acknowledge Equinor for supporting this research. The authors also recognize the academic licenses provided by dGB Earth Sciences for Opendtect, Schlumberger for Petrel, and Lloyd's Register for Interactive Petrophysics.

## REFERENCES

Abelha, M., Petersohn, E., 2018. The State of the Art of the Brazilian Pre-Salt Exploration. AAPG 2018 Annual Convention and Exhibition, Salt Lake City 30586, 531–549. https://doi.org/10.1306/30586Abelha2018

Al-Dossary, S., Marfurt, K.J., 2006. 3D volumetric multispectral estimates of reflector curvature and rotation. Geophysics 71. https://doi.org/10.1190/1.2242449

Alves, T., Fetter, M., Busby, C., Gontijo, R., Cunha, T.A., Mattos, N.H., 2020. A tectono-stratigraphic review of continental breakup on intraplate continental margins and its impact on resultant hydrocarbon systems. Marine and Petroleum Geology 117, 104341. https://doi.org/10.1016/j.marpetgeo.2020.104341

Alves, T.M., Fetter, M., Lima, C., Cartwright, J.A., Cosgrove, J., Gangá, A., Queiroz, C.L., Strugale, M., 2017. An incomplete correlation between pre-salt topography, top reservoir erosion, and salt deformation in deep-water Santos Basin (SE Brazil). Marine and Petroleum Geology 79, 300–320. https://doi.org/10.1016/j.marpetgeo.2016.10.015

Aminzadeh, F., de Groot, P., 2005. A neural networks based seismic object detection technique. Society of Exploration Geophysicists - 75th SEG International Exposition and Annual Meeting, SEG 2005 775–778. https://doi.org/10.1190/1.2144442

Ashraf, U., Zhang, H., Anees, A., Mangi, H.N., Ali, M., Ullah, Z., Zhang, X., 2020. Application of unconventional seismic attributes and unsupervised machine learning for the identification of fault and fracture network. Applied Sciences (Switzerland) 10. https://doi.org/10.3390/app10113864

Boyd, A., Souza, A., Carneiro, G., Machado, V., Trevizan, W., Santos, B., Netto, P., Bagueira, R., Polinski, R., Bertolini, A., 2015. Presalt Carbonate Evaluation for Santos Basin, Offshore Brazil. Petrophysics 56, 577–591.

Brouwer, F., Huck, A., 2011. An Integrated Workflow to Optimize Discontinuity Attributes for the Imaging of Faults, Attributes: New Views on Seismic Imaging–Their Use in Exploration and Production.

Chopra, S., 2011. Extracting meaningful information. CSEG Recorder 9–12.

Chopra, S., Marfurt, K., 2008. Gleaning meaningful information from seismic attributes. First Break 26, 43–53. https://doi.org/10.3997/1365-2397.2008012

Chopra, S., Marfurt, K., 2007a. Curvature attribute applications to 3D surface seismic data. The Leading Edge 26, 404–414. https://doi.org/10.1190/1.2723201

Chopra, S., Marfurt, K.J., 2007b. Seismic Attributes for Prospect Identification and Reservoir Characterization, Seismic Attributes for Prospect Identification and Reservoir Characterization. https://doi.org/10.1190/1.9781560801900

Cobbold, P.R., Meisling, K.E., Mount, V.S., 2001. Reactivation of an obliquely rifted margin, Campos and Santos basins, southeastern Brazil. AAPG Bulletin 85, 1925–1944. https://doi.org/10.4324/9780203960301

Correa, R.S.M., Pereira, C.E.L., Cruz, F.A.S., Lisboa, S.N.D., Junior, M.P.A., Carvalho, B.R.B.M., Souza, V.H.P., Rocha, C.H.A., Araujo, F.G., 2019. Integrated Seismic-Log-Core-Test Fracture Characterization, Barra Velha Formation, Pre-salt of Santos Basin. https://doi.org/10.1306/42425Correa2019

Da Silva, C. (2016). *Análise Geomecânica Dos Carbonatos Do Pré-Sal Da Bacia De Santos* [Pontifícia Universidade Católica do Rio de Janeiro (PUC-Rio)]. http://www.maxwell.vrac.pucrio.br/Busca_etds.php?strSecao=resultado&nrSeq=30291@1

Davison, I., Anderson, L., Nuttall, P., 2012. Salt deposition, loading and gravity drainage in the Campos and Santos salt basins. Geological Society Special Publication 363, 159–174. https://doi.org/10.1144/SP363.8

de Groot, P., 1998. An introduction to Neural Networks including Multi-Layer-Perceptrons, Radial-Basis-Functions and Unsupervised-Vector-Quantiser 1–11.

de Groot, P., Herald Ligtenberg, J., Meldahl, P., Heggland, R., 2001. SELECTING AND COMBINING TO ATTRIBUTES TO ENHANCE DETECTION OF SEISMIC OBJECTS. EAGE 63rd Conference & Technical Exhibition — Amsterdam, The Netherlands 3–6.

Farias, F., Szatmari, P., Bahniuk, A., França, A.B., 2019. Evaporitic carbonates in the pre-salt of Santos Basin – Genesis and tectonic implications. Marine and Petroleum Geology 105, 251–272. https://doi.org/10.1016/j.marpetgeo.2019.04.020

Fehmers, G.C., Höcker, C.F.W., 2003. Fast structural interpretation with structure-oriented filtering. Geophysics 68, 1286–1293. https://doi.org/10.1190/1.1598121

Fetter, M., Penteado, H., Madrucci, V., Spadini, A., 2018. The Paleogeography of the Lacustrine Rift System of the Pre-Salt in Santos Basin, Offshore Brazil. AAPG 2018 Annual Convention & Exhibition 11137, 39. https://doi.org/10.1306/11137Fetter2018

Gabrielsen, R.H., Braathen, A., 2014. Models of fracture lineaments - Joint swarms, fracture corridors and faults in crystalline rocks, and their genetic relations. Tectonophysics 628, 26–44. https://doi.org/10.1016/j.tecto.2014.04.022

Gamboa, L., Ferraz, A., Baptista, R., Santos Neto, E. V., 2019. Geotectonic controls on CO2formation and distribution processes in the Brazilian pre-salt basins. Geosciences (Switzerland) 9, 1–14. https://doi.org/10.3390/geosciences9060252

Gomes, P.O., Kilsdonk, B., Minken, J., Grow, T., Barragan, R., 2008. The outer high of the Santos Basin, Southern São Paulo Plateau, Brazil: pre-salt exploration outbreak, paleogeographic setting, and evolution of the syn-rift structures. AAPG International Conference and Exhibition, Cape Town, South Africa 10193, 26–29.

Hale, D., 2013. Methods to compute fault images, extract fault surfaces, and estimate fault throws from 3D seismic images. Geophysics 78. https://doi.org/10.1190/GEO2012-0331.1

Jaglan, H., Qayyum, F., Huck, H., 2015. Unconventional seismic attributes for fracture characterization. First Break 33, 101–109.

Jesus, C., Olho Azul, M., Moreira Lupinacci, W., Machado, L., 2019. Multiattribute framework analysis for the identification of carbonate mounds in the Brazilian presalt zone. Interpretation 7, T467–T476. https://doi.org/10.1190/int-2018-0004.1

Kumar, P.C., Sain, K., 2020. A machine learning tool for interpretation of Mass Transport Deposits from seismic data. Scientific Reports 10, 1–11. https://doi.org/10.1038/s41598-020-71088-6

Luo, Y., Marhoon, M., Al Dossary, S., Al-Faraj, M.N., 2002. 3D edge-preserving smoothing and applications. THE LEADING EDGE 71. https://doi.org/10.1190/1.2213050

Meisling, K.E., Cobbold, P.R., Mount, V.S., 2001. Segmentation of an obliquely rifted margin, Campos and Santos basins, southeastern Brazil. AAPG Bulletin 85, 1925–1944. https://doi.org/10.1306/8626d0b3-173b-11d7-8645000102c1865d

Meldahl, P., Heggland, R., Bril, B., De Groot, P., 2001. Identifying faults and gas chimneys using multiattributes and neural networks. Leading Edge (Tulsa, OK) 20. https://doi.org/10.1190/1.1438976

Meneguim, T.B.M.T.B., Proença, T.P.T., Pereira, C.E.L.P.C.E.L., De Almeida Junior, M.P.A.M.P., Da Silva, E.B.S.E.B., 2016. Effects of post stack Seismic data conditioning on impedance inversion for reservoir, Brazilian pre-salt, Santos Basin. 78th EAGE Conference and Exhibition 2016: Efficient Use of Technology - Unlocking Potential. https://doi.org/10.3997/2214-4609.201601340

Moreira, J.L.P., Madeira, C.V., Gil, J.A., 2007. Bacia de Santos. Boletim de Geociencias da Petrobras, , Rio de Janeiro, v. 15, n. 2, p. 531-549, maio/nov. 2007 531–549.

Oliveira, T., Cruz, N., Cruz, J., Cunha, R., Matos, M., 2019. Faults, Fractures and Karst Zones Characterization in a Pre-Salt Reservoir using Geometric Attributes 1–5. https://doi.org/10.22564/16cisbgf2019.139

Ribeiro da Silva, S.F.C., Pereira, E., 2017. Tectono-Stratigraphic Evolution of Lapa Field Pre-Salt Section, Santos Basin (Se Brazilian Continental Margin). Journal of Sedimentary Environments 2, 133–148. https://doi.org/10.12957/jse.2017.30052

Roberts, A., 2001. Curvature attributes and their application to 3D interpreted horizons. First Break 19, 85–100. https://doi.org/10.1046/j.0263-5046.2001.00142.x

Tingdahl, K.M., 2001. Improving seismic chimney detection using directional attributes. Developments in Petroleum Science 51, 157–173. https://doi.org/10.1016/S0376-7361(03)80013-4

Tingdahl, K.M., 1999. Improving seismic detectability using intrinsic directionality. Masters

Thesis 41.

Tingdahl, K.M., de Groot, P.F.M., 2003. Post-stack-dip- and azimuth processing. Journal of Seismic Exploration 12, 113–126.

Tingdahl, K.M., de Rooij, M., 2005. Semi-automatic detection of faults in 3-D seismic data. Geophysical Prospecting, 533–542.

Ysaccis, R., El-Toukhy, M., Moreira, L., 2019. Maximizing the value of seismic data for a better regional understanding and exploration assessment in the Santos Basin, Brazil 1–6. https://doi.org/10.22564/16cisbgf2019.130

Zoback, M.D., Barton, C.A., Brudy, M., Castillo, D.A., Finkbeiner, T., Grollimund, B.R., Moos, D.B., Peska, P., Ward, C.D., Wiprut, D.J., 2003. Determination of stress orientation and magnitude in deep wells. International Journal of Rock Mechanics and Mining Sciences 40, 1049–1076. https://doi.org/10.1016/j.ijrmms.2003.07.001

# APPENDIX 1A. FINAL CONSIDERATIONS

Studying carbonate reservoirs involves high complexity due to their heterogeneity and the geological events covering the most diverse scales. In that sense, three-dimensional seismic was an essential tool for understanding reservoirs spatially, even studying formations at great depths.

The pre-conditioning of the data consisted of removing acquisition footprints, coherent and random noises. Enhancing discontinuity characterization enabled us to gain new insights into the trigger mechanisms behind fracturing in the pre-salt rocks in the study area. Applying the SOF such as DSMF, DSDF, and EPS enhanced seismic amplitude and terminations of reflectors at the proximity of faults. These filters generated seismic attributes that demonstrated better delineation of discontinuities, improving the reliability of interpreting geological structures.

Implementing several seismic attributes that emphasized the discontinuities could identify the main structural trend and associated features to the relevant deformation events in the Santos Basin. It showed that extensional mechanisms derived the deformation on a regional scale. The analysis multi-attribute based on the UVQ identified the high probability of intense faulting in the study area, which will benefit the field development of the study area.

The workflow used in this research can be implemented in further studies on fracture characteristics in other areas with different tectonic regimes.

## APPENDIX 2A. WELL-TO-SEISMIC TIE

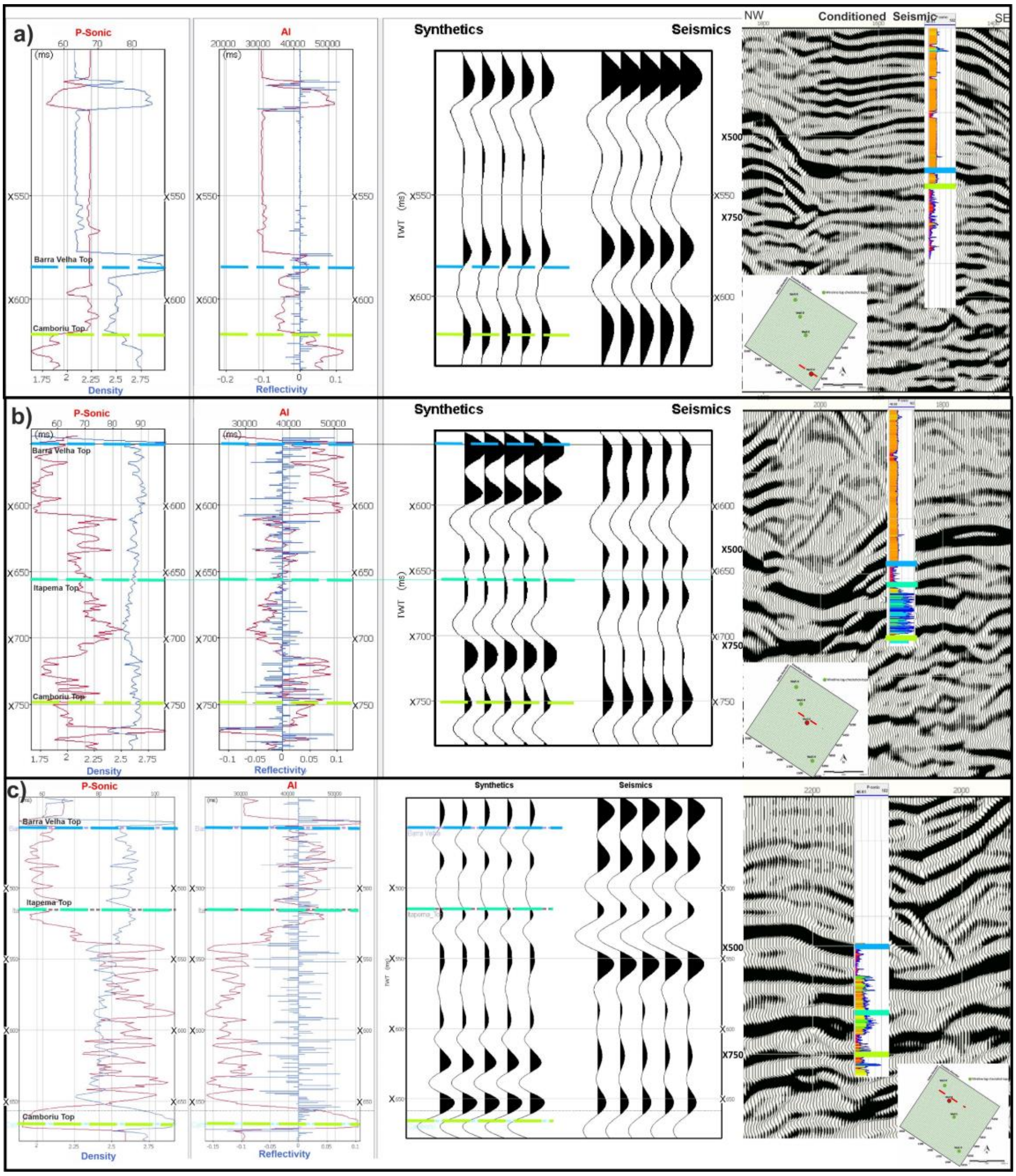


**Figure 1A.** The well-to-seismic tie for Well (a) D, (b) C, and (c) B using the conventional convolution of the reflectivity with the extracted wavelet from the conditioned seismic, producing the synthetic trace. The correlation coefficient was 68%, 71%, and 68%, respectively. The synthetic seismic is calibrated to associate the waveforms from the seismic with the stratigraphy for interpretation. The markers of the wells for Barra Velha, Itapema, and Camboriu Formations are represented by a blue, green, and yellow color, respectively.

## APPENDIX 2B. REPRESENTATIVE FREQUENCY SPECTRA AND VERTICAL RESOLUTION

The dominant vertical resolution on the intervals of the seismic data was calculated by analyzing a representative dominant frequency content from the time intervals regarding the main structures and the wells. It also used an average of interval velocity from the wells. The time intervals showed 1800-2500m/s for a shallow, 4500-4800 m/ for the intermediate, and 5000-5500 m/s for the deep interval. The vertical resolution was defined by the dominant wavelength, calculated by dividing the interval velocity by the dominant frequency. Then, one-fourth of the wavelength was the resolution of seismic data.

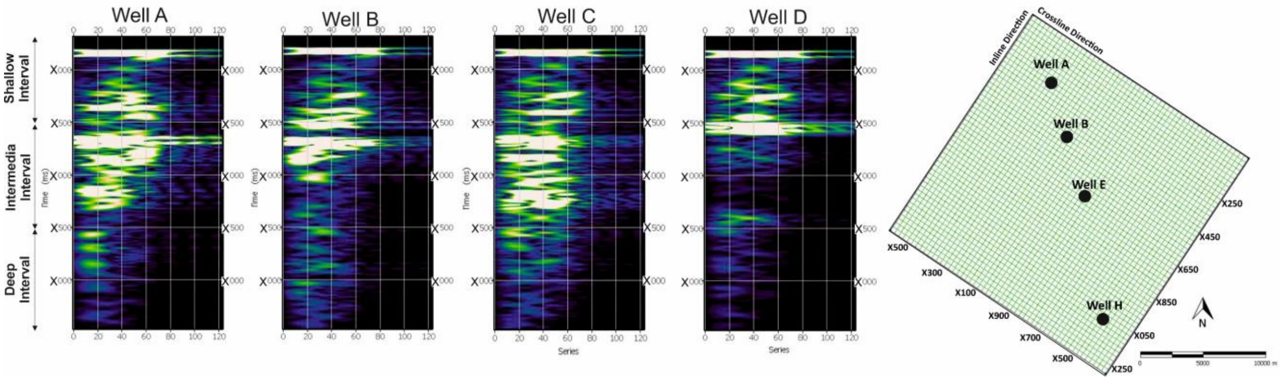


**Figure 1B.** Representative amplitude spectrum at each well location from original data, at shallow, intermediate, and deep intervals.

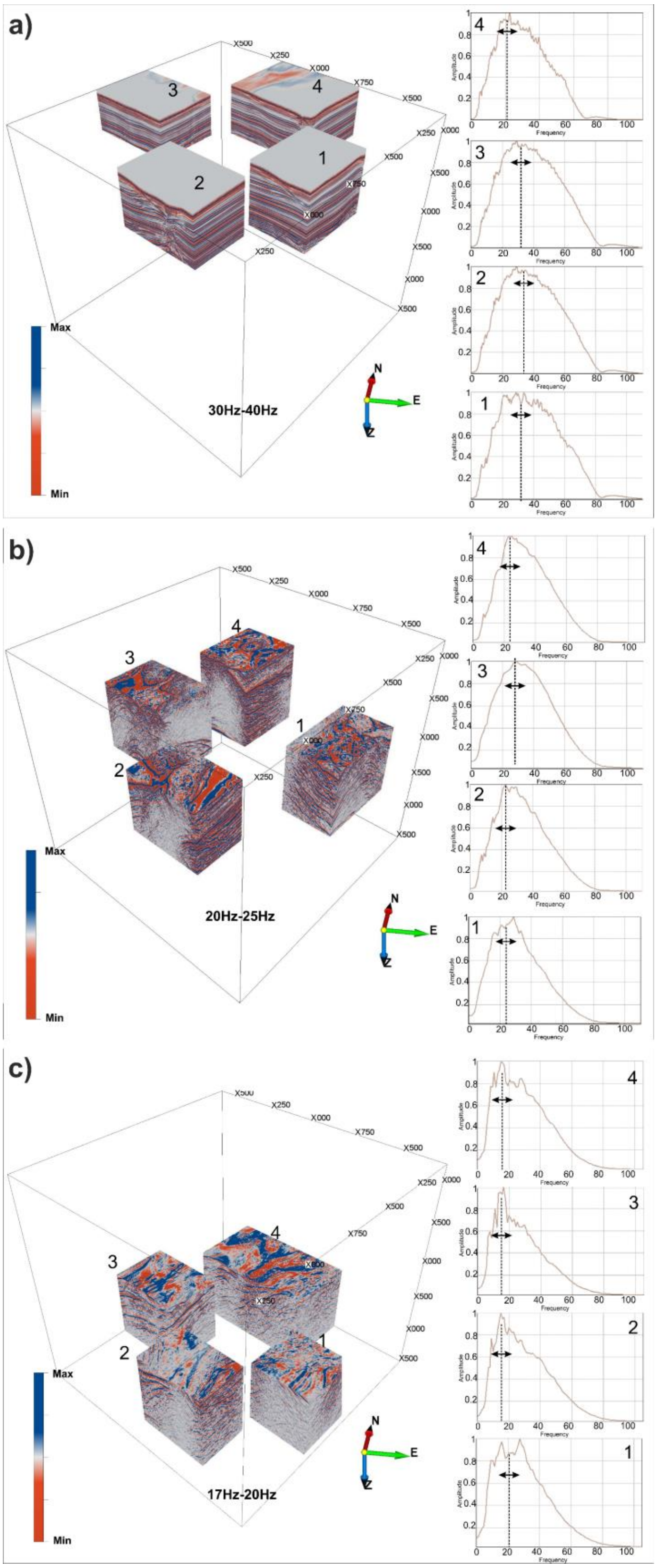


**Figure 2B.** Representative amplitude spectrum on the main structures from the original data. a) on the shallow, b) intermediate, and c) deep intervals.

## APPENDIX 3A. COMPARISON SEISMIC AND WELL STRUCTURAL ELEMENTS

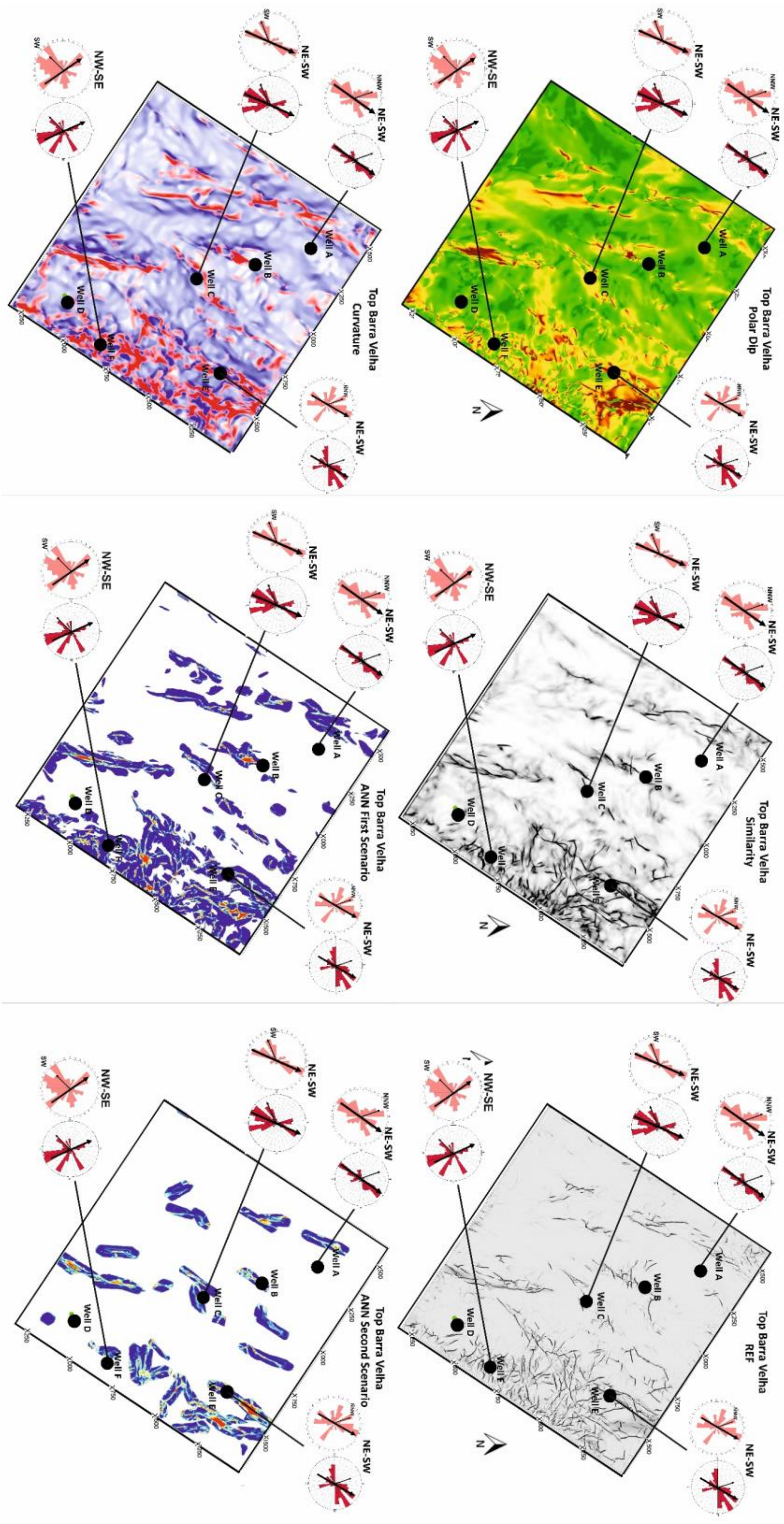


**Figure 2A.** Seismic attribute maps and well validation. Correlation between the computed seismic attributes and the borehole image log.